이학박사 학위논문

약제내성 삼중음성 유방암의 새로운 치료 표적으로서 RNA 결합 단백질 NONO의 기전에 대한 고찰

A Study on the Mechanism of RNA-Binding Protein NONO as a Novel Therapeutic Target in Drug Resistance of Triple-Negative Breast Cancer

울산대학교 대학원

의 학 과

김 성 진

A Study on the Mechanism of RNA-Binding Protein NONO as a Novel Therapeutic Target in Drug Resistance of Triple-Negative Breast Cancer

지 도 교 수 문 경 준

이 논문을 이학박사학위 논문으로 제출함

2023년 8월

울산대학교 대학원

의 학 과

김 성 진

김성진의 이학박사학위 논문을 인준함

심사위원　정 성 윤 (인)

심사위원　유 진 호 (인)

심사위원　황 정 진 (인)

심사위원　차 재 민 (인)

심사위원　문 경 준 (인)

울 산 대 학 교 대 학 원

2023 년 8 월

Abstract

Breast cancer (BC) is among the most prevalent types of cancer affecting women. The estrogen receptor (ER), progesterone receptor (PR), and human epidermal growth factor receptor (HER2) are important therapeutic targets in BC. However, triple-negative breast cancer (TNBC) has limited treatment options and no specific molecular targets, leading to poor clinical outcomes. Furthermore, TNBC is characterized by treatment failure owing to its aggressive nature, lymph node metastasis, and relatively high recurrence rate. This necessitates the identification of potential targets to enhance the therapeutic effect of TNBC treatment. RNA-binding proteins (RBPs) control messenger ribonucleic acid (mRNA) stability, splicing, translation efficiency, and the cellular distribution of proteins, thus significantly contributing to the regulation of various cellular functions. The human genome project (HGP) has identified more than 1500 structurally and functionally diverse RBPs. RBPs have recently demonstrated significant involvement in various human cancers, including BC, by influencing multiple oncogenic characteristics. This implies that RBPs are potential molecular targets for BC treatment. Genomic data were used in the present study to identify RBPs that exhibit specific expression patterns in TNBC. Consequently, RBP NONO, which contains a non-POU domain, was found to exhibit high expression levels in TNBC and to be correlated with unfavorable patient outcomes. The gene expression profile of NONO-depleted cells showed associations with cellular growth and proliferation, cell cycle regulation and cellular movement, and cell death and survival in TNBC cell lines. Surprisingly, the study findings indicate that NONO binds to and enhances the mRNA expression of the signal transducer and activator of transcription 3 (STAT3) in TNBC. Additionally, NONO directly binds to the STAT3 protein, resulting in enhanced preservation of its oncogenic function. We comprehensively screened a specific food and drug administration-approved candidate drug targeting NONO. The screening results demonstrated that auranofin effectively suppresses cell growth in TNBC, making it a potential NONO inhibitor. This implies that NONO serves as an upstream regulator of STAT3 at both the RNA and protein levels, thus influencing the growth and resistance mechanisms in these cancer cells. Overall, NONO exhibited great potential as a therapeutic target for the treatment of TNBC.

Keywords: RNA-binding protein; Triple-negative breast cancer; Non-POU domain containing octamer binding; Signal transducer and activator of transcription 3; Auranofin

Contents

Abstract ····· i

Contents ····· ii

List of figures ····· v

List of abbreviations ····· vii

Introduction ····· 1

Breast cancer ---------- 1

Treatment of breast cancer ---------- 1

Limitation of TNBC treatment ---------- 2

RNA-binding proteins ---------- 3

Implications of RBPs in cancer ---------- 4

RBPs as therapeutic targets in cancer ---------- 5

Purpose of the study ---------- 7

Materials and methods ····· 8

Cell lines ---------- 8

Cell proliferation assay ---------- 8

Colony forming assay ---------- 8

Cell migration and invasion ---------- 8

Wound healing assay ---------- 8

Flow cytometry cell cycle analysis ---------- 9

Sphere formation assay ---------- 9

Immunoprecipitation and western blotting ---------- 9

Immunofluorescence assay---------- 9

Short hairpin RNA---------- 10

Plasmid and luciferase assay----------10

Microarray analysis----------11

Quantitative real time polymerase chain reaction ----------11

Data processing ----------11

Statistical analysis ----------12

Hierarchical clustering ----------12

Chromatin immunoprecipitation assay ----------12

Short interfering RNA ---------- 13

RNA-immunoprecipitation----------13

Preparation of the chitosan-nanoparticle ----------13

Antitumor effectiveness of CH-NP-NONO siRNA ----------14

Protein structural homology modeling ----------14

High throughput drug screening----------14

Chemicals ----------15

Caspase 3/7 activity assay----------15

Tissue microarray and immunohistochemistry----------15

Results …… 15

Identification of NONO as an oncogenic RBP in TNBC----------16

NONO influences TNBC cell growth ----------25

NONO regulates STAT3 expression in TNBC ----------34

Mechanism of STAT3 regulation by NONO in TNBC ----------41

Clinical significance of the NONO-STAT3 interaction in TNBC----------54

Silencing NONO enhances the sensitivity of TNBC cells to chemotherapeutics----------61

Drug screening for inhibitors targeting NONO in TNBC ----------72

Discussion ----------79

Identification of the molecular function of NONO in TNBC----------79

NONO as therapeutic targets in TNBC----------81

Conclusion····· 85

References ····· 86

국문요약 ····· 97

List of figures

Figure 1. NONO as TNBC-specific RBP. ····· 18

Figure 2. NONO is associated with drug response in TNBC. ····· 20

Figure 3. NONO expression in TNBC. ····· 22

Figure 4. NONO expression is linked to patient survival in TNBC. ····· 23

Figure 5. NONO regulates cell growth in TNBC cells. ····· 26

Figure 6. NONO modulates cell cycle and caspase3/7 activity in TNBC cells. ····· 28

Figure 7. Depletions of NONO and its effect on migration. ····· 30

Figure 8. Depletions of NONO and its effect on invasion. ····· 32

Figure 9. Depletions of NONO and its effect on BC tumorigenesis. ····· 33

Figure 10. NONO regulates the cellular growth and movement associated genes in TNBC. ····· 35

Figure 11. NONO regulates STAT3 expression in TNBC. ····· 37

Figure 12. NONO regulates STAT3 gene expression and thereby governs TNBC cell growth. ····· 39

Figure 13. NONO binding sites in the STAT3 RNA. ····· 43

Figure 14. NONO binding sites affect STAT3 luciferase activity. ····· 45

Figure 15. NONO physically interacts with the STAT3. ····· 47

Figure 16. NONO colocalizes with STAT3 in TNBC cells. ····· 48

Figure 17. The direct interaction between NONO and STAT3 enables STAT3 to function as a transcription factor. ····· 50

Figure 18. NONO directly mediates the function of STAT3 in TNBC cells. ····· 52

Figure 19. STAT3 expression was linked to bad prognosis and correlated with NONO expression in TNBC. ····· 55

Figure 20. The clinical association between NONO-STAT3 in TNBC. ····· 57

Figure 21. NONO-STAT3 regulates the cellular growth and movement associated gene in TNBC. ····· 58

Figure 22. Patient prognosis was predicted based on the expression of NONO-STAT3 using a prediction model. ····· 59

Figure 23. Survival rates analysis of BC patients according to NONO expression levels. ·· 63

Figure 24. Clinical relevance of NONO and STAT3 in BC. ····· 65

Figure 25. Association of NONO and cancer stem cell (CSC) marker in BC. ····· 66

Figure 26. Inhibition of NONO expression enhances the responsiveness of TNBC cells to chemotherapy and radiation. ····· 68

Figure 27. NONO induces drug resistance in TNBC cells through the regulation of the STAT3 gene. ····· 70

Figure 28. FDA-approved drug screening for NONO inhibitors in TNBC. ····· 73

Figure 29. NONO inhibitory effect of Auranofin in TNBC. ····· 75

Figure 30. Modeling of the structure prediction of drug-target interaction. ····· 77

List of abbreviations

4EGI-1: EIF4E/eIF4G interaction inhibitor

4Ei-1: Eukaryotic translation initiation factor 4e nuclear import factor 1

AB: Antibody

Act D: Actinomycin D

Akt: Protein kinase B

ANOVA: Analysis of variance

ATCC: American Type Culture Collection

AUC: Area under curve

BC: Breast cancer

Bcl-2: B-cell lymphoma 2

BRB: Biometrics research branch

BRCA: Breast cancer gene

CCNB1: Cyclin B1

CCND1: Cyclin D1

cDNA: Complementary DNA

ChIP: Chromatin immunoprecipitation

CH-NP: Chitosan-nanoparticle

CHX: Cycloheximide

COX2: Cyclooxygenase 2

CRTC: CREB-regulated transcription coactivator

CS: Control signature

CSC: Cancer stem-like cell

DEAD: Asp-glu-ala-asp

DFS: Disease-free survival

DMEM: Dulbecco's Modified Eagle's Medium

DMSO: Dimethyl sulfoxide

DNA: Deoxyribonucleic acid

Dox: Doxorubicin

DSRM: Double-stranded RNA binding motif

EDTA: Ethylenediaminetetraacetic acid

EGFR: Epidermal growth receptor

eIF4E: Eukaryotic translation initiation factor 4E

eIF4F: Eukaryotic translation initiator factor 4F

eIF4G: Eukaryotic translation initiation factor 4 gamma

ER: Estrogen receptor

ESR1: Estrogen receptor 1

Ets-1: ETS proto-oncogene

F12: Nutrient mixture F-12

FACS: Fluorescence activated cell sorting

FBS: Fetal bovine serum

FCCS: Fluorescence cross-correlation spectroscopy

FDA: Food and drug administration

GEO: Gene expression omnibus

GFP: Green fluorescent protein

HDAC: Histone deacetylase

HER2: Human epidermal growth factor receptor

HGP: Human genome project

hnRNP: Heterogeneous nuclear ribonucleoproteins

HuR: Human antigen R

IC50: Half maximal inhibitory concentration

ID1: Inhibitor of DNA binding 1

IGF2BP1: Insulin-like growth factor 2 mRNA-binding protein 1

IHC: Immunohistochemistry

IL-6: Interleukin-6

Ils: Interleukins

IP: Immunoprecipitation

IPA: Ingenuity pathway analysis

JAK: Janus kinase

KH: K homology

KS: Knockdown signatures

LIN28: Lin-28 homolog

LINC00473: Long intergenic non-protein coding RNA 473

MAPK: Mitogen-activated protein kinase

MEK: Mitogen-activated protein kinase kinase

MMP: Matrix metalloproteinase

mRNA: Messenger ribonucleic acid

MSI: Musashi

mTOR: Mammalian target of rapamycin

MYC: Myc proto-oncogene protein

NAMPT: Nicotinamide phosphoribosyltransferase

NANOG: Nanog homeobox

NKI: Netherlands Cancer Institute

NONO: Non-POU domain containing octamer binding

Notch1: Neurogenic locus notch homolog protein 1

Oct4: Octamer-4

OS: Overall survival

PARP: Poly ADP-ribose polymerase

PBS: Phosphate buffered saline

PI3K: Phosphoinositide 3-kinase

PLK4: Polo-like kinase 4

PPIA: Peptidylprolyl isomerase A

PR: Progesterone receptor

qPCR: Quantitative real time polymerase chain reaction

RBP: RNA-binding protein

RFP: Red fluorescent protein

RNA-IP: RNA-immunoprecipitation

RNPC1: RNA-binding region-containing protein 1

ROC: Receiver operating characteristic

RPMI: Roswell Park Memorial Institute

RRM: RNA recognition motifs

SD: Standard deviation

SDS-PAGE: Sodium dodecyl sulfate-polyacrylamide gel electrophoresis

SFPQ: Splicing factor proline and glutamine rich

shRNA: Short hairpin RNA

siRNA: Short interfering RNA

SOX4: SRY-box transcription factor 4

STAT3: Signal transducer and activator of transcription 3

TCGA-BRCA: The Cancer Genome Atlas Breast Invasive Carcinoma

TF: Transcription factor

TIMP1: TIMP metallopeptidase inhibitor 1

TMA: Tissue microarray

TNBC: Triple-negative breast cancer

TP53: Tumor suppressor P53

TPP: Sodium tripolyphosphate

TrxR: Thioredoxin reductase

UNC: University of North Carolina

UTR: Untranslated regions

VEGF: Vascular endothelial growth factor

WB: Western blotting

Introduction

Breast cancer

Breast cancer (BC) is a prevalent cancer type among women [1, 2]. The estrogen receptor (ER), progesterone receptor (PR), and human epidermal growth factor receptor (HER2) are critical molecular markers and therapeutic targets for BC [1, 3]. The ER, which is expressed in most patients with BC, is a primary influencing factor and is correlated with prognosis [4]. Estrogen controls the activity of PR, the gene targeted by ER [5]. Additionally, the PR is linked to the overall survival (OS) or disease-free survival (DFS) of patients with BC [6]. Approximately 25% of patients with BC are HER2 positive and have an aggressive phenotype [7]. Endocrine therapy that targets estrogenic action can be used for the treatment of BC that grows in a hormone receptor-dependent manner; the expression of related receptors influences the response to endocrine therapy [6]. Conversely, the lack of molecular markers and therapeutic targets for triple-negative breast cancer (TNBC) tumors, which do not express the aforementioned key factors, significantly limits diagnosis and treatment [8]. TNBC is a BC subtype that accounts for approximately 24% of all BC cases [9]. Patients with TNBC are often younger than those without and exhibit aggressive tumors with relatively frequent lymph node metastases [10]. Moreover, compared with hormone receptor-positive BC, TNBC with more aggressive features has a higher rate of treatment failure and chemotherapy is its only authorized systemic treatment option [10, 11]. According to a previous study, patients with TNBC who responded to initial neoadjuvant treatment have a higher recurrence rate within five years than those with other cancer subtypes [12].

Treatment of breast cancer

Treatment for BC, including TNBC, depends on factors such as the patient's medical history, cancer type and stage, and the biology of the cancer cells. Several treatment options are available for BC. First, hormone therapy is commonly used to treat breast and prostate cancer and employs tamoxifen, fulvestrant, and aromatase inhibitors to block hormone production or interfere with hormone action to slow down cancer growth [13-15]. Second, chemotherapy utilizes drugs such as alkylating agents, antimetabolites, antimitotics, and antibiotics to prevent cancer cells from growing and dividing [16-18]. Third, targeted chemotherapy focuses on specific genes and proteins in cancer cells. HER2-targeted drugs such as trastuzumab are commonly used for the treatment of HER2-positive BC. Additionally, small molecule inhibitors are utilized in the management of TNBC. Poly ADP-ribose polymerase (PARP) inhibitors obstruct the activity of PARP, an enzyme that is crucial for DNA repair, resulting in

the accumulation of DNA damage and cancer cell death. This treatment is particularly effective for TNBC patients with breast cancer gene (BRCA) mutations. Furthermore, there are other available options in the form of small-molecule inhibitors, including those that target the mitogen-activated protein kinase (MAPK) pathway, such as mitogen-activated protein kinase kinase (MEK) inhibitors. Additionally, certain inhibitors impede the phosphoinositide 3-kinase (PI3K)/protein kinase B (Akt)/mammalian target of rapamycin (mTOR) (PI3K/Akt/mTOR) pathway, which plays a vital role in cellular proliferation and viability. Moreover, histone deacetylase (HDAC) inhibitors are employed to regulate gene expression [19-21]. Finally, immunotherapy, a novel approach to TNBC treatment, aims to strengthen the patient's immune system for the targeting and attack of cancer cells [22].

Limitation of TNBC treatment

Chemotherapy using anthracycline and taxane is the first-line treatment administered for TNBC because standard hormone or HER2-targeting therapies are ineffective in this patient population [23-25]. Although patients with TNBC exhibit an initial favorable response to chemotherapy, the long-term prognosis is unfavorable, with a significant risk of recurrence [26]. Adjuvant therapy has been found to be ineffective in the treatment of metastatic TNBC, resulting in a median survival duration of 13.3 months after the onset of metastasis [26, 27]. If chemotherapy proves unsuccessful, alternative treatment modalities, such as surgery and radiation, are considered [28]. Surgery, the primary treatment, is followed by radiation therapy to destroy or slow down cancer cell growth and alleviate symptoms regardless of the occurrence of metastasis [29]. Recently, immunotherapeutic agents like PD-L1 inhibitors have exhibited effectiveness in TNBC treatment by stimulating the immune system to target and attack cancer cells [30]. Unlike conventional treatments, immunotherapy targets cancer cells that are unresponsive to chemotherapy or radiation [31]. The limited treatment options primarily stem from drug resistance which can arise from various causes. Cancer cells develop genetic mutations that change the structure of proteins targeted by drugs. This prevents the drug from targeting the protein, thus reducing its therapeutic effect [32]. Cancer cells also reduce the expression of proteins that are targeted by drugs or activate drug elimination mechanisms that release drugs into extracellular pumps. This reduces the drug concentration and therapeutic effect [33]. Epidermal growth receptor (EGFR), tumor suppressor P53 (TP53), and HER2 genes help cancer cells develop resistance to drugs, and the overexpression of these genes causes cancer cells to develop drug resistance [34]. Cancer cells also avoid the toxic effects of drugs by altering their apoptotic pathways [35]. Therefore, alternative options should be considered to overcome drug resistance in TNBC treatment. They may include novel

therapies, promising drug combinations, new targeted therapies, or the integration of immunotherapy and chemotherapy in a combined treatment approach.

RNA-binding proteins

RNA-binding proteins (RBPs) are pivotal in governing a wide range of biological processes. RBPs contribute to various cellular processes by governing messenger ribonucleic acid (mRNA) stability, splicing, translation efficiency, and the cellular distribution of proteins [36]. One of the major functions of RBP is regulating mRNA stability. RBPs can bind to specific sequences or structures within mRNA molecules to determine their fate [37]. Certain RBPs prevent degradation by enhancing mRNA stability, while others reduce mRNA levels by promoting degradation. RBPs have substantial impact on the regulation of gene expression, as they control the stability of mRNA and influence the levels of specific proteins within cells [38]. Additionally, RBPs assume a crucial function in alternative splicing, which is responsible for generating multiple protein isoforms from a single gene [38]. Alternative splicing considerably enhances protein diversity, allowing cells to produce various protein variants with unique functions. RBPs bind to specific RNA sequences positioned at the exon-intron boundary and regulate the splicing machinery, thereby influencing the decision to include or exclude specific exons during mRNA processing [39]. Dysregulation of alternative splicing, resulting from RBP dysfunction, can lead to the production of abnormal protein isoforms associated with various diseases [40]. Translation, the conversion of mRNA to protein, is a key area affected by RBPs. RBPs can interact with specific regions of mRNA molecules and regulate translation efficiency [41]. They can promote or inhibit the recruitment of ribosomes to mRNA, influence the initiation of translation, or affect the movement of ribosomes along mRNA molecules [42]. This fine-tuning of translation allows cells to tailor protein synthesis to different conditions or stages of development. Apart from their involvement in mRNA metabolism, RBPs also play a role in facilitating the intracellular localization of proteins [43]. By binding to specific RNA sequences within coding or untranslated regions of mRNA, RBPs can affect the transport of mRNA molecules to specific cellular compartments. This localization affects protein targeting, stability, and function, thus affecting various cellular processes [44]. The Human Genome Project (HGP) has identified more than 1500 RBPs [45]. RBPs exhibit a wide range of structural and functional diversity that is crucial for the regulation of various cellular processes [46]. A number of RBPs have several specific basic domains, which consist of several repetitive sequences, and commonly include RNA recognition motifs (RRM), k homology (KH) domains, asp-glu-ala-asp (DEAD) motifs, double-stranded RNA binding motifs (DSRM), and zinc-finger domains. [45]. A previous study has

linked the abnormal expression or dysfunction of RBP to various human diseases [47]. For example, dysregulated expression or impaired activity of RBPs has been implicated in cancer development and progression. RBPs can influence cell proliferation, apoptosis, and metastasis by modulating the translation and stability of oncogenes or tumor suppressor genes [48].

Implications of RBPs in cancer

Several studies have indicated that the abnormal expression of RBPs is observed in a broad spectrum of human diseases, such as cancer, neurological disorders, and muscular atrophies [47, 49, 50]. By conducting comprehensive genome analyses, several RBPs have been identified as pivotal contributors to the development and progression of cancers, thus significantly influencing cell growth and proliferation [51-54]. Abnormal expression of RBPs is closely linked to the survival rate of individuals diagnosed with cancer [51, 55]. For example, in various cancer types, the aberrant expression of specific RBPs can result in the dysregulation of their mRNA targets [48, 56]. The human antigen R (HuR), an RBP, is commonly upregulated in various cancer types, and this overexpression is correlated with a poor prognosis. [57, 58]. Another aspect of RBP involvement in cancer is related to the dysregulation of post-transcriptional processes. Alterations in mRNA splicing, stability, or localization due to dysregulated RBP have implications for cancer as they can lead to abnormal cellular phenotypes [36]. For example, RBPs play a pivotal role in the advancement of cancer by modulating alternative splicing, leading to the generation of distinct isoforms of oncogenes and tumor suppressors [59]. RBPs also assume a crucial role in modulating oncogenes and tumor suppressors by regulating the stability, translation, and splicing of mRNAs encoding these pivotal proteins [60]. It is involved in epigenetic regulation that affects gene expression without making any changes to the DNA sequence [39, 61, 62]. The dysregulation of these RBPs disrupts the normal patterns of gene expression, thereby facilitating the initiation and progression of cancer [63]. Non-coding RNAs, such as microRNAs and long non-coding RNAs, can also interact with RBPs, which significantly contribute to cancer progression. The disruption of these interactions may also contribute to cancer [64, 65]. RBP is associated with anticancer drug resistance. By regulating genes associated with drug metabolism, drug transport, and the drug target, RBPs can modulate the response of cancer cells to therapeutic agents [66]. Given the pleiotropic involvement of RBPs in cancer, elucidating their role can unveil novel therapeutic targets and biomarkers for cancer diagnosis, prognosis, and treatment. However, the complexity of interactions between RNA and proteins and the multifunctionality of RBPs present significant challenges to research in this field.

RBPs as therapeutic targets in cancer

Small molecule inhibitors, ≤500 Da in size, can target the functions of RBPs in diverse human diseases, including cancer. Small molecule inhibitors are currently undergoing clinical trials and showing promising anticancer effects [56]. Eukaryotic translation initiator factor 4F (eIF4F), HuR, musashi (MSI) proteins, and lin-28 homolog (LIN28) are some of the RBPs being targeted by these small-molecule inhibitors [48]. In multiple cancer types, the overexpression of the eukaryotic translation initiation factor 4E (eIF4E), a component of eIF4F has been observed. Compounds such as ribavirin, a eukaryotic translation initiation factor 4E nuclear import factor 1 (4Ei-1), eIF4E/ eukaryotic translation initiation factor 4 gamma (eIF4G) interaction inhibitor (4EGI-1), and mTOR inhibitors, disrupt interactions between eIF4E and other proteins thus obstructing translation initiation through the cap-dependent mechanism and inducing apoptosis in cancer cells [67, 68]. Additionally, MnK inhibitors have been used to inhibit eIF4E phosphorylation resulting in reduced cell proliferation and metastasis in various cancer models [69]. HuR exhibits abnormal expression and localization in different types of cancer. Small molecule inhibitors, such as MS-444, target specific regions of HuR, blocking its RNA-binding activities and reducing HuR-mediated mRNA stabilization of genes involved in cancer progression [57]. MS-444 attenuates cytoplasmic HuR in glioblastoma cells, inducing apoptosis and decreasing cell invasion [70]. In colorectal cancer cells, MS-444 reduces the expression levels of cyclooxygenase 2 (COX2), resulting in growth inhibition and enhanced expression of genes associated with apoptosis [71]. High-throughput screenings have identified oleic acid and (−)-gossypol as potential inhibitors of MSI proteins [71, 72]. Ro 08-2750 (Ro) effectively inhibits the function of MSI2 by binding to its RRM1 domain, thus reducing the expression of target mRNAs involved in leukemogenesis [73]. The excessive expression of LIN28 in cancer hampers the normal maturation process of let-7, thereby facilitating tumor growth. Inhibitors such as compound 1632 disrupt LIN28 activity, resulting in the restoration of let-7 levels and inhibition of tumorigenesis [74]. In human prostate and liver cancer cells, compound 1632 demonstrated the ability to disrupt the action between LIN28 and pre-let-7 [75]. Targeted therapies are more advantageous than existing ones in terms of selectivity, efficacy, and tolerability. Small molecule inhibitors that specifically target RBPs have great potential [76]. RBPs possess unique RNA-binding domains or motifs that can recognize and interact with specific RNAs. Small molecule inhibitors disrupt the interaction between the RBP and its RNA target, effectively targeting the domain [77]. These features enable precise targeting of disease-associated RBPs while minimizing potential off-target effects on other cellular processes [78].

Altered regulation of RBPs has been associated with numerous diseases, including drug resistance [79, 80]. The utilization of small molecule inhibitors to target RBPs enables the modulation of several facets of RNA metabolism, including mRNA stability, splicing, and translation [81]. For instance, heterogeneous nuclear ribonucleoproteins (hnRNP) A1 regulates alternative splicing of pre-mRNAs, including genes involved in apoptosis like b-cell lymphoma (Bcl)-x, thus contributing to chemotherapy resistance [82]. The overexpression of MSI1 is linked to drug resistance in glioblastoma and colorectal cancer, as it binds and regulates target mRNAs, including neurogenic locus notch homolog protein 1 (Notch1) involved in cell survival [83]. HuR, involved in mRNA stabilization and regulation, contributes to drug resistance through permeability glycoprotein (P-glycoprotein) and Bcl-2 mRNA [84]. Insulin-like growth factor 2 mRNA-binding protein 1 (IGF2BP1) interaction mRNA of insulin-like growth factor 2 (IGF2) and Myc proto-oncogene protein (MYC), which are associated with cell survival and proliferation, conferring chemotherapy resistance in various cancer types [85, 86].

RBPs are vital in governing a wide array of cellular processes, encompassing drug efflux, apoptosis, DNA repair, and drug metabolism. Specific RBPs have been identified as key factors in the development of drug resistance, controlling the expression of target genes associated with mechanisms of drug resistance [66]. Certain proteins involved in disease processes were considered "non-therapeutic" owing to the absence of enzymatic active sites or accessible binding pockets [87]. However, because RBPs interact with RNA, the utilization of small-molecule inhibitors to target these proteins offers a novel strategy for modulating the function of previously undruggable targets [88]. Therefore, we propose that targeting RBPs with small-molecule inhibitors may effectively influence gene expression, overcome drug resistance, and treat diseases with complex etiology.

Purpose of the study

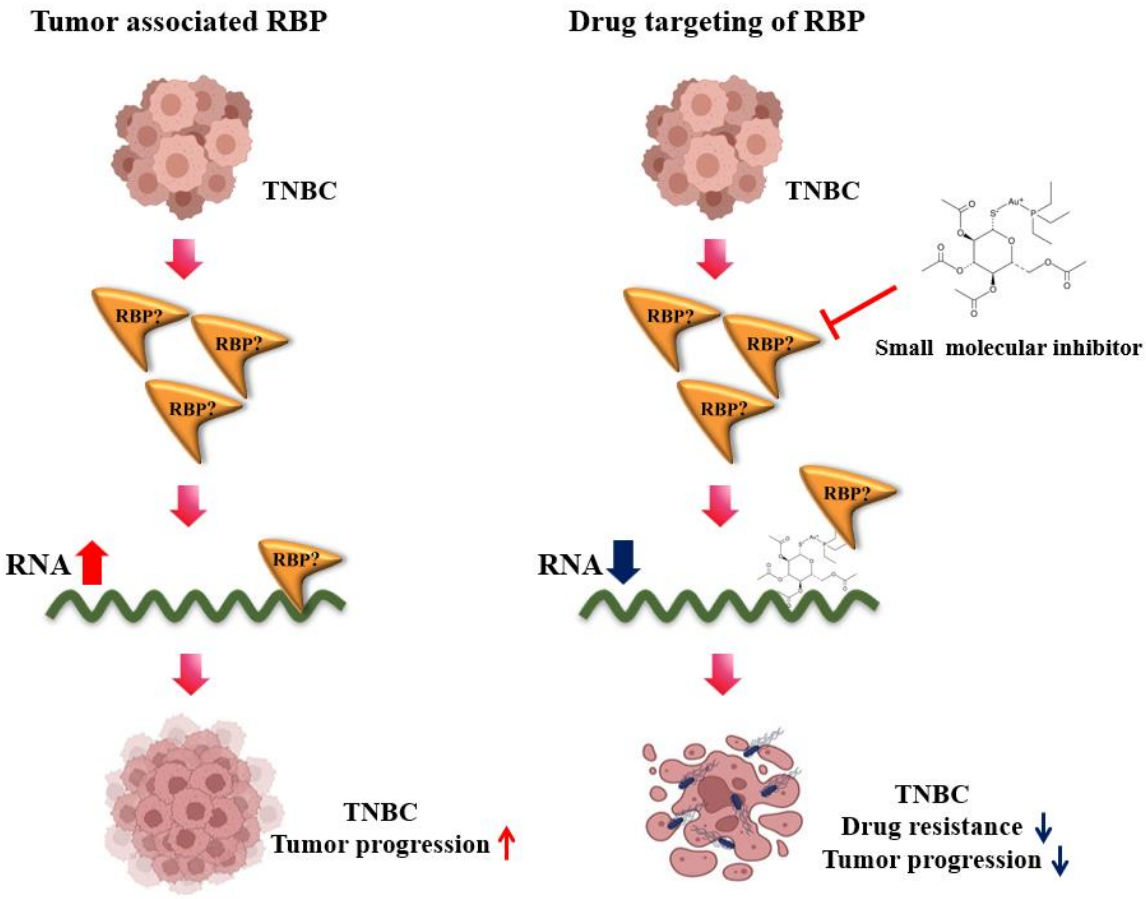

Drug-resistant TNBC does not respond favorably to conventional therapies, highlighting the need for new therapies. By identifying RBPs associated with drug resistance in TNBC, we aimed to overcome drug resistance through the regulation of oncogene expression and development of novel therapeutics. The primary objectives of this study were as follows:

1. To identify specific RBPs associated with drug resistance in the TNBC patient database.

2. To validate the functional importance of RBPs using *in vitro* and *in vivo* models.

3. To examine interactions between RBPs and target RNAs.

4. To investigate potential therapeutics by identifying small molecules or compounds that can modulate the activity or expression of the target RBP based on RBP and target RNA.

Materials and Methods

Cell lines

Human cancer cell lines were procured from the American Type Culture Collection (ATCC). The cells were maintained in a humidified incubator at 37 °C with 5 % CO2 using either Dulbecco's Modified Eagle Medium (DMEM) or Roswell Park Memorial Institute (RPMI) 1640 medium (HyClone). The culture media were supplemented with 10% fetal bovine serum (FBS) and 1% antibiotic-antimycotic (Gibco) [89, 90].

Cell proliferation assay

The specified cell lines were seeded in triplicate at a density of 3×10^3 cells per well in 96-well plates. Cell viability was assessed using a CCK8 assay (Dojindo) according to the manufacturer protocol. Following the addition of the CCK-8 reagent, the cells were incubated at 37 °C for 1 h. Cell viability was assessed by measuring the absorbance at a wavelength of 450 nm.

Colony forming assay

In total, 3×10^3 cells per well were seeded in 6-well plates cultured in DMEM or RPMI media for 1 to 2 weeks. To determine colony formation, the cells were fixed with methanol and stained with a 0.05% crystal violet solution for 30 min.

Cell migration and invasion

For the cell migration and invasion assay, a cell density of 4×10^4 cells per well was seeded in the upper chamber (Corning) using media devoid of FBS. Matrigel (Corning) was applied as a pre-coat to the upper chambers in the invasion assay; however, the cell migration assay did not require a coating step. The lower chamber was filled with a medium containing 10 % FBS as a supplement. After incubation for 24 h, the cells on the lower side of the chamber were fixed using 4% paraformaldehyde and subsequently stained with 0.05% crystal violet. Cotton swabs were used to remove the matrigel as well as any non-migrated and non-invaded cells.

Wound healing assay

For the wound healing assay, cells were seeded at a density of 5×10^5 cells per well in 6-well plates and incubated at 37 °C for 24 h. Once the cells reached full confluence, a scratch or wound was created across the monolayer using sterile 200 μL pipette tips, and then washed. After removing the detached

cells by washing with medium, images of the scratch/wound were captured at 0 and 12 h. The percentage of wound closure was calculated and analyzed based on these images.

Flow cytometry cell cycle analysis

Cells were detached using trypsinization and subsequently collected through centrifugation. Afterwards, the cells were washed twice with phosphate buffered saline (PBS) and fixed with cold 70 % ethyl alcohol at -20 °C for 1 h. After another round of PBS washing, the cells were treated with RNase A and stained with propidium iodide at a concentration of 20 μg/mL, followed by incubation at 37 °C for 30 min. The cells were analyzed using a CytoFLEX (Beckman) flow cytometer.

Sphere formation assay

In total, 5×10^3 cells per well were seeded in ultra-low attachment 6-well plates and cultured for 10 days. The spheres were cultured in DMEM/nutrient mixture F-12 (F12) medium supplemented with B27 supplement (Gibco), 20 ng/mL epidermal growth factor, and 20 ng/mL basic fibroblast growth factor. Subsequently, the spheres were imaged and manually counted.

Immunoprecipitation and western blotting

Immunoprecipitation (IP) and western blotting (WB) experiments were conducted following established protocols [89-91]. First, cellular lysates were obtained by treating the cells with lysis buffer comprising 50 mM Tris (pH 7.4), 150 mM NaCl, 1% Triton X-100, and 1 mM ethylenediaminetetraacetic acid (EDTA), and supplemented with protease inhibitors (Roche) and phosphatase inhibitors (GenDEPOT). Following centrifugation at 13,500 g for 30 min at 4 °C, the supernatants containing the desired components were collected. To prepare for IP, the cell lysates underwent a pre-clearing step using protein A/G beads. Subsequently, the lysates were incubated for 4 h with protein A/G beads conjugated to antibodies specific to non-POU domain-containing octamer-binding (NONO) and signal transducer and activator of transcription 3 (STAT3). The immunocomplexes were washed four times with a cell extraction buffer. Eluted samples or whole-cell lysates were separated using sodium dodecyl sulfate-polyacrylamide gel electrophoresis (SDS-PAGE), and the proteins were subsequently detected using specific antibodies. The antibodies employed in this study included NONO (Millipore or Bethyl), STAT3 (Cell signaling or Abcam), phospho-STAT3 (Cell signaling), β-actin (Cell signaling), FLAG (Cell signaling), and MYC (Cell signaling).

Immunofluorescence assay

Immunofluorescence assays were conducted following established protocols, as described in a previous report [91]. The immunofluorescence staining procedure employed anti-NONO (Millipore) and anti-STAT3 (Cell signaling) antibodies.

Short hairpin RNA

Short hairpin NONO (TRCN0000286628; TRCN0000294049) and short hairpin green fluorescent protein (GFP) (SHC005) clones were procured from Sigma. The co-transfection of 293FT cells was conducted by employing the Lipofectamine® 2000 Reagent (Invitrogen) and lentiviral packaging plasmids psPAX2 and pMD2.G. After a transfection period of 48 h, the viral supernatants were gathered and combined. To infect the target cells, the filtered viral supernatant was mixed with a culture medium containing 8 μg/mL polybrene as a supplement. After a 24 h incubation period, the infectious supernatant was discarded, and the selection of infected cells was initiated 48 h after infection.

Plasmids and luciferase assay

The construction of STAT3 complementary DNA (cDNA), STAT3-reporter, and NONO cDNA have previously been documented [92, 93]. To produce the reporter plasmids containing the 3' untranslated regions (UTRs) of STAT3, custom-designed oligonucleotides were utilized to target the putative NONO binding site, following the procedure depicted in Figures 1–13A-B. The oligonucleotides included wild-type sequences for M1-1, M1-2, M2, M3, and M4 with the following designs: M1-1 wild-type forward: 5'- AAACTAGCGGCCGCTAGTCTGTCTCCAGGCAGGAGGACTT-3', reverse: 5'-CTAGAAGTCCTCCTGCCTGGAGACAGACTAGCGGCCGCTAGTTT-3'; M1-2 wild-type forward: 5'-AAACTAGCGGCCGCTAGTCTACCTTCAGGCAGGTCCTACT-3', reverse: 5'-CTAGAGTAGGACCTGCCTGAAGGTAGACTAGCGGCCGCTAGTTT-3'; M2 wild-type forward: 5'-AAACTAGCGGCCGCTAGTCTCTGCTCCTGGAACACACCTT-3'; reverse: 5'-CTAGA AGGTGTGTTCCAGGAGCAGAG ACTA GCGGCCGCTAGTTT-3'; M3 wild-type forward: 5'-AAACTAGCGGCCGCTAGTGAACCTGGGAGGCGGAGGTTGT-3', reverse: 5'-CTAGACAACCTCCGCCTCCCAGGTTCACTA GCGGCCGCTAGTTT-3'; and M4 wild-type forward: 5'-AAACTAGCGGCCGCTAGTGTAATCCCAGCACTGTGGGAGT-3', reverse: 5'-CTAGA CTCCCACAGTGCTGGGATTACACTAGCGGCCGCTAGTTT-3'. The oligonucleotides containing PmeI and XbaI restriction sites were annealed and then inserted into pmirGLO dual-luciferase expression vectors (Promega) through cloning. To create mutations in the seed region of the NONO binding site, mutant oligos were inserted into pmirGLO vectors, as depicted in Figures 1–13A–B. The sequences were confirmed using an automated sequencer. To conduct luciferase-based reporter assays,

the cells were transfected with reporter genes and plasmids using the Dual-Glo® Luciferase Assay System (Promega). Dual-Luciferase® Reporter Assay System (Promega) was utilized according to the manufacturer's instructions. After 48 h, the cells were collected to assess luciferase activity, which was then normalized to *Renilla* activity (n=3).

Microarray analysis

Microarray analysis was conducted following the established methodology outlined in previous studies [89-91]. Summarily, the specified cell lines were subjected to total RNA extraction using a mirVana RNA Isolation labeling kit (Ambion). In total, 500 ng RNA was utilized for labeling and hybridization, according to the manufacturer's protocols (Illumina). The bead chips were scanned using an Illumina BeadArray Reader (Illumina) for data acquisition. The obtained microarray data were normalized using the quantile normalization method available in the LIMMA package, a tool within the R language environment for the analysis of microarray data. To simplify the analysis, the expression levels of each gene were logarithmically transformed (log2) prior to further analysis. The resulting data have been deposited in the Gene Expression Omnibus (GEO) database under accession number GSE117927.

Quantitative real time polymerase chain reaction

RNA extraction was performed using the Trizol extraction method according to the manufacturer's instructions (Invitrogen). Gene-specific TaqMan primers were utilized for quantitative real-time polymerase chain reaction (qPCR) analysis on an ABI Prism StepOneTM real-time PCR system. Gene expression analysis was conducted using the SensiFAST™ Probe Hi-ROX One-Step Kit (Bioline). The expression of each gene was normalized to the expression of the human peptidylprolyl isomerase A (PPIA) gene. The following primers were utilized in this study: PPIA (ABI), NONO (IDT), STAT3 (IDT), cyclin B1 (CCNB1) (ABI), cyclin D1 (CCND1) (ABI), nanog homeobox (NANOG) (ABI), and Octamer 4 (OCT4) (ABI).

Data processing

The gene expression dataset was acquired from the Gene Expression Omnibus (GEO) database (GSE76275; GSE21653; GSE65216; GSE31519; GSE58812; GSE22226; GSE16446;) and TCGA portal (https://www.cbioportal.org/). Prior to analysis, all the data were normalized using the quantile normalization method implemented in the R programming language.

Statistical analysis

The quantitative data were expressed as the mean ± standard deviation (SD) obtained from three independent experiments. A two-tailed Student's t-test was employed to assess the statistical significance of differences between two groups. To compare three or more groups, we conducted one-way analysis of variance (ANOVA) followed by Tukey's post hoc analysis, which facilitated the assessment of the statistical differences between the groups. Statistical significance was set at $p < 0.05$. To assess the correlation between two continuous variables, we employed the Pearson correlation coefficient. Receiver operating characteristic (ROC) curve analysis was conducted to assess the correlation between gene expression levels. The area under the curve (AUC) was calculated using the concordance index as a measure of predictive accuracy. The corresponding p-values were calculated using a one-sided Wilcoxon's rank test to assess statistical significance. The class comparison method of the BRB-array tools package was utilized to identify genes that exhibited differential expression between two array groups. Gene expression differences in the profile data were deemed statistically significant if the p-value was below 0.001. Clustering analysis was conducted using the clustering algorithm and the results were visualized using treeview. Kaplan-Meier survival plots were employed to assess the correlation with patient survival and analyzed using log-rank test. The optimal cutoff value for gene expression in survival analysis was determined using the R package [94].

Hierarchical clustering

Hierarchical clustering analysis was performed using complete linkage and Euclidean distance as a similarity measure to visualize the expression patterns of differentially expressed transcripts. The criteria used to identify differentially expressed genes included a minimum fold change of 1.5 and a raw p-value below 0.05, based on the independent t-test. Data analysis and visualization of the differentially expressed genes were carried out utilizing R version 3.5.3.

Chromatin immunoprecipitation assay

Chromatin immunoprecipitation (ChIP) assays were performed using a Magnetic ChIP assay kit (Pierce) according to the manufacturer's instructions. MDA-MB-231 cells were treated with 1% formaldehyde for 10 min to crosslink the proteins and DNA, and then quenched with glycine. Following a cold PBS wash, the cells were exposed to 1.5 µL micrococcal nuclease at 37 °C for 15 min. The chromatin containing crosslinked proteins was subjected to immunoprecipitation using the designated antibodies, and the isolated DNA fragments were subsequently analyzed using qPCR. The following

primers were used to amplify the promoter region of CCND1: forward primer 5'-CGAACACCTATCGATTTTGCTAA-3' and reverse primer 5'-TTGACCAGTCGGTCCTTGCGG-3'.

Short interfering RNA

The short interfering RNAs (siRNAs) targeting NONO and the non-specific siRNA had the following target sequences: siNONO-1: 5′-CUCAGUAUGUGUCCAACGA-3′, siNONO-2: 5′-CAAACGUCGCCGAUACUAA-3′, siNONO-3: 5′-GAUGGAAGCUGCACGCCAU-3′, and siCon: 5' UUCUCCGAACGUGUCACGU-3'. The cells were transfected with 100 pmol of siRNA (Sigma) using Lipofectamine® RNAiMAX reagent (Invitrogen) according to the manufacturer's instructions and incubated for 48 h.

RNA-immunoprecipitation

Cells were grown in 15-cm plates until they reached approximately 80–90% confluency. After the incubation period, the cells were washed with PBS. RNA-immunoprecipitation (IP) was carried out using a magnetic chromatin immunoprecipitation kit obtained from Active Motif according to the manufacturer's instructions. Immunoprecipitation was performed using anti-rabbit-NONO antibodies and anti-rabbit-IgG antibodies as controls. The RNA obtained from the immunoprecipitated complexes was purified using EZBlue (Sigma) and treated with DNase1 to remove any contaminating DNA. The immunoprecipitated RNA was then quantified using a qPCR kit with a STAT3 probe provided by IDT.

Preparation of the chitosan-nanoparticle

Chitosan (CH) used in this study, characterized by a low molecular weight and a deacetylation degree of 75–85%, was purchased from Sigma. Sodium tripolyphosphate (TPP) and acetic acid were also purchased from Sigma. The preparation of siRNA-incorporated chitosan-nanoparticles (CH-NP) involved the electrostatic interaction between positively charged chitosan (CH), negatively charged sodium tripolyphosphate (TPP), and siRNA. To form the CH-NP/siRNA complex, a CH solution (2 mg/mL, 1% acetic acid) was mixed with predetermined concentrations of TPP (0.25% w/v) and siRNA (1 μg/μL). The mixture was stirred continuously at 25°C, resulting in the spontaneous formation of CH-NP/siRNA. Following incubation for 30 min at 4°C, the CH-NP/siRNA complex was collected by centrifugation at 13,000 rpm for 50 min at 4°C. The size and surface charge of the CH-NP were determined using a dynamic light scattering photometer (HORIBA). The encapsulation efficiency of siRNA was assessed by measuring the absorbance at 260 nm using spectrophotometry and the

supernatant obtained from centrifugation of the CH-NP.

Antitumor effectiveness of CH-NP-NONO siRNA.

Female BALB/c nude mice weighing 20 g and aged 7 weeks were obtained from OrientBio. All animal procedures and maintenance conditions were approved by the Konkuk University Institutional Animal Care and Use Committee (Approval #: KU17188). Tumor growth was induced by subcutaneously injecting 1×10^6 MDA-MB-231 cells in 50 μL HBSS into each mouse (n=5 mice per group). A 5 μg dose of CH-NP-control siRNA (5'-UUCUCCGAACGUGUCACGU[dT][dT]-3') or CH-NP-NONO siRNA (5'-GAUGGAAGCUGCACGCCAU[dT][dT]-3') was intravenously administered to each mouse twice a week. The treatment regimen was continued until the control group showed moribund signs, which typically occurred at approximately 4 to 5 weeks. At this point, all mice were euthanized. The lengths and widths of the tumors were measured using calipers, and their volumes calculated as follows: tumor volume (mm^3) = length × $(width)^2/2$. The weights of the tumors were also documented.

Protein structural homology modeling

SWISS-MODEL web server (http://swissmodel.expasy.org) [95] was utilized for homology-based structural modeling of NONO (accession ID: NP_001138880.1) and STAT3 (accession ID: NP_001356441). The templates selected for modeling were human splicing factor proline and glutamine-rich (SFPQ) (PDB ID: 4WIJ) for NONO and mouse STAT3 (PDB ID: 1BG1) for STAT3, with sequence similarities of 73.6% and 99.8%, respectively. The SWISS-MODEL yielded QMEAN4 Z-scores of 1.61 and -2.41 for NONO and STAT3, respectively. ClusPro 2.0, utilizing the hydrophobic-favored scoring scheme [96], was employed for computational docking simulations. AutoDock Vina (ver. 1.1.2), a widely used protein-ligand docking method, was employed for molecular docking analyses. The file format was prepared using AutoDock Tools (ver. 1.5.6) obtained from the Scripps Research Institute, CA, USA. The binding affinities for the compounds were assessed based on negative Gibbs free energy (ΔG) scores (kcal/mol) [97]. The docking structures were visualized using PyMOL software from DeLano Scientific.

High throughput drug screening

After infecting MDA-MB-231 cells with the pCDH-GFP-NONO viral vector, they were seeded at a density of 1.0×10^3 cells per well in 96-well plates After incubation for 24 h, the cells were treated with compounds from the drug library (Enzo) at a final concentration of 5 μM in 0.5%

dimethyl sulfoxide (DMSO) (v/v) (Sigma). After a 24-h incubation period, the cells were fixed using 4% paraformaldehyde (Sigma) and subsequently rinsed with PBS (Welgene) for 10 min. The fluorescence intensity of GFP was assessed using the Operetta High Content Screening System (Perkin Elmer), and subsequent data analysis was performed utilizing Harmony 3.5.1 high-content imaging and analysis software (Perkin Elmer).

Chemicals

Auranofin, digoxin, colchicine, and podophyllotoxin were obtained from Sigma.

Caspase 3/7 activity assay

The specified cell lines were plated in white 96-well plates at a density of 4×10^3 cells/well. Caspase 3/7 activity was measured in the cells using the Caspase-Glo® 3/7 activity assay (Promega) according to the manufacturer's instructions. Upon the addition of the assay reagent and incubation for 30 min at room temperature, the luminescence intensity of the cells was assessed using an *Alpha PLUS (Multi-Label) Plate Reader* (Pekin Elmer).

Tissue microarray and immunohistochemistry

TMA and IHC were conducted following the established protocols [98, 99] and using tissue samples obtained from patients who had undergone primary breast cancer surgery between 1993 and 1998 at Asan Medical Center in Seoul, Korea. The TMA was stained with an anti-NONO antibody (Bethyl) for analysis.

Results

Identification of NONO as an oncogenic RBP in TNBC

Previous studies report that RBPs are promising targets for therapeutic interventions in TNBC treatment owing to their implicated oncogenic roles [100]. Therefore, we screened genomic data to identify TNBC-specific RBPs using approaches previously tested for elucidating unexplored functions of oncogenes [89, 90]. We aimed to identify differentially expressed RBPs between TNBC and non-TNBC subtypes, leveraging the well-established Netherlands Cancer Institute (NKI) [101] and University of North Carolina (UNC) [102] cohorts, considering the relatively poor prognosis associated with TNBC. Class comparison analysis was performed for the two subtypes of breast cancer (TNBC vs non-TNBC) [103]. In total, 23 RBPs were identified as potential candidates associated with TNBC, as depicted in Figure 1A. The findings were validated using the Cancer Genome Atlas Breast Invasive Carcinoma (TCGA-BRCA) dataset, as illustrated in Figure 1B, of these RBPs, while 18 RBPs were highly expressed in TNBC and 5 RBPs in non-TNBC, suggesting that individual RBPs have specificity depending on BC subtypes. Using ROC curves [104], we identified RBPs that exhibited significant association with chemotherapy responsiveness, a crucial factor affecting the survival of patients with TNBC. Among the identified RBPs, 10 were linked to chemotherapy responsiveness. NONO exhibited the lowest p-value and was selected for further investigation (Figures 2A–B).

NONO, a non-POU domain-containing octamer-binding protein has been implicated in various molecular functions across different types of cancer, including gastric [105], prostate [106], and lung cancer [107]. However, its clear mechanisms in cancer have not been clearly identified. Furthermore, NONO function in TNBC is not comprehensively understood. Therefore, we focused on the elucidation of NONO function in TNBC (Figure 1-3A), analysis of independent BC datasets demonstrated a significant increase in NONO mRNA expression in TNBC compared to non-TNBC. This finding was confirmed by the results obtained from TMA analysis (Figures 3B–C).

Subsequently, we investigated the potential association between NONO expression and survival of patients with BC, specifically in the context of TNBC. Decreased levels of NONO were correlated with enhanced OS throughout the patient cohort, as depicted in Figure 4A [108]. This could be attributed to the unfavorable survival outcomes observed among patients with TNBC, who exhibit high expression of NONO. Notably, within the TNBC subgroup, a decreased level of NONO was consistently associated with more optimized prognosis across multiple TNBC datasets, as shown in Figure 4B. Furthermore,

TCGA data analysis revealed that the prognostic significance of NONO expression was particularly pronounced in patients with TNBC compared to those without, as depicted in Figure 4C.

These findings indicate a robust association between NONO expression and prognosis, indicating that NONO could be a promising indicator of clinical outcomes in TNBC.

A

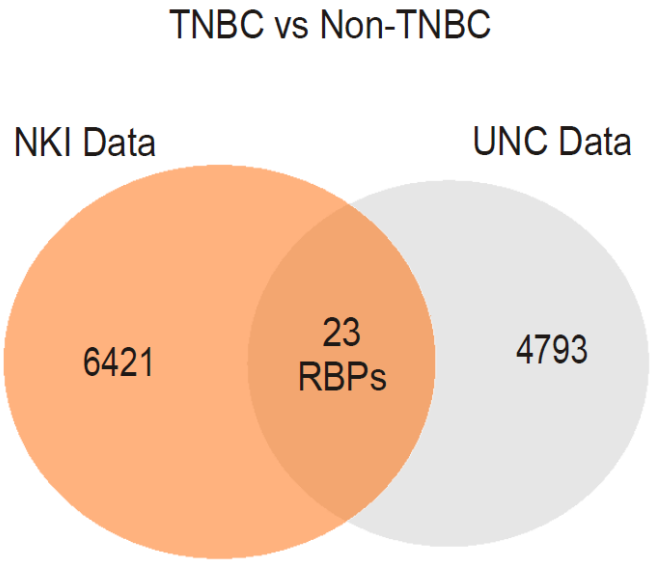
TNBC vs Non-TNBC
NKI Data
UNC Data
6421
23
RBPs
4793

B

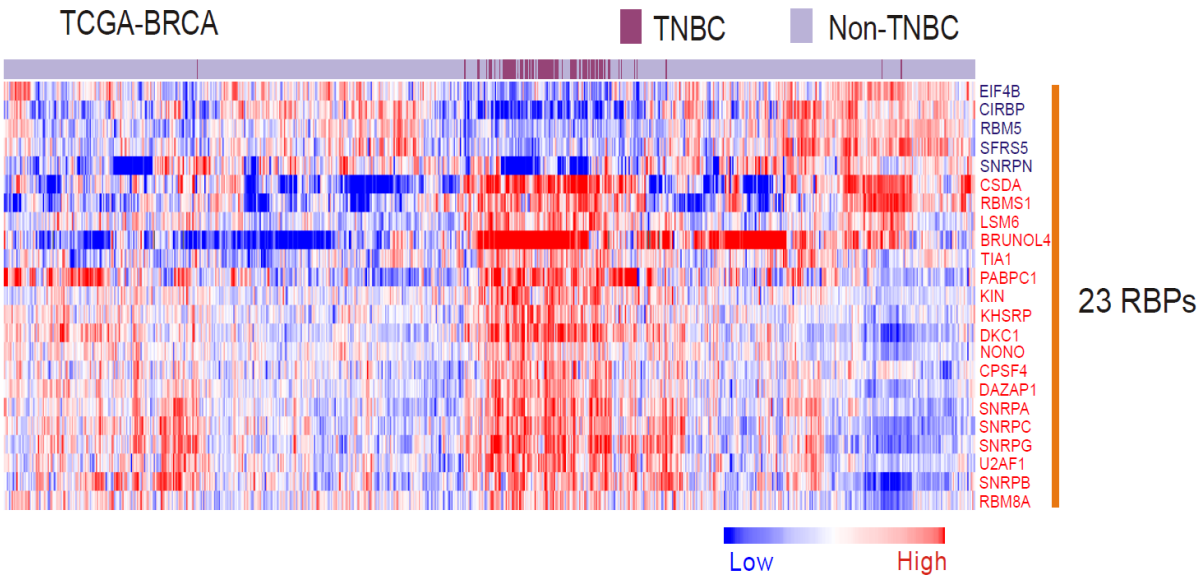
TCGA-BRCA
TNBC
Non-TNBC
EIF4B
CIRBP
RBM5
SFRS5
SNRPN
CSDA
RBMS1
LSM6
BRUNOL4
TIA1
PABPC1
KIN
KHSRP
DKC1
NONO
CPSF4
DAZAP1
SNRPA
SNRPC
SNRPG
U2AF1
SNRPB
RBM8A
23 RBPs
Low
High

Figure 1. NONO as TNBC-specific RBP.

(A) Venn diagram illustrates the genes that exhibit significant differential expression between TNBC and non-TNBC in two separate BC patient cohorts. A univariate test was conducted using class comparison analysis in the BRB array tool, and it was supplemented with a multivariate permutation test involving 10,000 random permutations. A significance threshold of $p < 0.001$ was used to identify genes with significantly different expression levels between the two groups of tissues analyzed in each comparison. (B) The TCGA-BRCA cohort revealed a consistent upregulation or downregulation of 23 RBP genes. The heatmap displays samples, with colored bars indicating the expression levels of the respective RBPs.

A

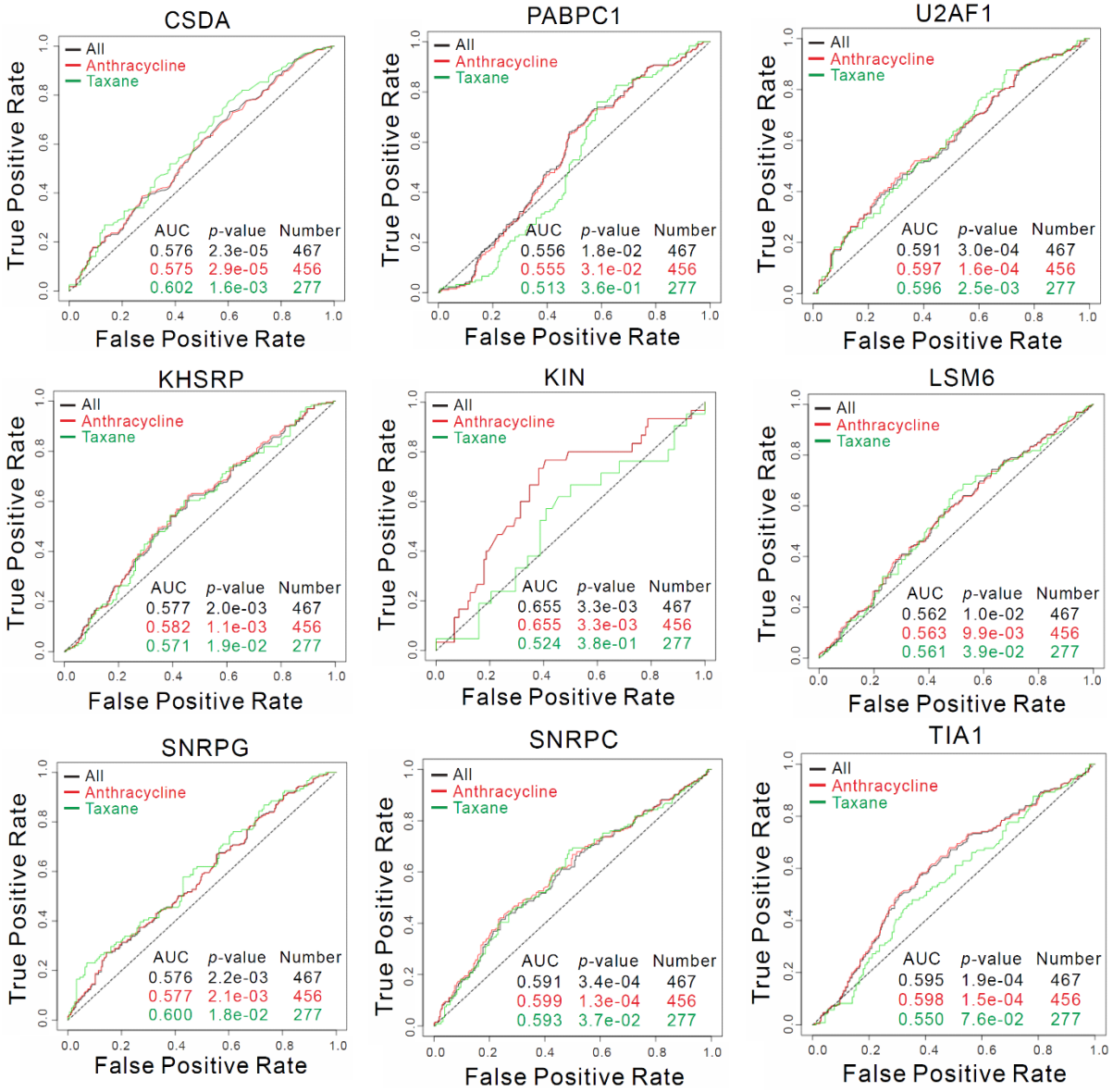
CSDA
All
Anthracycline
Taxane
AUC p-value Number
0.576 2.3e-05 467
0.575 2.9e-05 456
0.602 1.6e-03 277
PABPC1
AUC p-value Number
0.556 1.8e-02 467
0.555 3.1e-02 456
0.513 3.6e-01 277
U2AF1
AUC p-value Number
0.591 3.0e-04 467
0.597 1.6e-04 456
0.596 2.5e-03 277
KHSRP
AUC p-value Number
0.577 2.0e-03 467
0.582 1.1e-03 456
0.571 1.9e-02 277
KIN
AUC p-value Number
0.655 3.3e-03 467
0.655 3.3e-03 456
0.524 3.8e-01 277
LSM6
AUC p-value Number
0.562 1.0e-02 467
0.563 9.9e-03 456
0.561 3.9e-02 277
SNRPG
AUC p-value Number
0.576 2.2e-03 467
0.577 2.1e-03 456
0.600 1.8e-02 277
SNRPC
AUC p-value Number
0.591 3.4e-04 467
0.599 1.3e-04 456
0.593 3.7e-02 277
TIA1
AUC p-value Number
0.595 1.9e-04 467
0.598 1.5e-04 456
0.550 7.6e-02 277
True Positive Rate
False Positive Rate

B

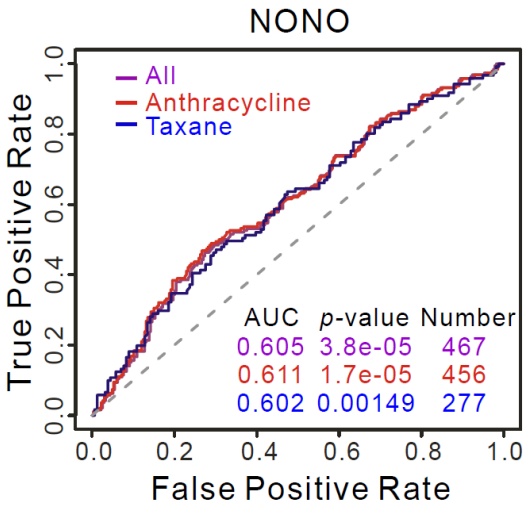
NONO
All
Anthracycline
Taxane
AUC p-value Number
0.605 3.8e-05 467
0.611 1.7e-05 456
0.602 0.00149 277
True Positive Rate
False Positive Rate

Figure 2. NONO is associated with drug response in TNBC.

(A-B) ROC curve analysis was conducted to assess the predictive probability of RBPs expression for chemotherapy responsiveness in the BC cohorts. The correlation between RBPs gene expression levels and chemo-response was evaluated using ROC curve analysis. The area under the curve (AUC) was calculated as a measure of predictive accuracy, and the concordance index was used for estimation. The significance of the results was assessed using a one-sided Wilcoxon's rank test, and corresponding p-values were obtained.

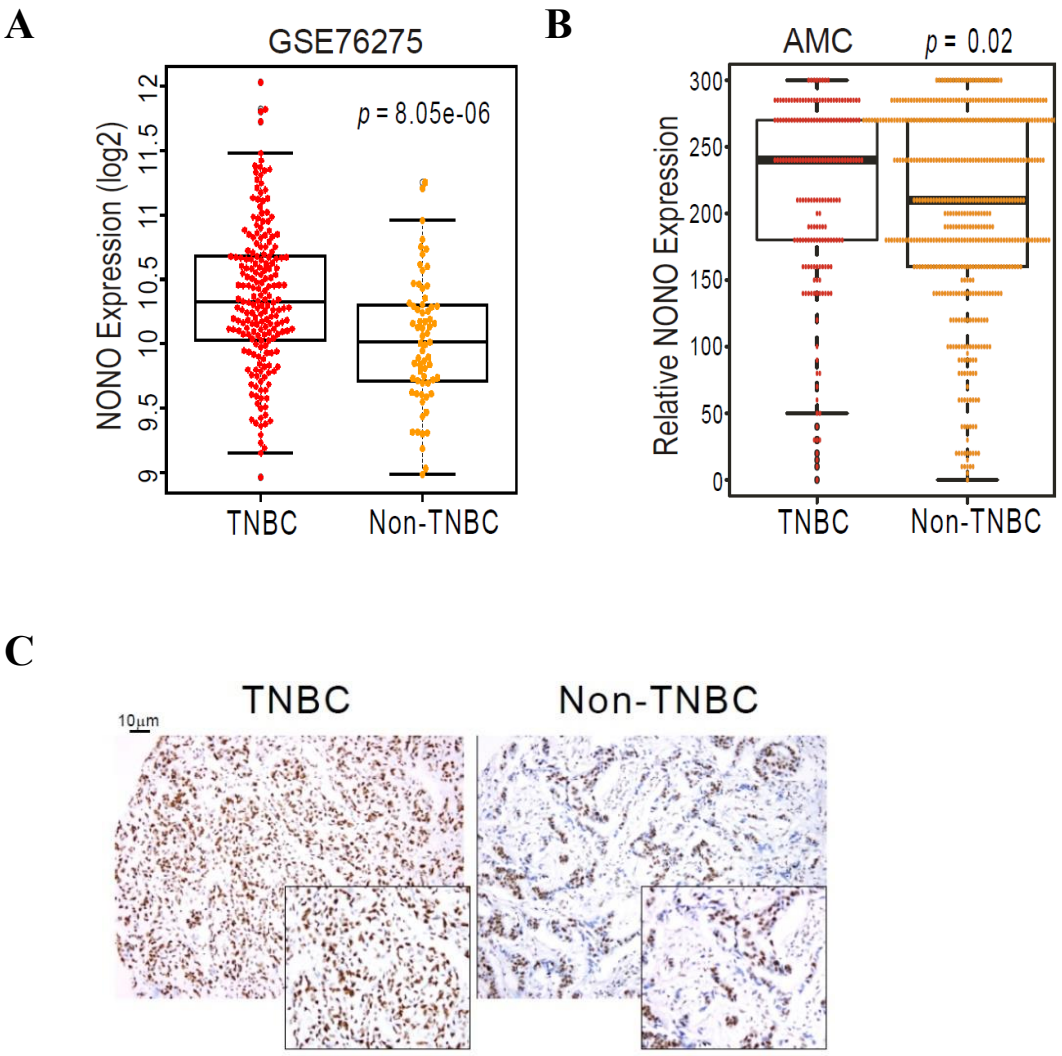

Figure 3. NONO expression in TNBC.

(A) mRNA expression levels of NONO (log2) were TNBC compared to non-TNBC. Error bar displays SD value. Two-tailed Student's t-test was performed to calculate the p-values. (B) Quantitative analysis of the TMA data was conducted to determine the relative expression of NONO in breast tissues. The relative expression was calculated by multiplying the stained intensity. Error bar displays SD value. Two-tailed Student's t-test was performed to calculate the p-values. (C) Immunohistochemical analysis were performed for TNBC and Non-TNBC. Scale bar = 10 μm.

A

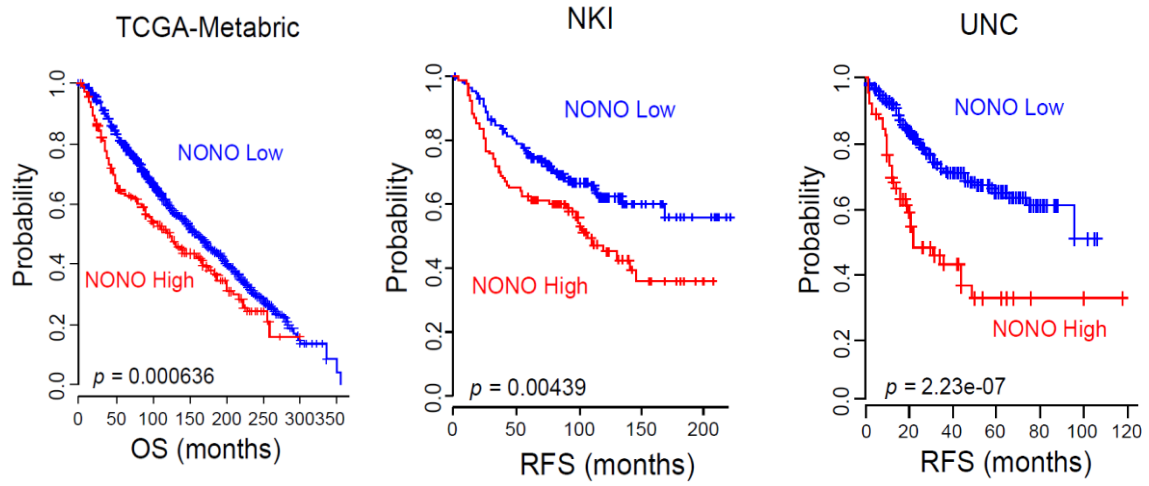
TCGA-Metabric
NONO Low
NONO High
p = 0.000636
Probability
OS (months)
NKI
NONO Low
NONO High
p = 0.00439
Probability
RFS (months)
UNC
NONO Low
NONO High
p = 2.23e-07
Probability
RFS (months)

B

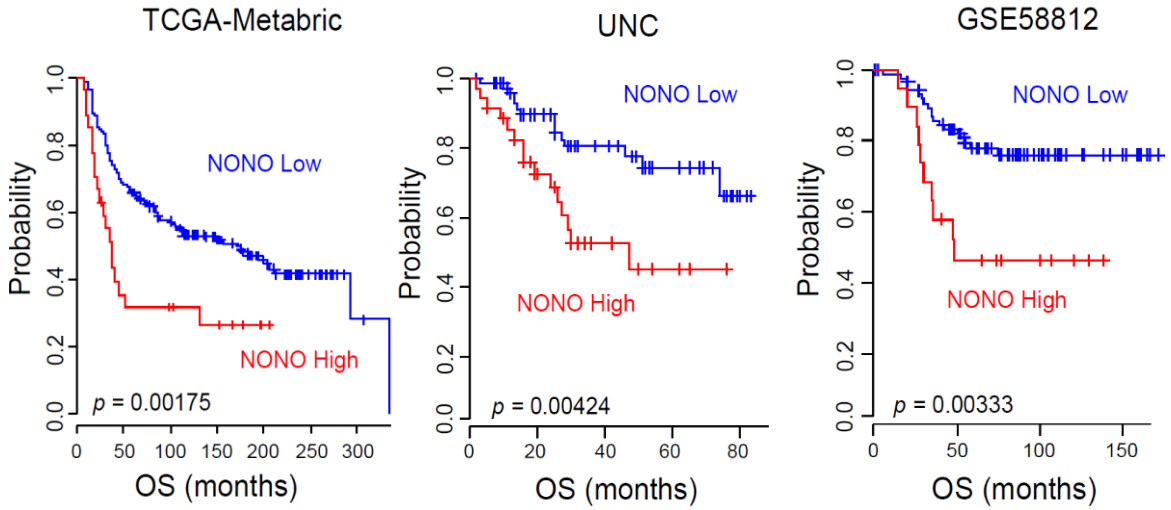
TCGA-Metabric
NONO Low
NONO High
p = 0.00175
Probability
OS (months)
UNC
NONO Low
NONO High
p = 0.00424
Probability
OS (months)
GSE58812
NONO Low
NONO High
p = 0.00333
Probability
OS (months)

C

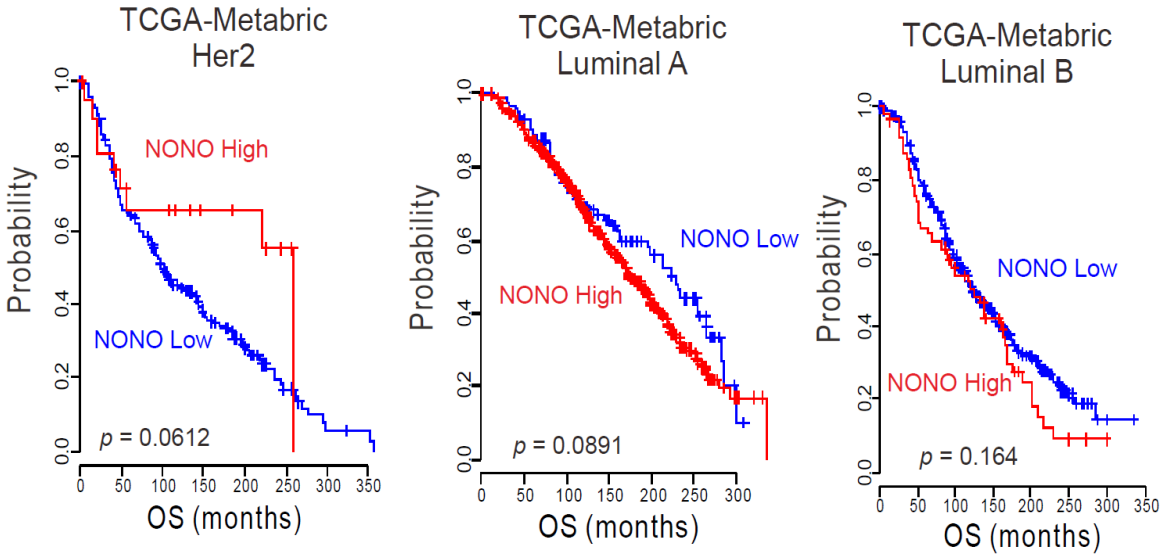
TCGA-Metabric
Her2
NONO High
NONO Low
p = 0.0612
Probability
OS (months)
TCGA-Metabric
Luminal A
NONO Low
NONO High
p = 0.0891
Probability
OS (months)
TCGA-Metabric
Luminal B
NONO Low
NONO High
p = 0.164
Probability
OS (months)

Figure 4. NONO expression is linked to patient survival in TNBC.

(A) Patients in the specified BC cohorts, including TNBC cohorts or TNBC-specific cohorts (B-C), were stratified into two groups based on their relative NONO expression levels: a group with relatively high NONO expression and a group with relatively low NONO expression. These groups were then used for plotting and further analysis. Significant differences between these groups were observed and assessed using the log-rank test. RFS, recurrence-free survival.

NONO influences TNBC cell growth

To explore the potential oncogenic function of NONO, its impact on cancer cell growth was assessed. Hs 578T and MDA-MB-231 cell lines were infected with lentivirus vectors carrying shNONO to achieve stable knockdown of NONO expression (Figure 5A). Silencing NONO in all tested cell lines notably suppressed cancer cell growth and colony formation, as observed in Figures 5B–C. Cells for which NONO was silenced exhibited a significant alteration in cell cycle distribution, characterized by an increase in the sub-G1 fraction and a reduction in the number of cells in the S-phase (Figure 6A); NONO-silenced cells exhibited an increase in caspase3/7 activity compared to parental cells (Figure 6B), suggesting that NONO is involved in modulating apoptotic activity and affects the growth of cancer cells. Oncogenic potential is not limited to effects on cell cycle distribution and apoptosis but also on cancer features such as cancer cell migration and invasion. We conducted multiple migration assays, including a conventional migration assay that measures cell passage through a non-matrigel-coated chamber. The results demonstrated significant inhibition of cell migration upon the silencing of NONO. Additionally, both the migration assay and wound healing scratched assay yielded consistent findings, supporting the inhibitory effect of NONO on cell migration (Figures 7A–B). Furthermore, a cell invasion assay was conducted on a matrigel-coated surface, and the results revealed a significant decrease in the invasion of TNBC cells upon the knockdown of NONO (Figure 8A). Subsequently, the influence of NONO on tumor growth was investigated in a mouse model. In vivo knockdown of NONO was achieved using siRNA nanoparticles (CH-NP; chitosan nanoparticles), leading to a significant inhibition of tumor growth (Figure 9A) and suppression of cell proliferation marker Ki-67 expression (Figure 9B). Summarily, the comprehensive findings from this study strongly validate the oncogenic function of NONO in TNBC. The results demonstrate its significant impact on cell growth, migration, and invasion, highlighting its crucial involvement in cancer progression and survival within the context of TNBC. Therefore, the targeting of NONO, an important RBP, is a promising therapeutic approach toward effectively suppressing cancer cell growth in this aggressive subtype of BC.

A

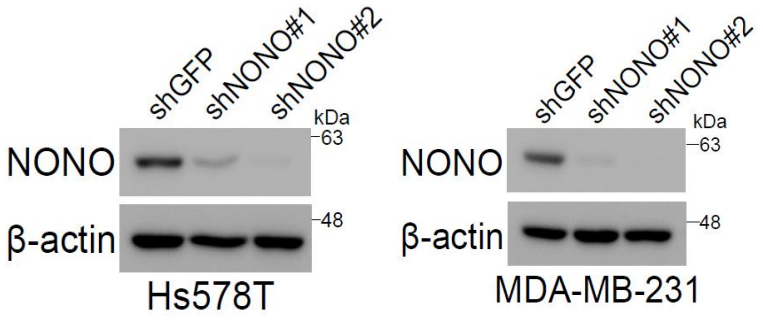
shGFP
shNONO#1
shNONO#2
kDa
NONO
63
β-actin
48
Hs578T
MDA-MB-231

B

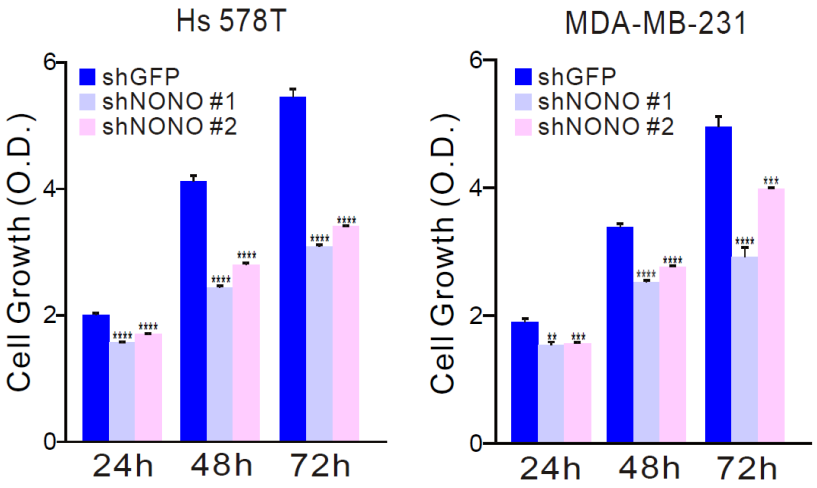
Hs 578T
MDA-MB-231
shGFP
shNONO #1
shNONO #2
Cell Growth (O.D.)
24h
48h
72h

C

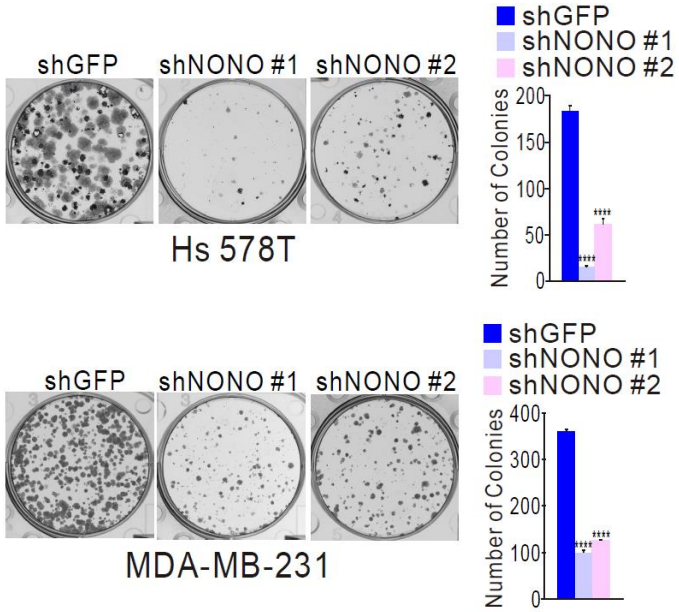
shGFP
shNONO #1
shNONO #2
Hs 578T
MDA-MB-231
Number of Colonies

Figure 5. NONO regulates cell growth in TNBC cells.

(A) The specified Hs 578T and MDA-MB-231 cells were transfected with shNONO or control shRNA (shGFP), and subsequent analysis was performed using WB with a NONO AB. (B) The cells that were infected were subjected to a proliferation assay using the CCK8 assay. Data presented are the mean ± SD of three independent experiments. Statistical analysis was performed using one-way ANOVA with Tukey's post hoc analysis, (**$p < 0.01$, ***$p < 0.005$, and ****$p < 0.001$ *vs* shGFP). (C) The colony formation assay was used to quantify the clonogenic survival of the infected cells. Data presented are the mean ± SD of three independent experiments. Statistical analysis was performed using one-way ANOVA with Tukey's post hoc analysis, (****$p < 0.001$ *vs* shGFP).

A

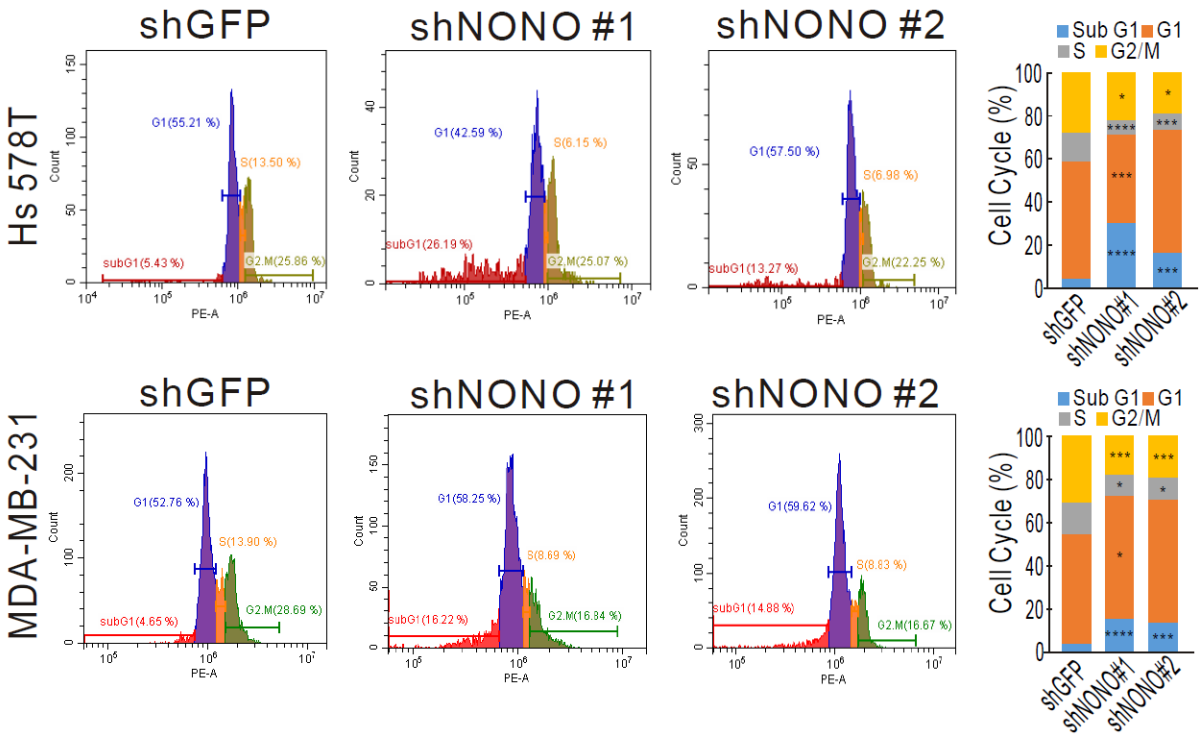
shGFP
shNONO #1
shNONO #2
Hs 578T
MDA-MB-231
Count
PE-A
G1(55.21 %)
S(13.50 %)
G2.M(25.86 %)
subG1(5.43 %)
G1(42.59 %)
S(6.15 %)
G2.M(25.07 %)
subG1(26.19 %)
G1(57.50 %)
S(6.98 %)
G2.M(22.25 %)
subG1(13.27 %)
G1(52.76 %)
S(13.90 %)
G2.M(28.69 %)
subG1(4.65 %)
G1(58.25 %)
S(8.69 %)
G2.M(16.84 %)
subG1(16.22 %)
G1(59.62 %)
S(8.83 %)
G2.M(16.67 %)
subG1(14.88 %)
Sub G1
G1
S
G2/M
Cell Cycle (%)
shGFP
shNONO#1
shNONO#2

B

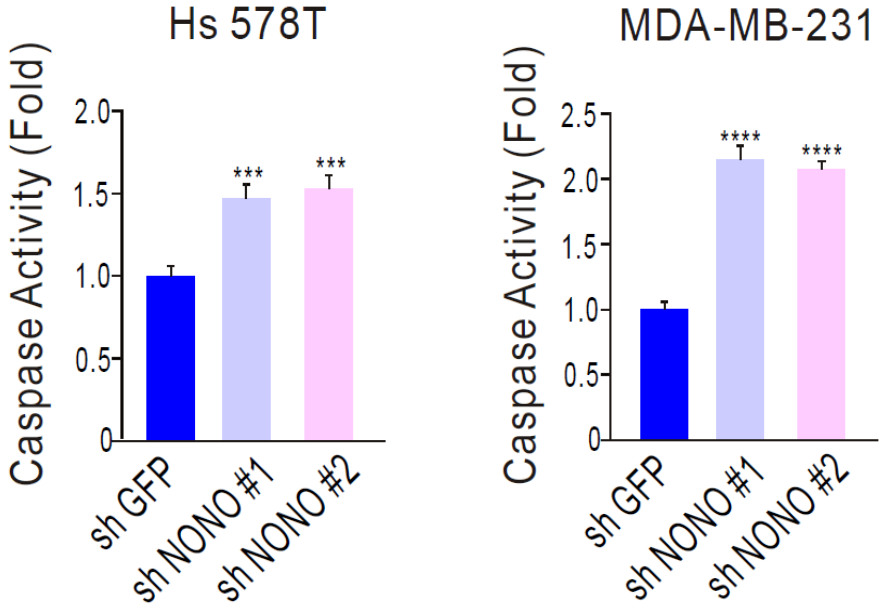
Hs 578T
MDA-MB-231
Caspase Activity (Fold)
sh GFP
sh NONO #1
sh NONO #2

Figure 6. NONO modulates cell cycle and caspase3/7 activity in TNBC cells.

(A) The lentivirus-infected Hs578T and MDA-MB-231 cells were subjected to fluorescence-activated cell sorting (FACS) analysis to examine the cell cycle distribution. (B) Caspase 3/7 activity was measured in Hs578T and MDA-MB-231 cells after infection with either shNONO or shGFP. All data presented are the mean ± SD of three independent experiments. Statistical analysis was performed using one-way ANOVA with Tukey's post hoc analysis, (*$p < 0.05$, ***$p < 0.005$, and ****$p < 0.001$ *vs* shGFP).

A

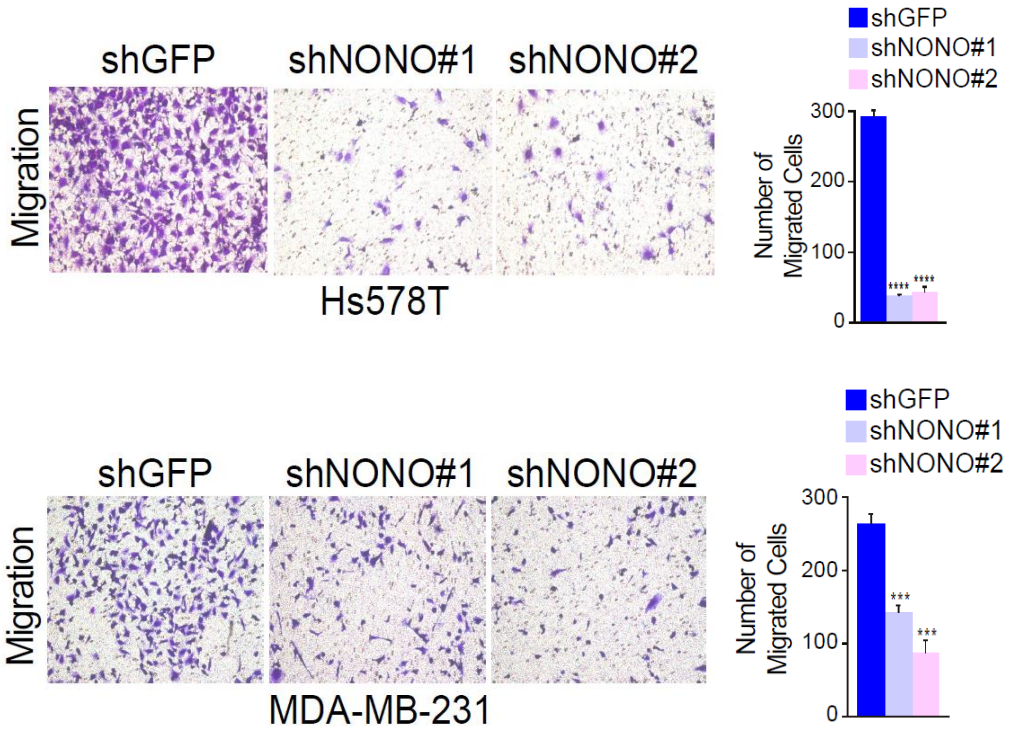
shGFP
shNONO#1
shNONO#2
Migration
Hs578T
Number of Migrated Cells
300
200
100
0
****
****
shGFP
shNONO#1
shNONO#2
shGFP
shNONO#1
shNONO#2
Migration
MDA-MB-231
Number of Migrated Cells
300
200
100
0
***
***
shGFP
shNONO#1
shNONO#2

B

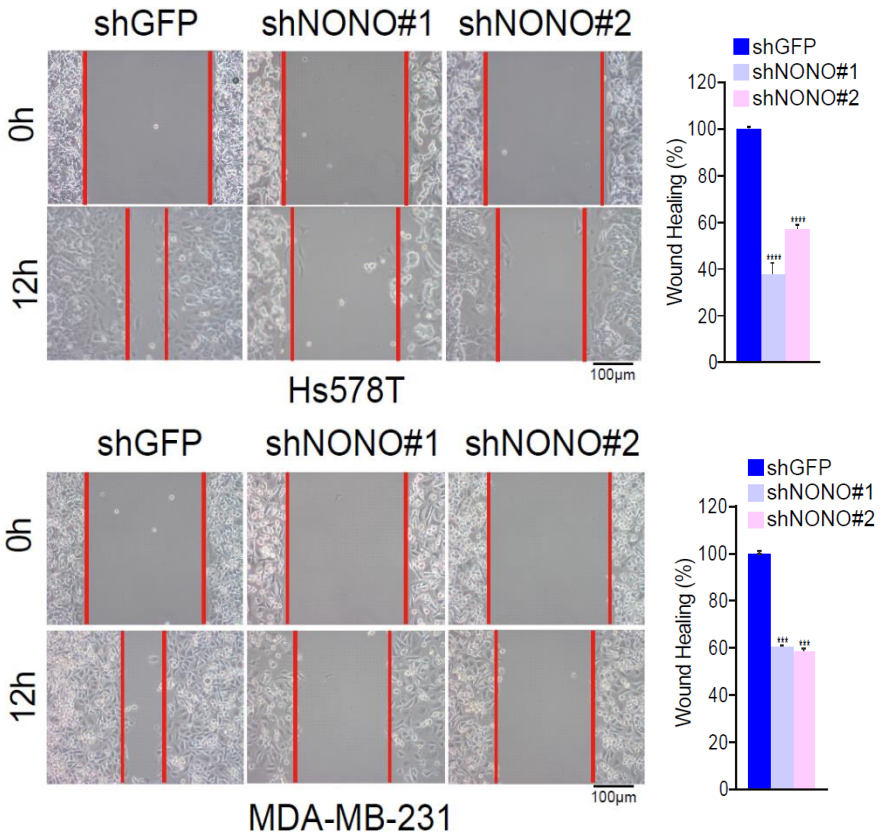
shGFP
shNONO#1
shNONO#2
0h
12h
100μm
Hs578T
Wound Healing (%)
120
100
80
60
40
20
0
shGFP
shNONO#1
shNONO#2
shGFP
shNONO#1
shNONO#2
0h
12h
100μm
MDA-MB-231
Wound Healing (%)
120
100
80
60
40
20
0
shGFP
shNONO#1
shNONO#2

Figure 7. Depletions of NONO and its effect on migration.

(A) Cell migration assays were performed using Boyden chambers on the infected cells. The assays were conducted for 24 hours without extracellular matrix, and the migratory capacity of the cells was assessed by counting the number of stained cells. Data presented are the mean ± SD of three independent experiments. Statistical analysis was performed using one-way ANOVA with Tukey's post hoc analysis, (***$p < 0.005$, and ****$p < 0.001$ *vs* shGFP). (B) The migration of infected cells was assessed using a wound healing assay, which involved measuring the areas devoid of cells at 0 and 12 hours to quantify the extent of migration. Data presented are the mean ± SD of three independent experiments. Statistical analysis was performed using one-way ANOVA with Tukey's post hoc analysis, (***$p < 0.005$, and ****$p < 0.001$ *vs* shGFP). Scale bar = 100 µm.

A

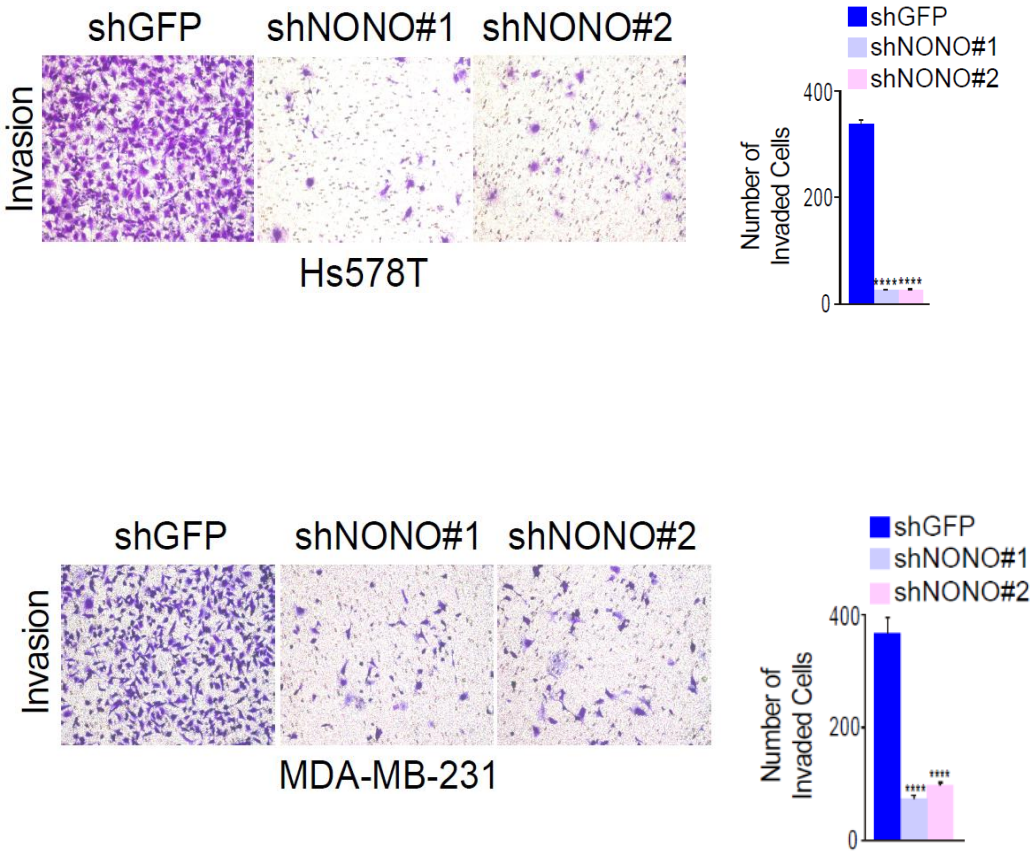

Figure 8. Depletions of NONO and its effect on invasion.

Cell invasion was evaluated using Boyden chambers, where the chambers were coated with matrigel to simulate the extracellular matrix. The cells in the invasion assay were incubation at a temperature of 37°C for a duration of 24 hours. Subsequently, the cells were stained with crystal violet and quantified to determine the extent of invasion. Data presented are the mean ± SD of three independent experiments. Statistical analysis was performed using one-way ANOVA with Tukey's post hoc analysis, (****$p <$ 0.001 *vs* shGFP).

A

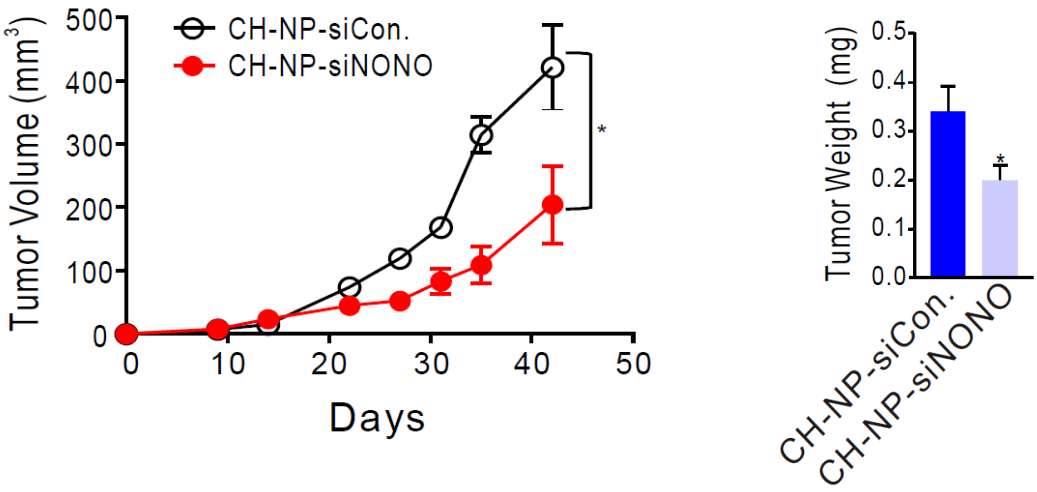

B

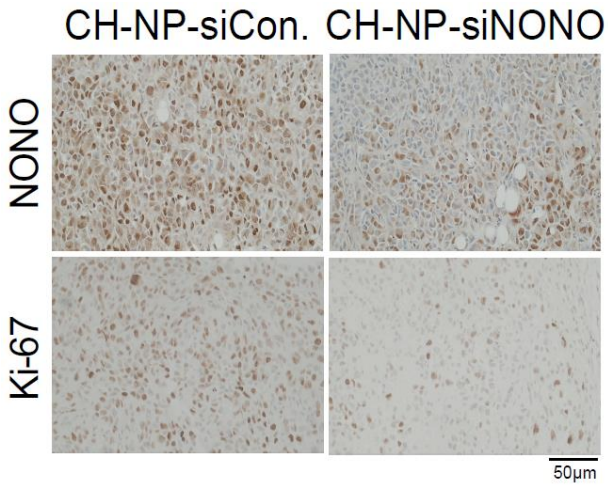

Figure 9. Depletions of NONO and its effect on BC tumorigenesis.

(A) BALB/c nude mice were injected with MDA-MB-231 cells, and subsequently, the mice were administered the specified siRNA. The tumor volumes and weights were measured, with a total of 5 mice included in the study. Error bar displays SD value. Two-tailed Student's t-test was performed to calculate the p-values, (*$p < 0.05$). (B) Representative IHC analysis of mouse samples were performed. Scale bar = 50 μm.

NONO regulates STAT3 expression in TNBC

To elucidate the role of NONO in cancer cell growth and gain insights into the underlying mechanisms, gene expression profiles were generated in Hs 578T and BT-20 cells following the silencing of NONO. An analysis of gene expression profiles revealed a set of 138 mRNA transcripts that exhibited consistent differential expression upon the silencing of NONO in both TNBC cell lines (Figure 10A). This profile exhibits oncogenic factors such as polo-like kinase 4 *(PLK4)*, SRY-box transcription factor 4 *(SOX4)*, *STAT3*, and TIMP metallopeptidase inhibitor 1 *(TIMP1)*. Moreover, multiple genes are differentially regulated by NONO (Figure 10B). To validate these findings, the observed changes in gene expression identified through profiling analysis were validated by performing qPCR (Figure 10C). Pathway analysis was conducted using ingenuity pathway analysis (IPA) with the set of 138 genes that were identified as being regulated by NONO. The results from IPA indicate that the 138 genes regulated by NONO are functionally associated with various biological processes relevant to cancer progression, including cell growth and proliferation, cell cycle regulation, and cell movement and migration. These findings are consistent with those illustrated in Figures 1-5, 1-6, 1-7, 1-8, and 1-9 (Figure 10C). Out of those oncogenic factors, given the well-established role of STAT3 as an oncogenic transcription factor (TF) in TNBC, we prioritized investigating its potential relationship with NONO as a downstream target [109, 110]. The inhibition of STAT3 signaling has been identified as a promising therapeutic strategy in cancer, including TNBC. It is currently under extensive investigation as a potential target for cancer therapy [111, 112]. Subsequently, we investigated the role of NONO in modulating the activity of the STAT3 signaling pathway. WB and qPCR were conducted to confirm the gene expression profiling results. The analysis confirmed that the expression of STAT3 and its downstream targets, including *CCNB1* and *CCND1*, was significantly reduced in Hs 578T and MDA-MB-231 cells after infection with shNONO (Figures 11A–B). Furthermore, *in vivo* experiments demonstrated that the knockdown of NONO resulted in a reduction in STAT3 expression (Figures 11C–D).

We aimed to determine whether the oncogenic properties of NONO were dependent on STAT3 activation. While cell growth, invasion, and migration were suppressed upon NONO silencing, reintroduction of the STAT3 gene enhanced cell growth in TNBC cells with NONO silencing (Figures 12A–E). This suggests that the growth-promoting effects mediated by NONO are dependent on STAT3 expression. Collectively, the study results indicate that NONO has a positive regulatory role on STAT3 signaling, and this activation of STAT3 contributes to the cancer-promoting properties of NONO.

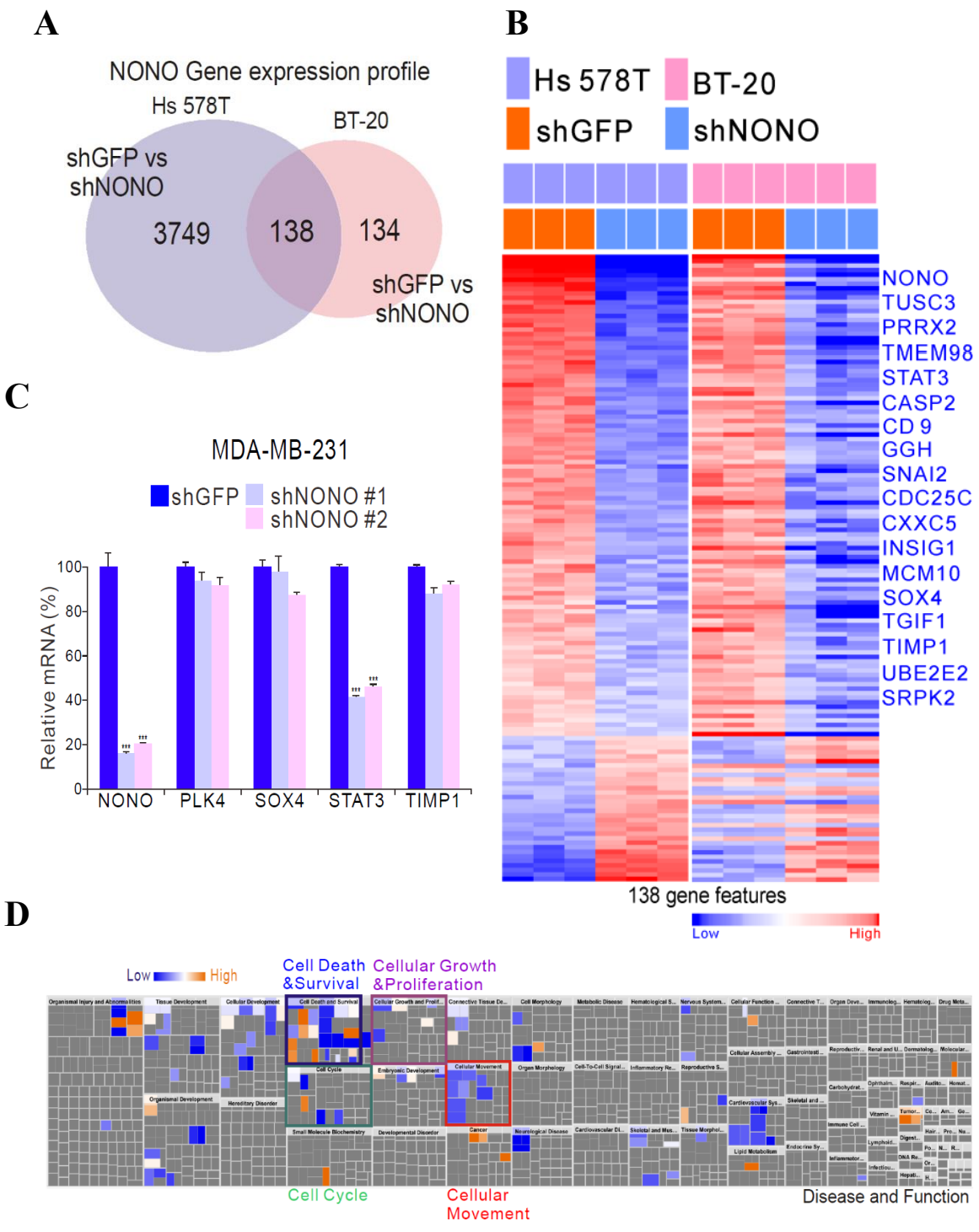
A
NONO Gene expression profile
Hs 578T
BT-20
shGFP vs shNONO
3749
138
134
shGFP vs shNONO
B
Hs 578T
BT-20
shGFP
shNONO
NONO
TUSC3
PRRX2
TMEM98
STAT3
CASP2
CD 9
GGH
SNAI2
CDC25C
CXXC5
INSIG1
MCM10
SOX4
TGIF1
TIMP1
UBE2E2
SRPK2
138 gene features
Low
High
C
MDA-MB-231
shGFP
shNONO #1
shNONO #2
Relative mRNA (%)
100
80
60
40
20
0
NONO
PLK4
SOX4
STAT3
TIMP1
D
Low
High
Cell Death &Survival
Cellular Growth &Proliferation
Cell Cycle
Cellular Movement
Disease and Function

Figure 10. NONO regulates the cellular growth and movement associated genes in TNBC.

(A) Gene expression profiles associated with the knockdown of NONO expression using shNONO in TNBC cell lines revealed distinct gene expression signatures. Genes within the Venn diagram were chosen through class comparison analysis using the BRB array tool, applying a significance threshold of $p < 0.001$. (B) Gene expression profiling is displayed in a matrix format, where the colors represent the relative expression levels of the genes. Red color represents relatively high expression, whereas blue color represents relatively low expression. The scale bar provided indicates the log2-transformed scale used for expression values. (C) expression levels of oncogenic factor genes were analyzed using qPCR in MDA-MB-231 cells following NONO silencing. Data presented are the mean ± SD of three independent experiments. Statistical analysis was performed using one-way ANOVA with Tukey's post hoc analysis, (***$p < 0.005$ *vs* shGFP). (D) IPA was performed to analyze the differentially expressed genes following NONO inhibition.

A

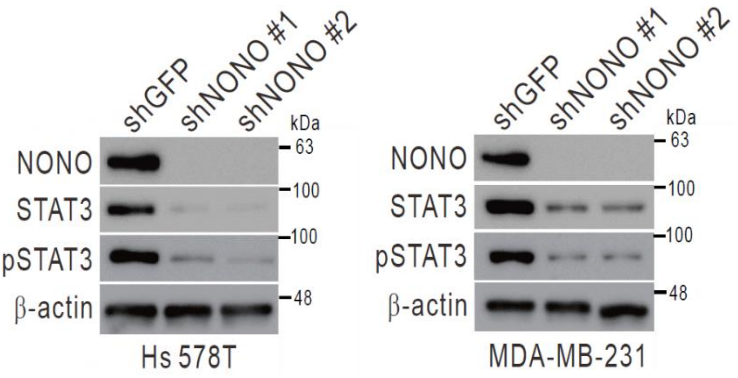
shGFP
shNONO #1
shNONO #2
kDa
NONO
STAT3
pSTAT3
β-actin
63
100
100
48
Hs 578T
MDA-MB-231

B

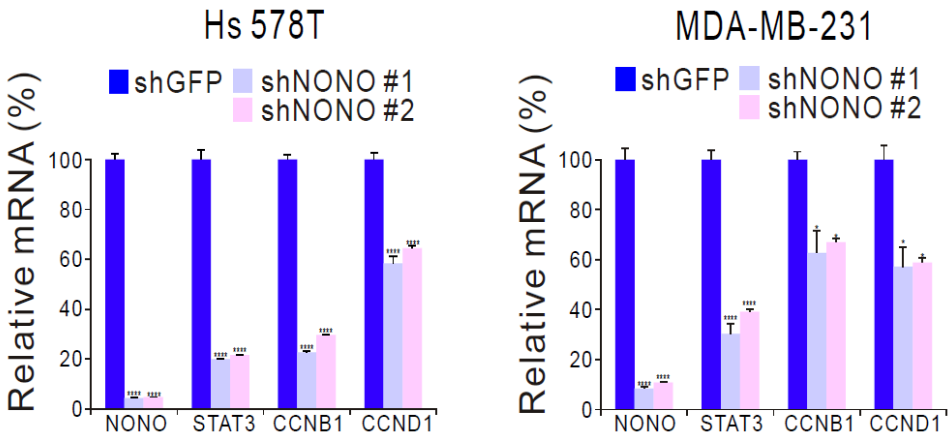
Hs 578T
MDA-MB-231
shGFP
shNONO #1
shNONO #2
Relative mRNA (%)
NONO
STAT3
CCNB1
CCND1

C

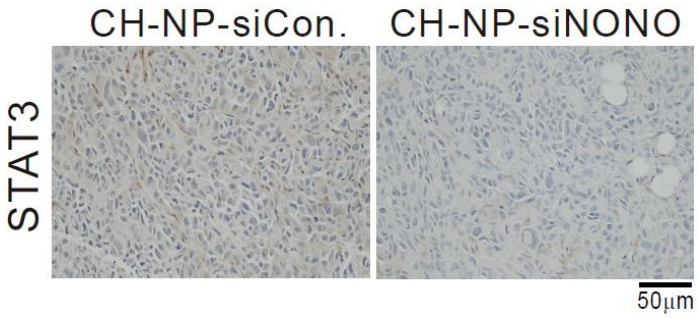
CH-NP-siCon.
CH-NP-siNONO
STAT3
50μm

D

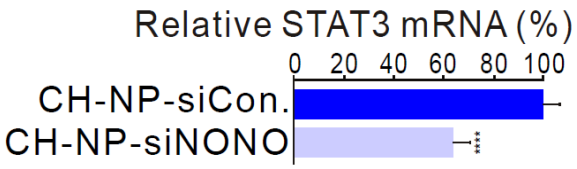
Relative STAT3 mRNA (%)
0 20 40 60 80 100
CH-NP-siCon.
CH-NP-siNONO

Figure 11. NONO regulates STAT3 expression in TNBC.

(A) WB analysis was conducted to examine the expression of STAT3-associated genes in Hs 578T and MDA-MB-231 cells following NONO silencing. (B) TNBC cells were infected with the specified lentivirus, and the expression of NONO was analyzed using qPCR. Data presented are the mean ± SD of three independent experiments. Statistical analysis was performed using one-way ANOVA with Tukey's post hoc analysis, (*$p < 0.05$, and ****$p < 0.001$ *vs* shGFP). (C-D) Representative IHC image Scale bar = 50 μm. (C) and qPCR (D) Analysis was performed after knockdown NONO in a xenograft model. Data presented are the mean ± SD of three independent experiments. Two-tailed Student's t-test was performed to calculate the p-values, (****$p < 0.001$ *vs* siCon).

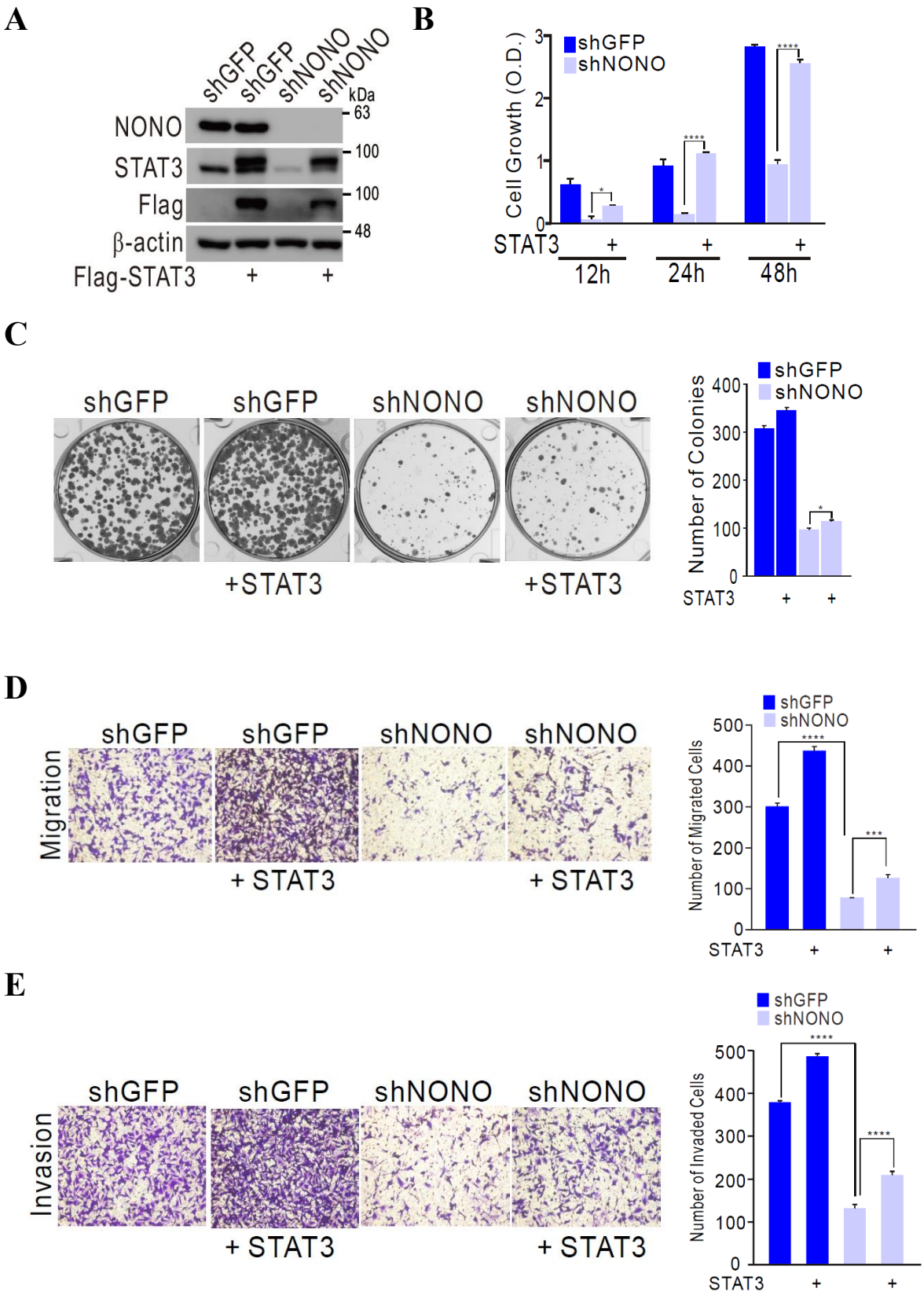
A
shGFP
shGFP
shNONO
shNONO
kDa
NONO
STAT3
Flag
β-actin
63
100
100
48
Flag-STAT3 + +
B
shGFP
shNONO
Cell Growth (O.D.)
STAT3 + + +
12h
24h
48h
C
shGFP
shGFP
shNONO
shNONO
+STAT3
+STAT3
shGFP
shNONO
Number of Colonies
STAT3 + +
D
shGFP
shGFP
shNONO
shNONO
Migration
+ STAT3
+ STAT3
shGFP
shNONO
Number of Migrated Cells
STAT3 + +
E
shGFP
shGFP
shNONO
shNONO
Invasion
+ STAT3
+ STAT3
shGFP
shNONO
Number of Invaded Cells
STAT3 + +

Figure 12. NONO regulates STAT3 gene expression and thereby governs TNBC cell growth.

(A-E) Rescue experiments, MDA-MB-231 cells were initially infected with either shGFP or shNONO, and subsequently, the transfection of the Flag-STAT3 plasmid into these cells. (A) Following the transfection and infection, the cells were subjected to various analyses. WB analysis was conducted to assess the levels of protein expression. (B) Cell viability and growth were assessed using the CCK8 assay (C) Clonogenic survival was measured using the colony formation assay (D) Cell migration was evaluated using Boyden chamber assays (E) and cell invasion was assessed using Boyden chambers coated with matrigel as an extracellular matrix. (B-E) Data presented are the mean ± SD of three independent experiments. Statistical analysis was performed using one-way ANOVA with Tukey's post hoc analysis, ($^{*}p < 0.05$, $^{***}p < 0.005$, and $^{****}p < 0.001$).

Mechanism of STAT3 regulation by NONO in TNBC

To further comprehend the mechanism through which NONO modulates STAT3 gene expression and sustains its oncogenic functions in TNBC, we investigated the interaction between NONO and the STAT3 RNA. Usually, RBPs directly bind to the 3' UTR region of their target gene RNA. Previous research has indicated that NONO can bind to specific response elements within the 3' UTR region [113]. Based on a defined sequence, we examined the binding sites of NONO within the *STAT3* locus and ranked the NONO binding sites on the locus (Figure 13A). We identified five putative NONO binding sites on STAT3 locus (Figure 13B). Furthermore, we performed RNA-IP experiments to validate the interaction between NONO and STAT3 RNA, and demonstrated the interaction between NONO and STAT3 RNA in MDA-MB-231 cells (Figure 13C). To investigate the functional significance of the NONO-STAT3 RNA interaction, we created reporter constructs that included the NONO-binding sites identified within the STAT3 locus. Both wild-type and mutant reporter constructs were generated and subsequently co-transfected with NONO cDNA into the cells for further investigation. NONO significantly enhanced the activity of the wild-type reporter construct. Among the tested mutations in the NONO-binding sites, the mutant M4 site (CAGCACUG) showed the lowest reporter activity, indicating that this specific binding site plays a crucial role in the interaction between NONO and STAT3 RNA (Figure 14A).

STAT3 functions as a TF and engages in interactions with various proteins to maintain its biological functions in cancer cells [114]. Furthermore, to determine its role in RNA-level regulation of STAT3 gene expression, we investigated whether NONO influences STAT3 function through direct protein-protein interactions. Interestingly, through co-immunoprecipitate experiments, we observed a physical interaction between endogenous and exogenous STAT3 and NONO proteins (Figure 15A), suggesting a direct association between the two proteins. To further assess this interaction, we employed fluorescence cross-correlation spectroscopy (FCCS) analysis in live cells where GFP-STAT3 and red fluorescent protein (RFP)-NONO were co-expressed. The relative cross-correlation amplitude in this experiment indicates the strength of interaction. Significantly higher cross-correlation amplitudes were observed between GFP-STAT3 and RFP-NONO, indicating a stronger interaction than the cross-correlation amplitudes observed between GFP and RFP-NONO monomers (Figure 16A). To assess the structural characteristics of the NONO/STAT3 complex, we conducted a protein-protein docking simulation utilizing ClusPro, a widely-used docking algorithm [96]. The docking model generated exhibited favorable binding characteristics, as indicated by the ClusPro scores for the center and the

lowest energy regions were -908.5 and -1006.3, respectively (Figure 16B). This suggests that NONO and STAT3 can potentially form a stable and specific docking conformation, supporting their interaction at the protein level.

Immunofluorescence staining demonstrated the co-localization of NONO and STAT3 in the nucleus (Figure 16C), indicating their functional interaction. Furthermore, the binding of NONO protein to the promoter region of the CCND1 gene, a recognized target of STAT3, was observed (Figure 17A). Ectopically and endogenously expressed NONO directly interacts with STAT3 and the reporter assay with a STAT3 promoter revealed that NONO activates STAT3 transcriptional activity (Figure 17B). In addition, suppressed promoter activity by NONO silencing was rescued by the reintroduction of STAT3, indicating that the transcriptional activity of STAT3 is regulated by NONO (Figure 17C). Because NONO modulates STAT3 transcriptional activity by direct interaction, we hypothesized that NONO might also influence the stability of STAT3, given that RBPs impact the stability of RNA and proteins to uphold cellular functions [115]. Following treatment of the protein synthesis inhibitor, cycloheximide (CHX), the protein levels of STAT3 were assessed in NONO-silenced cells. Interestingly, as depicted in Figure 18A, STAT3 exhibited accelerated degradation in cells with suppressed NONO expression upon CHX treatment. Actinomycin D (Act D) yielded similar results (Figures 18B–C), demonstrating that NONO modulates STAT3 stability. Therefore, the data obtained suggest that NONO contributes to STAT3 regulation through direct interaction and influences STAT3 stability, thereby contributing to its oncogenic function as a transcriptional regulator.

A

NONO -binding Rank	Motif	*STAT3* Locus
1		Chr17: 42,313,859 ~ 42,313,866 (M1-1) Chr17: 42,323,456 ~ 42,323,463 (M1-2)
2		Chr17: 42,367,511 ~ 42,367,518 (M2)
3		Chr17: 42,344,645 ~ 42,344,652 (M3)
4		Chr17: 42,345,015 ~ 42,345,022 (M4)

B

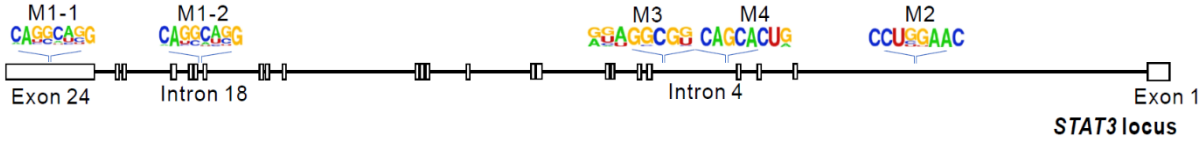

C

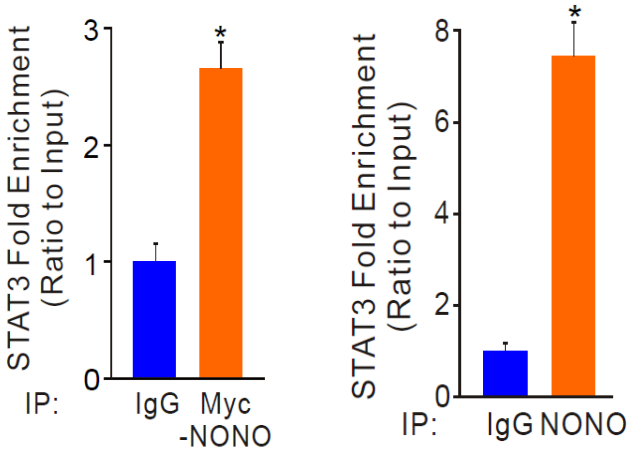

Figure 13. NONO binding sites in the STAT3 RNA.

(A) Based on RNA immunoprecipitation-sequencing, the identified NONO-binding sequences on the STAT3 locus exhibit an abundance of enriched RNA motifs. (B) The sequence of the STAT3 locus was aligned. (C) RNA-IP was carried out using either anti-Myc antibodies or endogenous NONO AB in MDA-MB-231 cells overexpressing Myc-NONO or in regular MDA-MB-231 cells. Following RNA-IP, the cells were subjected to qPCR using the specified probes for analysis. Data presented are the mean ± SD of three independent experiments. Two-tailed Student's t-test was performed to calculate the p-values, (*$p < 0.05$ *vs* IgG).

A

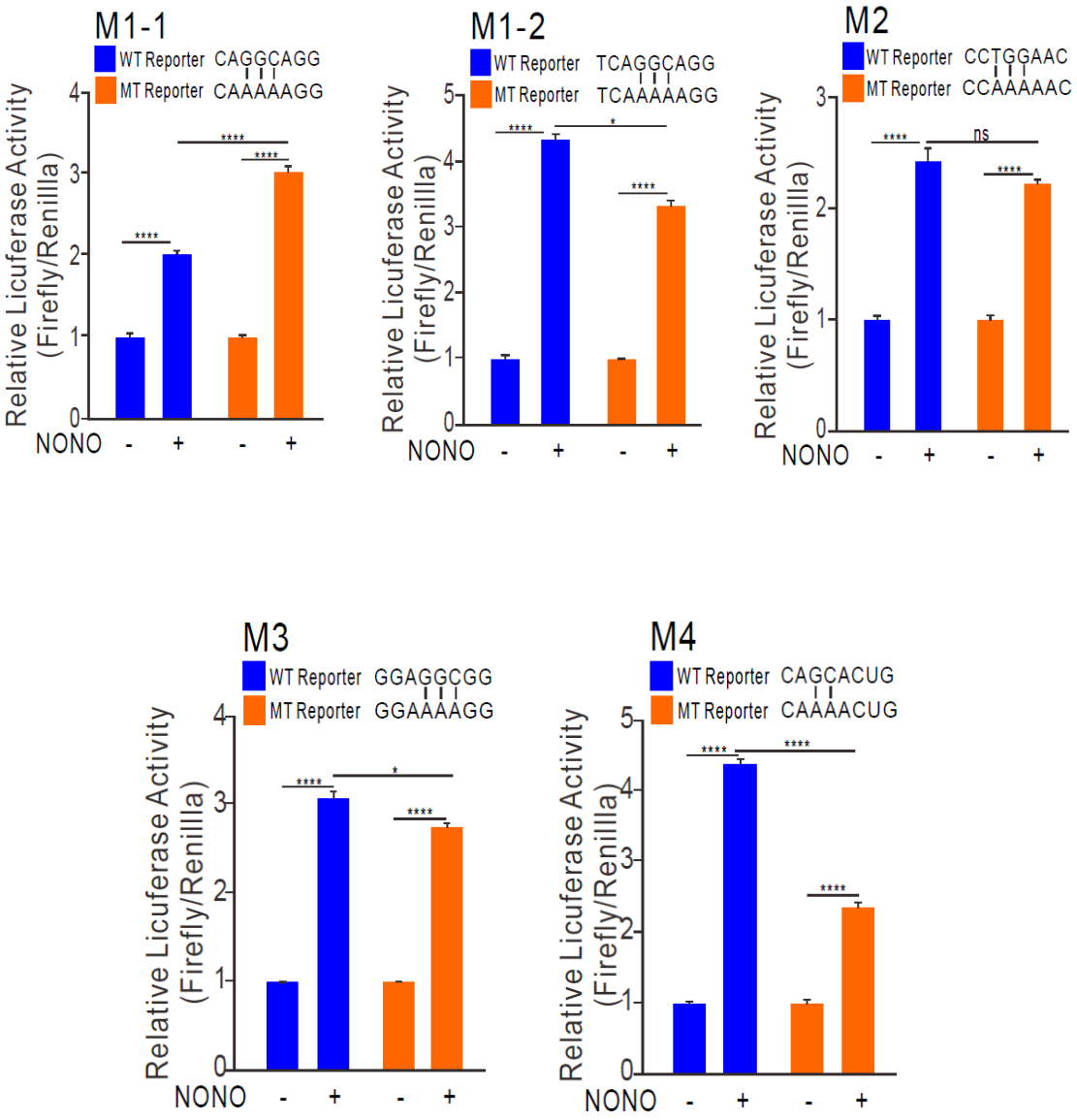
M1-1
WT Reporter CAGGCAGG
MT Reporter CAAAAAGG
M1-2
WT Reporter TCAGGCAGG
MT Reporter TCAAAAAGG
M2
WT Reporter CCTGGAAC
MT Reporter CCAAAAAC
ns
M3
WT Reporter GGAGGCGG
MT Reporter GGAAAAGG
M4
WT Reporter CAGCACUG
MT Reporter CAAAACUG
Relative Licuferase Activity (Firefly/Renillla)
NONO - + - +

Figure 14. NONO binding sites affect STAT3 luciferase activity.

(A) A dual-luciferase assay was performed in HEK293T cells using a luciferase reporter vector containing either the wild-type or mutant-type sequence of the STAT3 locus. The luciferase activities were assessed following the transfection of the specified constructs. Data presented are the mean ± SD of three independent experiments. Statistical analysis was performed using one-way ANOVA with Tukey's post hoc analysis, (*$p < 0.05$, and ****$p < 0.001$).

A

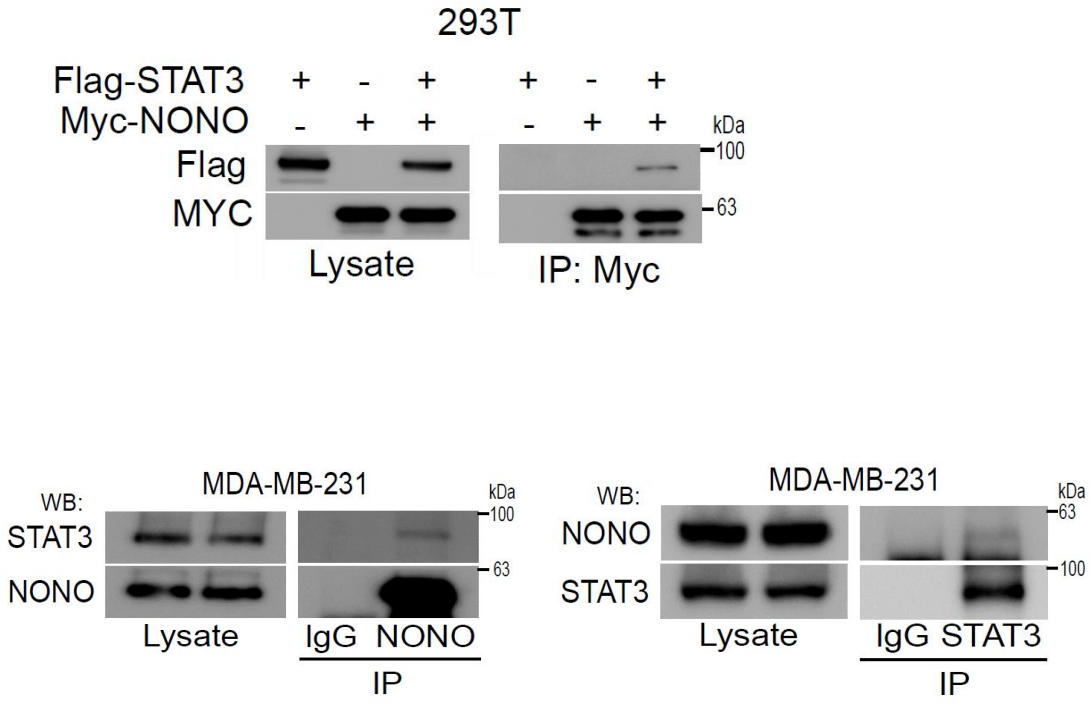

Figure 15. NONO physically interacts with STAT3.

(A) Flag-STAT3 or Myc-NONO constructs were individually or co-transfected into HEK293T cells. Subsequently, the cells were lysed, and co-immunoprecipitation was conducted using Myc antibodies. WB was then performed using Myc and Flag AB (upper panel). Cell lysates from MDA-MB-231 cells were subjected to immunoprecipitation using IgG AB, NONO AB (lower panel), and STAT3 AB (right panel). WB was then conducted using AB against STAT3 and NONO.

A

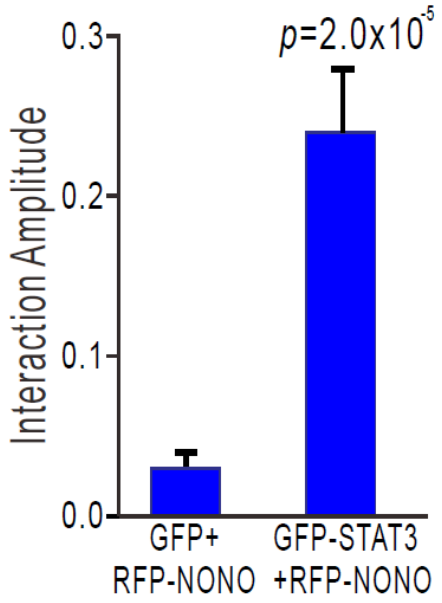
p=2.0x10-5
Interaction Amplitude
0.3
0.2
0.1
0.0
GFP+
RFP-NONO
GFP-STAT3
+RFP-NONO

B

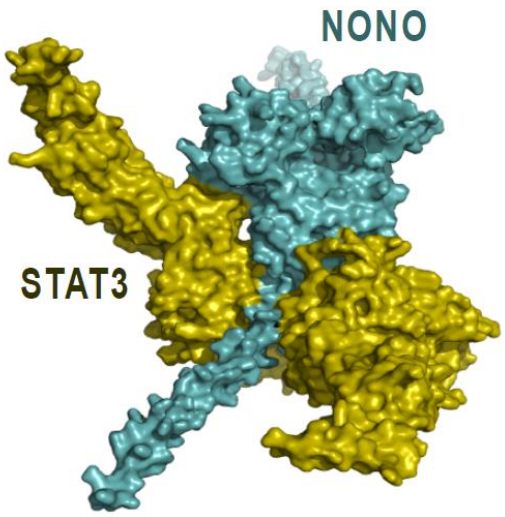
NONO
STAT3

C

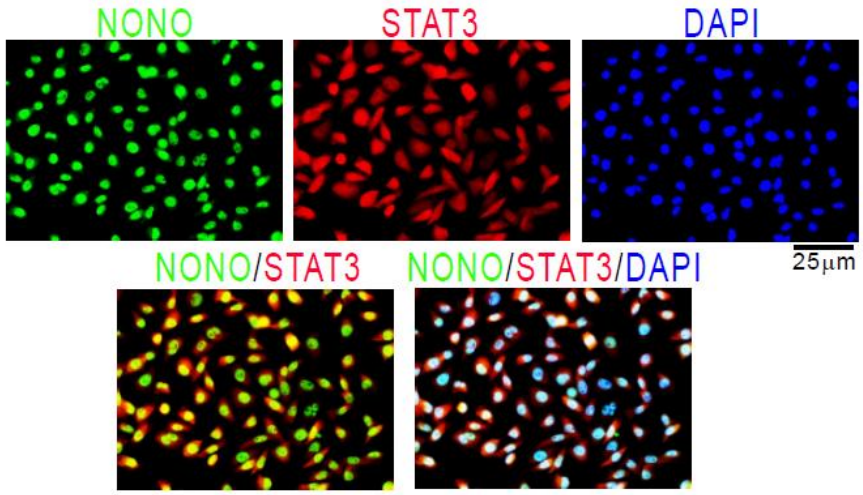
NONO
STAT3
DAPI
25μm
NONO/STAT3
NONO/STAT3/DAPI

Figure 16. NONO colocalizes with STAT3 in TNBC cells.

(A) The amplitudes of protein interactions were determined by analyzing the correlation functions obtained from cells expressing both GFP and RFP. Data presented are the mean ± SD of three independent experiments. Two-tailed Student's t-test was performed to calculate the p-values. (B) Using ClusPro, a computational docking model of human NONO (cyan) and STAT3 (olive) was generated. (C) Cellular co-localization of NONO and STAT3 was examined in MDA-MB-231 cells. Immunostaining was performed on the cells using the specified AB and the resulting images were captured using microscopy. Scale bar = 25 μm.

A

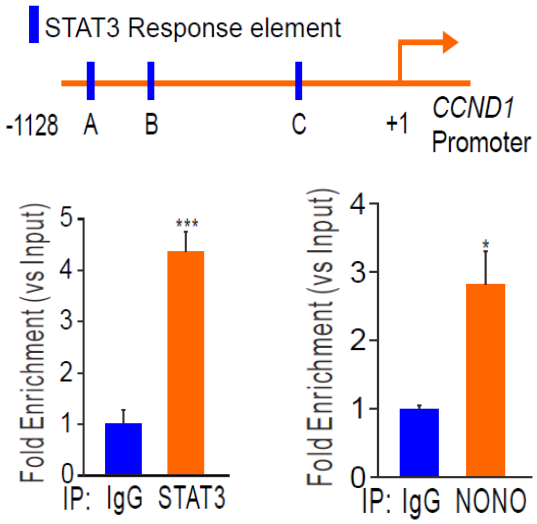
STAT3 Response element
-1128
A
B
C
+1
CCND1
Promoter
Fold Enrichment (vs Input)
IP: IgG
STAT3
IP: IgG
NONO

B

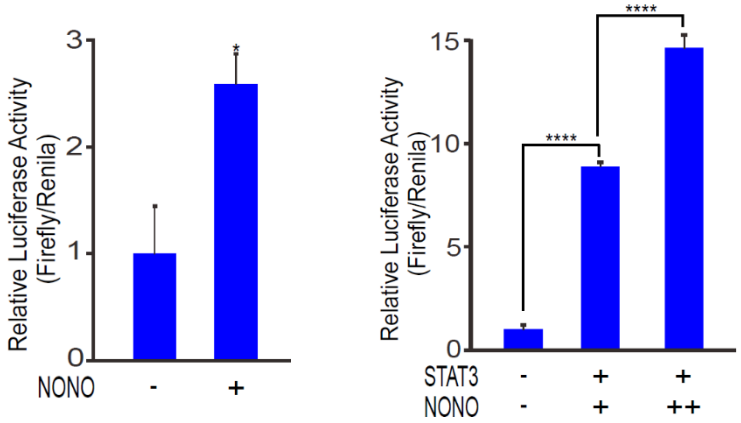
Relative Luciferase Activity
(Firefly/Renila)
NONO
STAT3
NONO

C

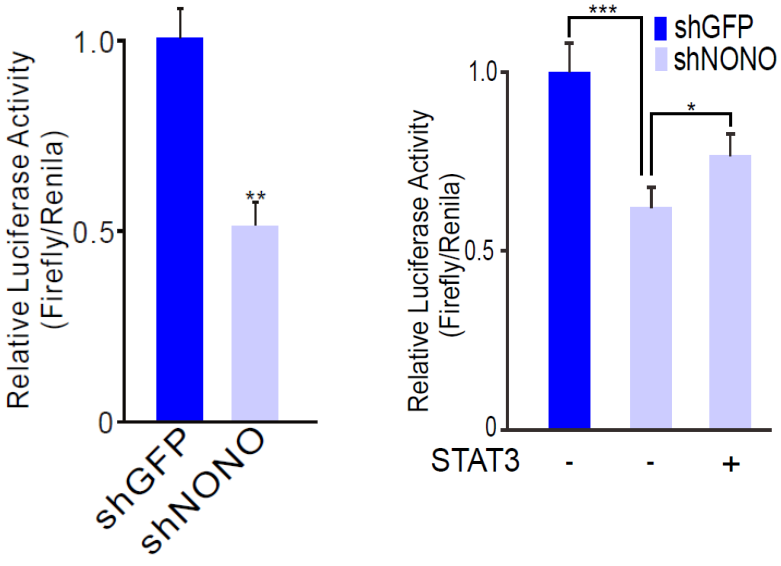
Relative Luciferase Activity
(Firefly/Renila)
shGFP
shNONO
STAT3

Figure 17. The direct interaction between NONO and STAT3 enables STAT3 to function as a transcription factor.

(A) A diagram illustrating the *CCND1* promoter region was created. ChIP assays were conducted in MDA-MB-231 cells using AB specific to STAT3 or NONO. Analysis of the recruitment of NONO to the CCDN1 promoter through STAT3 was performed using primers designed specifically for this region. IgG was utilized as an internal control in the analysis. Data presented are the mean ± SD of three independent experiments. Two-tailed Student's t-test was performed to calculate the p-values, ($^{*}p < 0.05$, and $^{***}p < 0.005$ *vs* IgG). (B) A dual-luciferase reporter gene assay was performed in HEK293T cells to assess the activity level of STAT3 after transfecting NONO, STAT3, and a STAT3-reporter construct. Data presented are the mean ± SD of three independent experiments. Statistical analysis was performed using two-tailed Student's t-test or one-way ANOVA with Tukey's post hoc analysis, ($^{*}p < 0.05$, and $^{****}p < 0.001$). (C) The STAT3-reporter construct was introduced into MDA-MB-231 cells infected with shNONO or shGFP and the and the impact of this infection was counteracted by reintroducing STAT3. Subsequently, luciferase activity was measured in the cells. Data presented are the mean ± SD of three independent experiments. Statistical analysis was performed using two-tailed Student's t-test or one-way ANOVA with Tukey's post hoc analysis, ($^{*}p < 0.05$, $^{**}p < 0.01$, and $^{***}p < 0.005$).

A

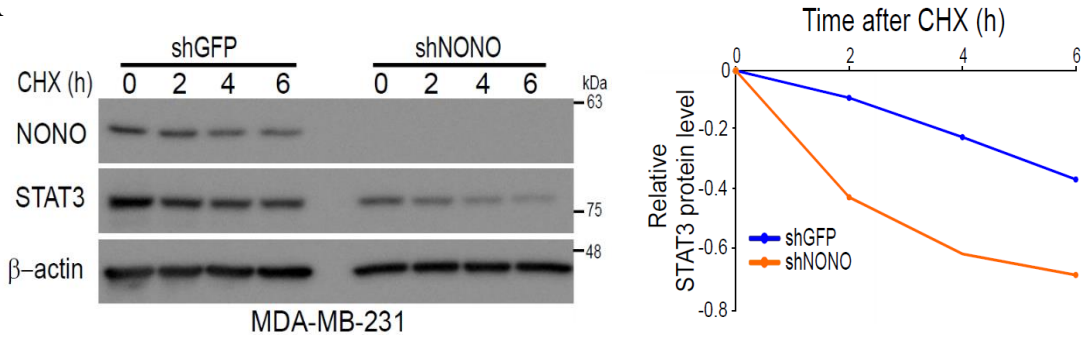
shGFP
shNONO
CHX (h)
0 2 4 6
0 2 4 6
kDa
NONO
STAT3
β–actin
63
75
48
MDA-MB-231
Time after CHX (h)
Relative STAT3 protein level
shGFP
shNONO

B

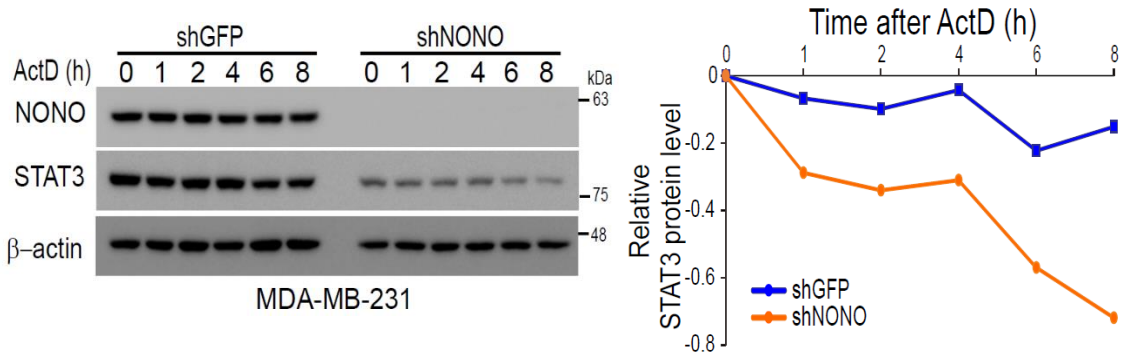
shGFP
shNONO
ActD (h)
0 1 2 4 6 8
0 1 2 4 6 8
kDa
NONO
STAT3
β–actin
63
75
48
MDA-MB-231
Time after ActD (h)
Relative STAT3 protein level
shGFP
shNONO

C

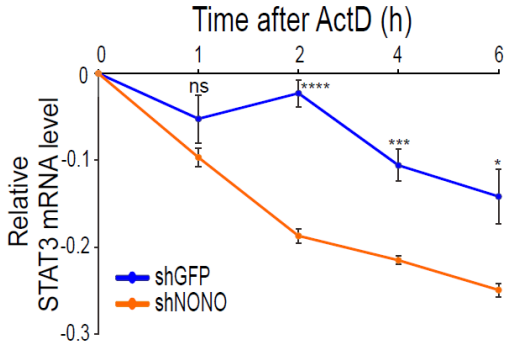
Time after ActD (h)
Relative STAT3 mRNA level
ns
****
***
*
shGFP
shNONO

Figure 18. NONO directly mediates the function of STAT3 in TNBC cells.

(A-C) Stable cell lines were established by transfecting MDA-MB-231 cells with either shNONO or shGFP. Following transfection, the cells were treated with DMSO, CHX (50 μg/ml), or Act D (1 μM) and then harvested at specified time intervals. (A and B) Protein extraction was performed on the designated cells, and WB analysis was conducted using the specified AB. The graphs represent the relative quantities of STAT3 protein normalized to the levels of ß-actin in the WB. The protein expression levels were analyzed using ImageJ software. The protein half-life was determined based on the relative level of STAT3 protein. (C) Total RNA was extracted from the specified cells and qPCR was performed for analysis. The RNA half-life was determined based on the relative level of STAT3 RNA. Data presented are the mean ± SD of three independent experiments. Statistical analysis was performed using one-way ANOVA with Tukey's post hoc analysis, (*$p < 0.05$, ***$p < 0.005$, and ***$p < 0.005$ *vs* shGFP).

Clinical significance of the NONO-STAT3 interaction in TNBC

Considering the association of NONO with clinical outcomes and its potential direct regulation of STAT3, the clinical significance of STAT3 was investigated using samples obtained from patients with BC. As anticipated, the expression of STAT3 was significantly elevated in TNBC tissues compared to non-TNBC tissues (Figure 19A) and there was a positive correlation between STAT3 mRNA and NONO mRNA expression (Figure 19B). Kaplan-Meier analysis of dichotomized STAT3 gene expression indicated a correlation between elevated STAT3 expression and poor clinical outcomes in TNBC patients (Figure 20A). Elevated levels of both NONO and STAT3 were strongly related to poor patient survival (Figure 20B). NONO and STAT3, acting as transcriptional regulators, exert oncogenic properties by influencing downstream gene expression. The investigation aimed to explore the shared gene networks between NONO and STAT3 by analyzing the gene expression profiles obtained from silencing both factors in MDA-MB-231 cells [116] (GSE85579). A Venn diagram was depicted, illustrating a significant number of genes identified as downstream targets of both NONO and STAT3 factors (Figure 21A), indicating potential dependency of NONO biological activity on STAT3. To gain further insight into the common gene network feature of NONO and STAT3, we analyzed 272 gene signatures using IPA (Figure 21B). The analysis indicated that the shared gene signatures between NONO and STAT3 were strongly associated with cancer cell growth, proliferation, cell cycle regulation, cell death, cellular movement, and migration. These findings are consistent with the observations presented in Figure 10C. Subsequently, the clinical significance of these shared gene signatures was assessed using a previously established prediction approach that integrates multiple algorithms [91, 117] (Figure 22A). As anticipated, the shared gene expression signatures demonstrated a significant association with patient survival and disease recurrence in patients with BC, as determined by the predicted outcomes derived from different classifiers [117]. Patients who exhibited knockdown signatures (KS) yielded a relatively favorable prognosis, while those with the opposite patterns yielded relatively poor outcomes (Figure 22B). Collectively, these findings indicate a functional association between NONO and STAT3 and highlight its potential impact on clinical outcomes in TNBC.

A

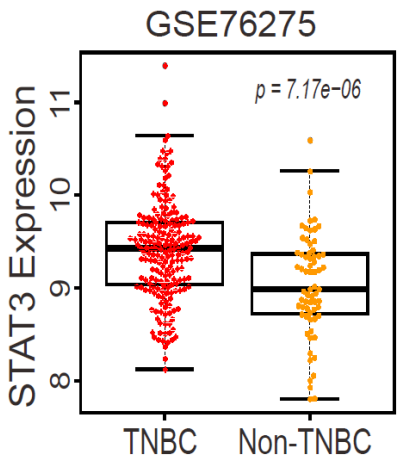
GSE76275
p = 7.17e-06
STAT3 Expression
8
9
10
11
TNBC
Non-TNBC

B

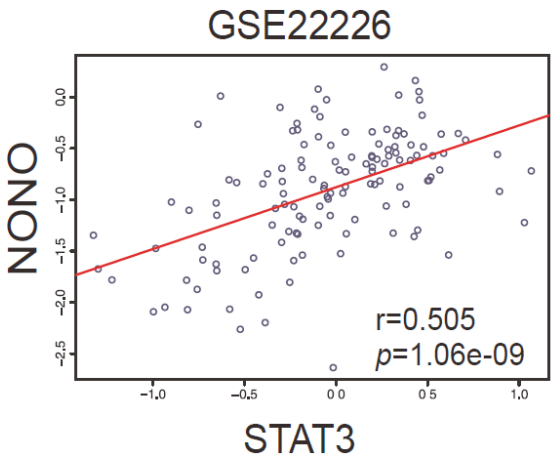
GSE22226
NONO
r=0.505
p=1.06e-09
STAT3

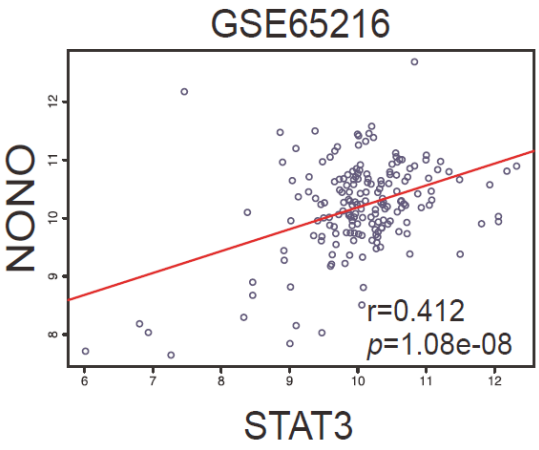
GSE65216
NONO
r=0.412
p=1.08e-08
STAT3

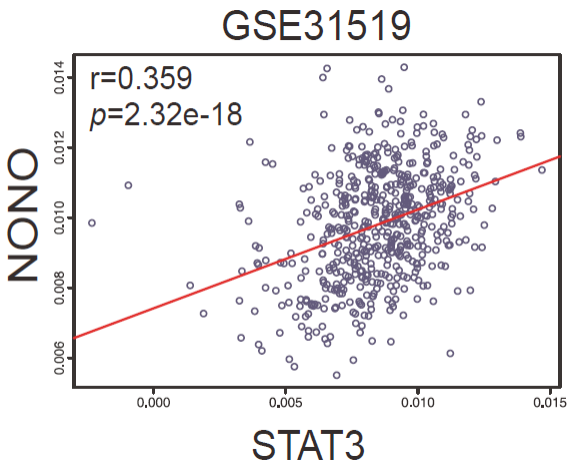
GSE31519
r=0.359
p=2.32e-18
NONO
STAT3

Figure 19. STAT3 expression was linked to a bad prognosis and correlated with NONO expression in TNBC.

(A) expression of STAT3 in patients with both TNBC and non-TNBC patients in the BC cohort. Error bar displays SD value. Two-tailed Student's t-test was performed to calculate the p-values. (B) correlation between NONO and STAT3 gene expression was assessed in the specified population of BC, which included cohorts of TNBC patients. Scatter plots depict the relationship between NONO and STAT3 expression levels in the cohorts of TNBC patients.

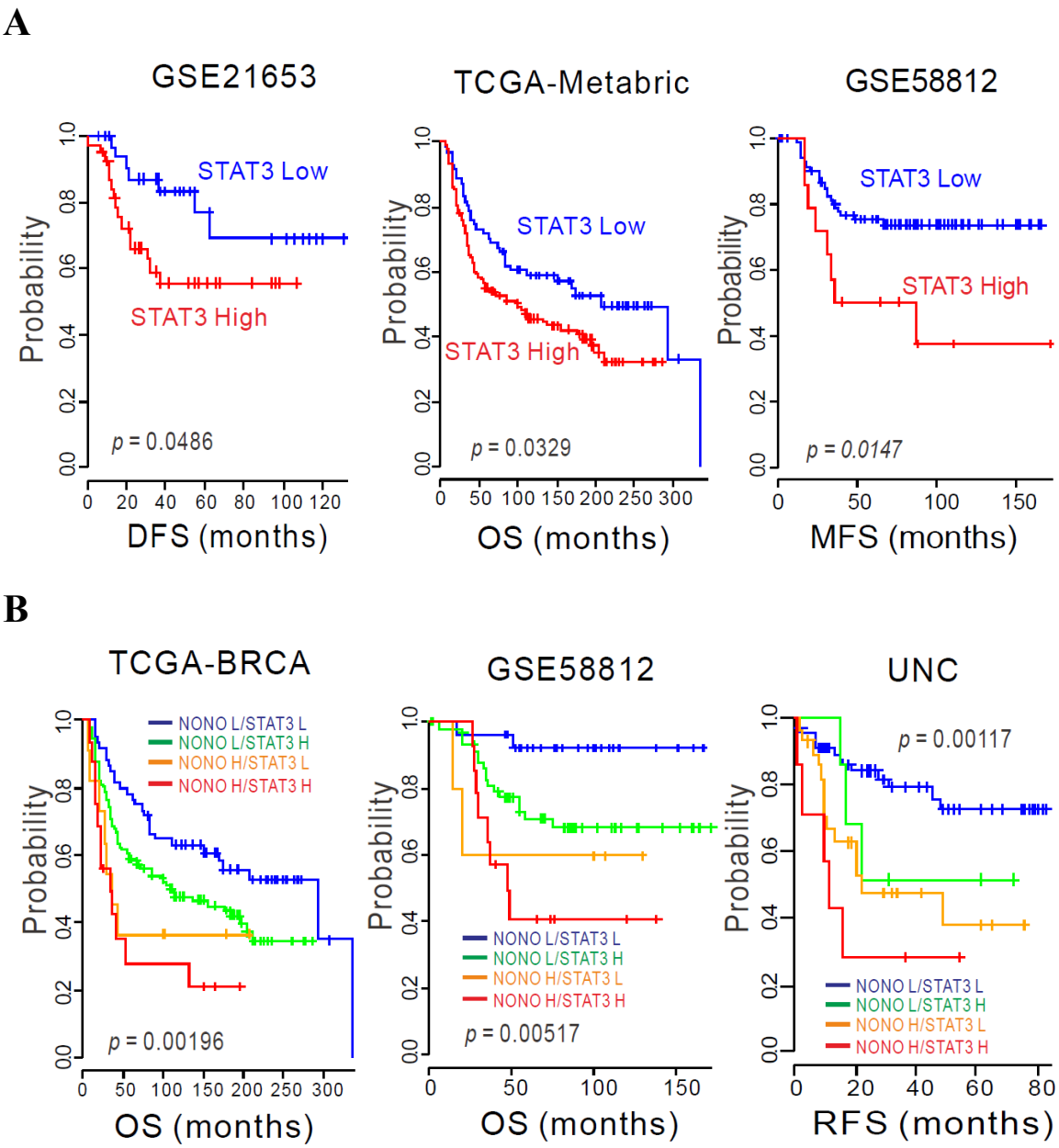

Figure 20. The clinical association between NONO and STAT3 in TNBC.

(A-B) Based on the relative expression levels of NONO and STAT3, patient cohorts were classified into two or four groups. The differences between the groups were found to be statistically significant (log-rank test). MFS, metastasis-free survival; RFS, recurrence-free survival.

A

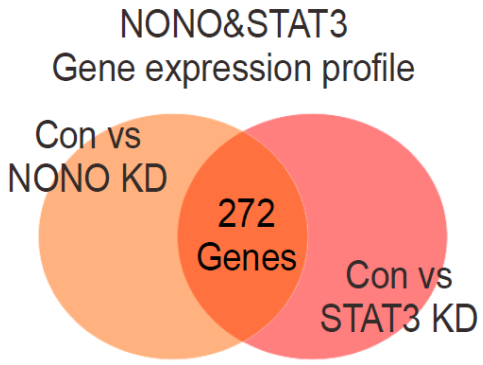

B

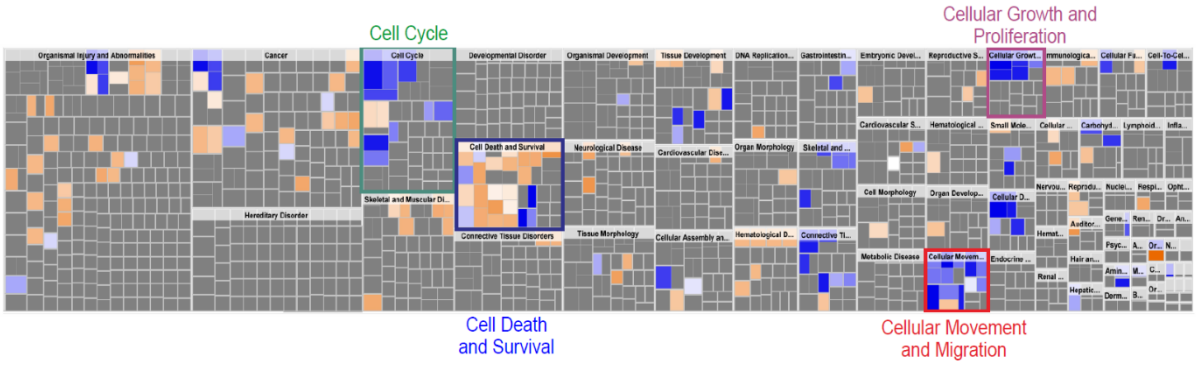

Figure 21. NONO-STAT3 regulates the cellular growth and movement associated gene in TNBC.

(A) The gene expression profile specific to the depletion of NONO or STAT3 expression using shRNA or siRNA, respectively, was examined in MDA-MB-231 cells. Genes present in the Venn diagram were chosen by applying a two-sample Student's t-test ($P < 0.001$) and considering those with a fold change greater than 1.5. The orange and pink circles in the diagram represent genes with expression patterns that are significantly correlated with the depletion of NONO or STAT3, respectively. (B) IPA was performed to analyze the differentially expressed genes following the silencing of NONO and STAT3.

A

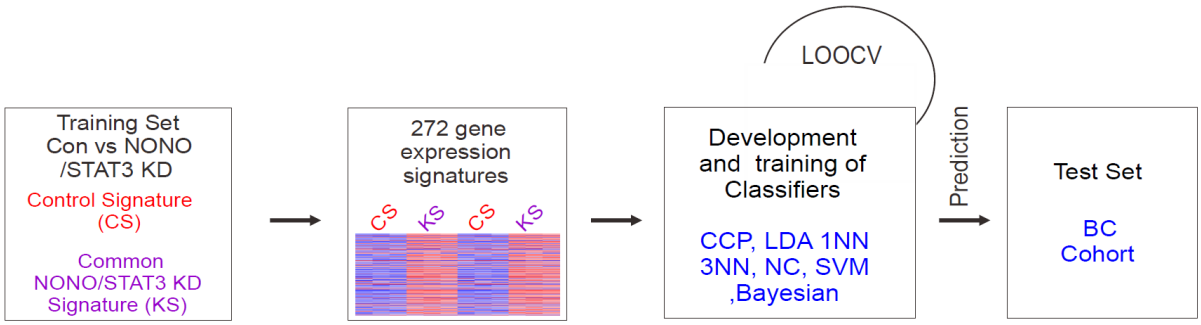
Training Set
Con vs NONO
/STAT3 KD
Control Signature
(CS)
Common
NONO/STAT3 KD
Signature (KS)
272 gene
expression
signatures
CS
KS
CS
KS
LOOCV
Development
and training of
Classifiers
CCP, LDA 1NN
3NN, NC, SVM
,Bayesian
Prediction
Test Set
BC
Cohort

B

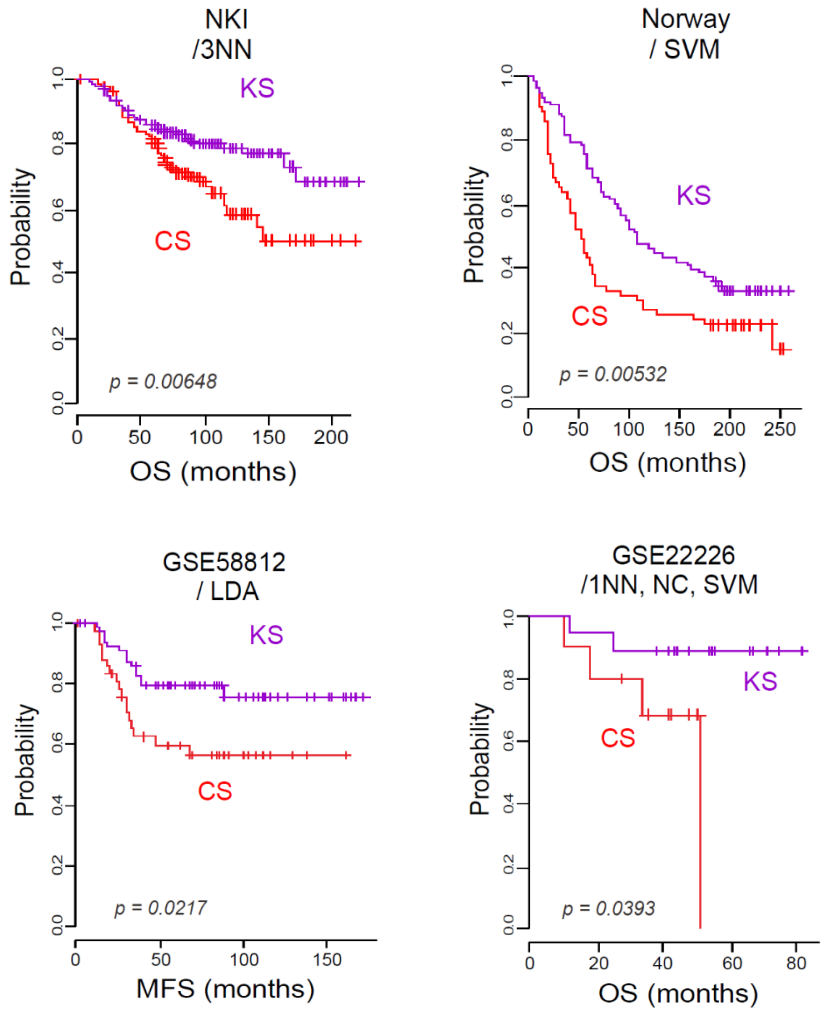
NKI
/3NN
KS
CS
p = 0.00648
Probability
OS (months)
Norway
/ SVM
KS
CS
p = 0.00532
Probability
OS (months)
GSE58812
/ LDA
KS
CS
p = 0.0217
Probability
MFS (months)
GSE22226
/1NN, NC, SVM
KS
CS
p = 0.0393
Probability
OS (months)

Figure 22. Patient prognosis was predicted based on the expression of NONO-STAT3 using a prediction model.

(A) A schematic diagram illustrating the generation of a prediction model and the evaluation of predicted outcomes were developed based on the shared gene expression signature of NONO and STAT3 in MDA-MB-231 cells. A shared gene expression signature was employed to construct a set of classifiers, which assessed the extent to which the expression pattern of BC patients resembled the shared signature. This comparison involved distinguishing between the control signature (CS) and knockdown signature (KS). (B) Kaplan-Meier plots predicting OS or MFS in BC patients from the specified cohorts were generated using the gene expression signature as a classifier. The differences between the groups were found to be statistically significant (log-rank test). MFS, metastasis-free survival; LOOCV, Leave-One-Out Cross-Validation; CCP, compound covariate predictor; LDA, linear discriminator analysis; 1NN, one nearest neighbor; 3NN, three nearest neighbors; NC, nearest centroid; SVM, support vector machines.

Silencing of NONO enhances the sensitivity of TNBC cells to chemotherapy

The responsiveness to chemotherapy and radiation therapy is considered an indicator of clinical outcomes in patients with TNBC [11, 118]. Because genomic analysis revealed a correlation between elevated NONO expression and poor prognosis in patients with TNBC and as shown in Figures 4A–B, NONO was found to be strongly related to responsiveness to chemotherapy. Further in-depth analysis was performed to examine the potential association between NONO expression and response to treatment. Epirubicin, a commonly utilized anthracycline drug, is extensively employed in the treatment of TNBC. Based on genomic data obtained from epirubicin-treated ER-negative patients, high expression of NONO translated to poor prognoses. Additionally, survival analysis was performed among chemotherapy and radiation-treated patients with TNBC. As expected, high NONO expression was associated to poor prognosis (Figure 23A). Additionally, a significant increase in NONO expression was observed in non-responders compared to responders (Figure 23B). Moreover, high levels of NONO were linked to poor prognosis among patients with TNBC or basal-like tumors who had received chemotherapy or radiation therapy. Additionally, the expression of both NONO and STAT3 was identified as a contributing factor in the progression of drug resistance (Figure 24A). These findings suggest that NONO influences the sensitivity of TNBC to drug treatments.

Previous studies have indicated that drug resistance in cancer cells exhibits characteristics of cancer stem-like cells (CSCs), and STAT3 has been identified as a key component contributing to the proliferation of CSCs [119]. Given the involvement of NONO in the regulation of STAT3 and its association with drug resistance, we investigated whether NONO affects the proliferation of CSC through the regulation of STAT3. As expected, the sphere formation assay revealed a significant decrease in the proliferation of CSCs in NONO. As expected, the sphere formation assay revealed a significant reduction in the proliferation of CSCs in NONO-knockdown cancer cells (Figure 25A); the decreased proliferation of CSCs was restored by reintroducing STAT3 (Figure 25B), which rescued the reduction in CSC marker expression caused by NONO silencing (Figure 25C). Additionally, NONO and CSC markers NANOG and POU5F1/Oct4 in TNBC patients were found to be correlated (Figure 25D). These findings clearly indicate that NONO plays a regulatory role in CSC proliferation through STAT3. Moreover, NONO contributes to drug resistance by influencing CSC proliferation.

Subsequently, we examined the relationship between NONO expression and response to chemotherapy or radiation using TNBC cell lines with silenced NONO expression. Cell viability assays were conducted in MDA-MB-231 cells using chemotherapy agents commonly employed for TNBC

treatment. Interestingly, silencing NONO expression in MDA-MB-231 cells rendered them sensitive to doxorubicin (Dox), a commonly used therapy for patients with TNBC (Figure 26A), indicating that NONO could potentially be involved in conferring resistance of TNBC cells to Dox treatment. Moreover, response to radiation and cisplatin chemotherapy was enhanced in MDA-MB-231 cells with silenced NONO expression (Figures 26B–C) and the drug's half maximal inhibitory concentration (IC50) was lower in cells with silenced NONO expression than in the parental cells (Figure 27A). Furthermore, the experiment on recovery showed that resistance to chemotherapeutic drugs was dependent on the presence of STAT3 expression (Figure 27B-C). These findings suggest that the inhibition of NONO enhances the effectiveness of chemotherapy and radiation in TNBC models.

A

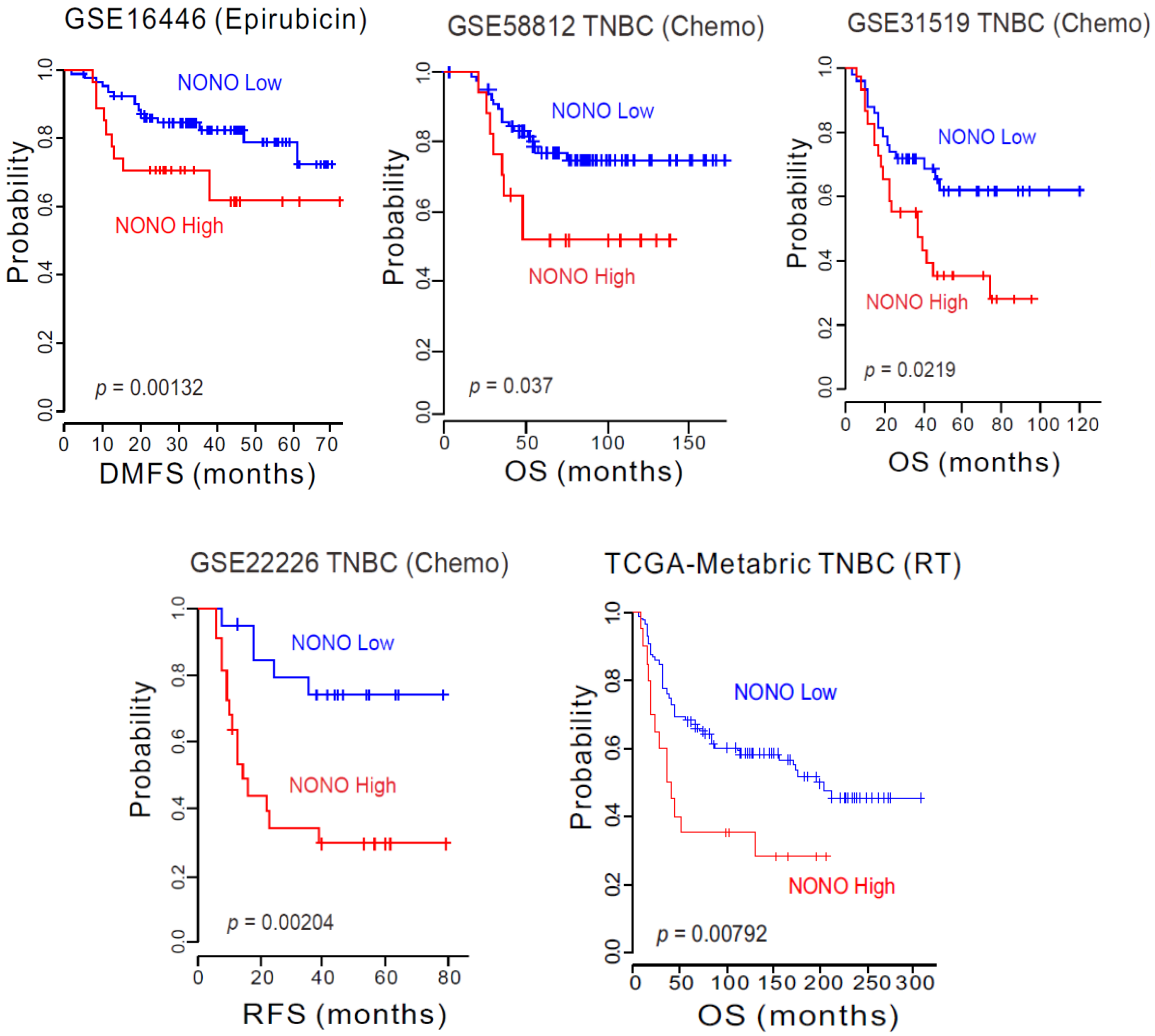
GSE16446 (Epirubicin)
NONO Low
NONO High
Probability
p = 0.00132
DMFS (months)
GSE58812 TNBC (Chemo)
NONO Low
NONO High
Probability
p = 0.037
OS (months)
GSE31519 TNBC (Chemo)
NONO Low
NONO High
Probability
p = 0.0219
OS (months)
GSE22226 TNBC (Chemo)
NONO Low
NONO High
Probability
p = 0.00204
RFS (months)
TCGA-Metabric TNBC (RT)
NONO Low
NONO High
Probability
p = 0.00792
OS (months)

B

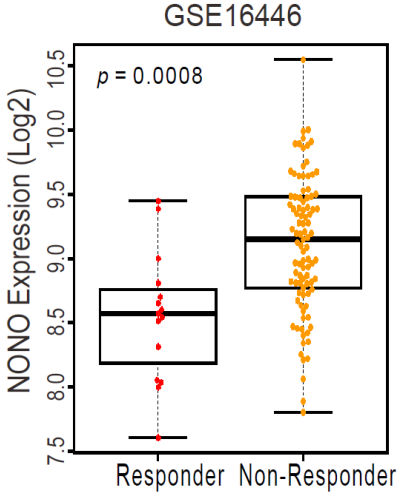
GSE16446
p = 0.0008
NONO Expression (Log2)
Responder
Non-Responder

Figure 23. Survival rate analysis of BC patients according to NONO expression levels.

(A) Kaplan-Meier survival plots illustrating OS, RFS, or DMFS outcomes in patients from the specified cohorts. The differences between the groups were found to be statistically significant (log-rank test). RFS, recurrence-free survival; DMFS, distant metastasis-free survival. (B) Expression levels of NONO in the mentioned patient groups. Error bar displays SD value. Two-tailed Student's t-test was performed to calculate the p-values.

A

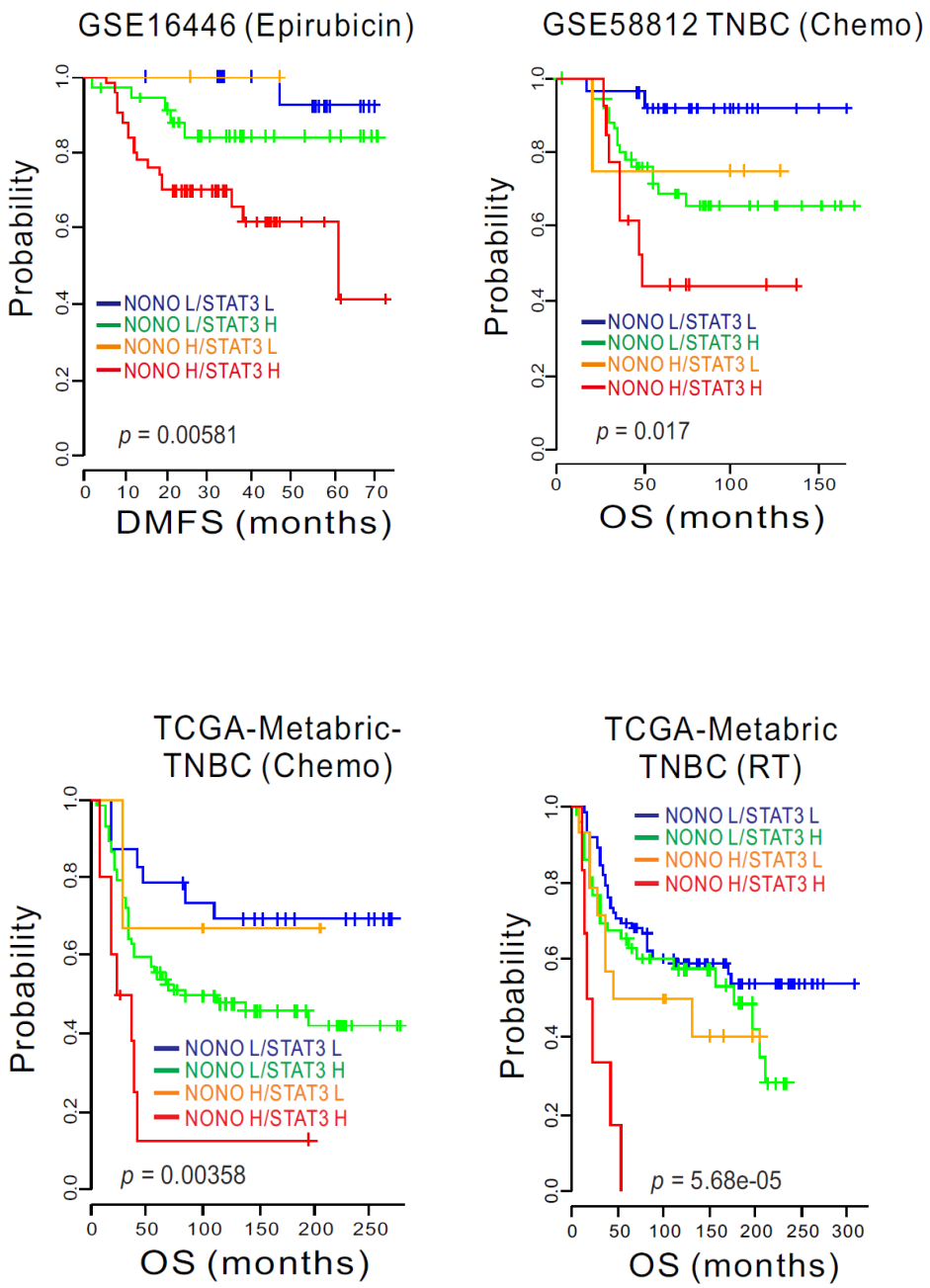

Figure 24. Clinical relevance of NONO and STAT3 in BC.

(A) Kaplan-Meier survival plots showing OS or DMFS outcomes in patients from the specified cohorts. The differences between the groups were found to be statistically significant (log-rank test). DMFS, distant metastasis-free survival.

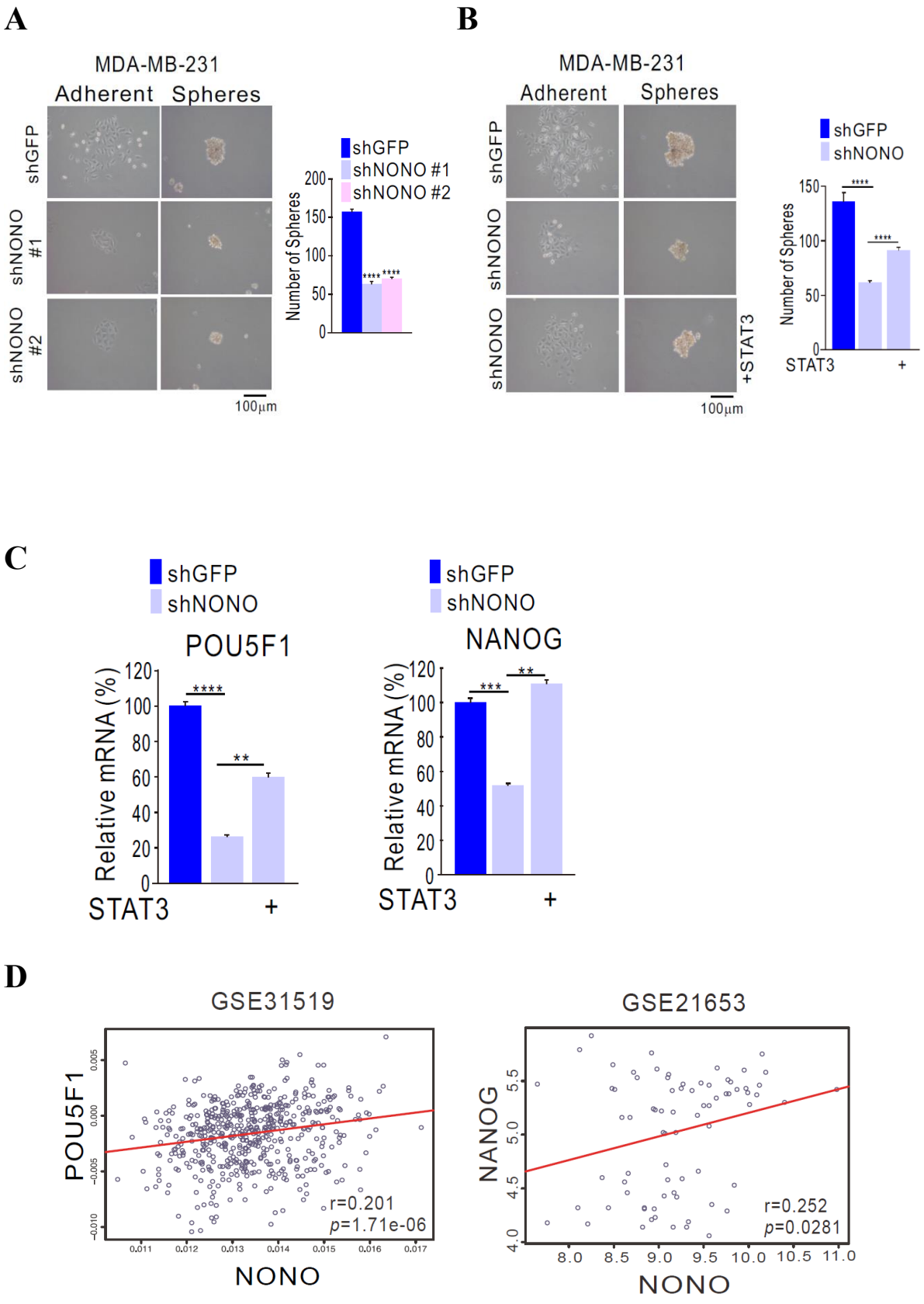
A
MDA-MB-231
Adherent
Spheres
shGFP
shNONO #1
shNONO #2
100μm
shGFP
shNONO #1
shNONO #2
Number of Spheres
B
MDA-MB-231
Adherent
Spheres
shGFP
shNONO
+STAT3
100μm
shGFP
shNONO
Number of Spheres
STAT3
+
C
shGFP
shNONO
POU5F1
Relative mRNA (%)
STAT3
+
shGFP
shNONO
NANOG
Relative mRNA (%)
STAT3
+
D
GSE31519
POU5F1
NONO
r=0.201
p=1.71e-06
GSE21653
NANOG
NONO
r=0.252
p=0.0281

Figure 25. Correlation of NONO and cancer stem cell (CSC) marker in BC.

(A-C) Representative images Scale bar = 100 μm, quantification of sphere formation and mRNA expression levels was performed using qPCR in MDA-MB-231 cells. (C) MDA-MB-231 cells were subjected to infection with specific shRNAs and transfection with STAT3 cDNA. All data presented are the mean ± SD of three independent experiments. Statistical analysis was performed using one-way ANOVA with Tukey's post hoc analysis, (**$p < 0.01$, ***$p < 0.005$, and ****$p < 0.001$). (D) correlation between NONO and POU5F1 or NANOG gene expression was analyzed in the specified TNBC patient cohorts. Scatter plots depict the relationship between NONO and correlated genes in the cohorts of TNBC patients.

A

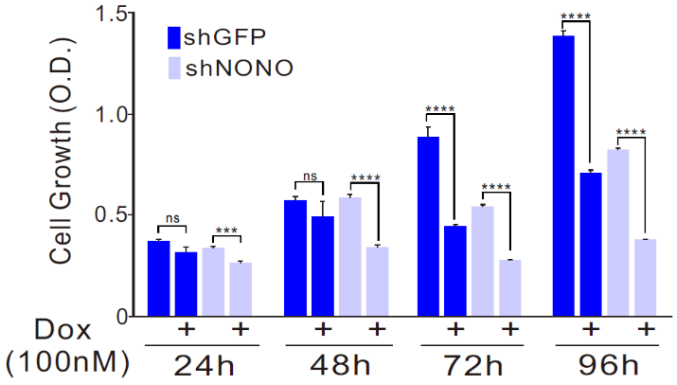
Cell Growth (O.D.)
1.5
1.0
0.5
0
shGFP
shNONO
ns
***
****
Dox
(100nM)
+ +
24h
48h
72h
96h

B

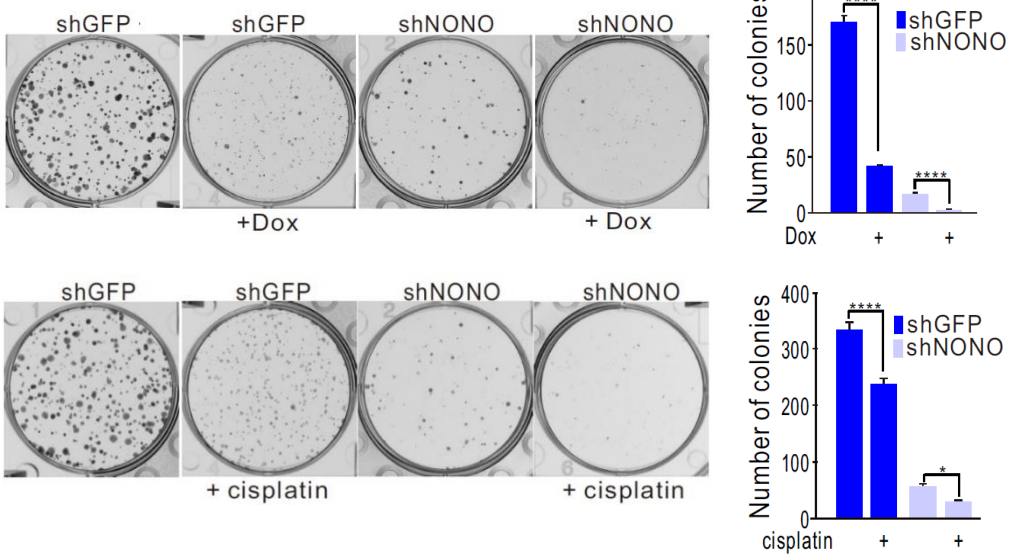
shGFP
shGFP
shNONO
shNONO
+Dox
+ Dox
Number of colonies
200
150
100
50
0
****
Dox
+ +
+ cisplatin
+ cisplatin
400
300
200
100
*
cisplatin

C

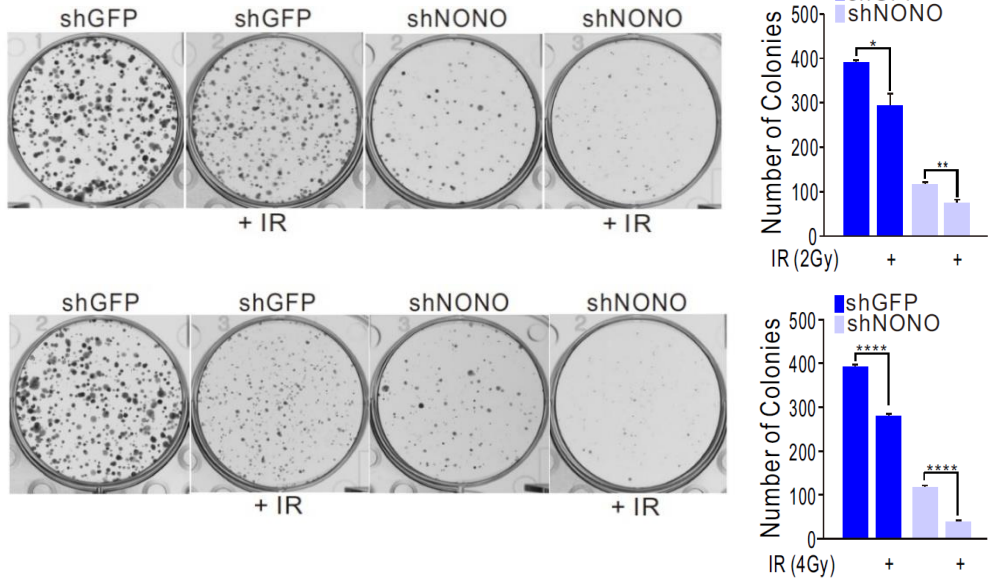
shGFP
shGFP
shNONO
shNONO
+ IR
+ IR
Number of Colonies
500
400
300
200
100
0
*
**
IR (2Gy)
+ +
****
IR (4Gy)

Figure 26. Inhibition of NONO expression enhances the responsiveness of TNBC cells to chemotherapy and radiation.

(A) MDA-MB-231 cells were transduced with shNONO or shGFP and subsequently exposed to Dox treatment for the specified durations. The cells were later subjected to CCK8 assay for analysis. (B-C) clonogenic survival was assessed and measured using a colony formation assay. silenced NONO cells were treatment with Dox (upper panel) cisplatin (lower panel) or (C) IR and stained cells were counted. All data presented are the mean ± SD of three independent experiments. Statistical analysis was performed using one-way ANOVA with Tukey's post hoc analysis, (*$p < 0.05$, **$p < 0.01$, ***$p < 0.005$, and ****$p < 0.001$).

A

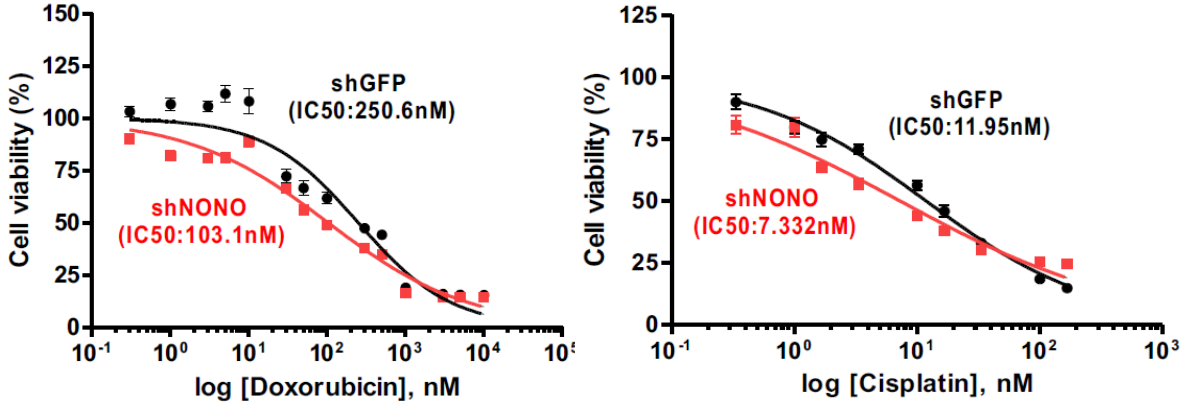
Cell viability (%)
shGFP
(IC50:250.6nM)
shNONO
(IC50:103.1nM)
log [Doxorubicin], nM
Cell viability (%)
shGFP
(IC50:11.95nM)
shNONO
(IC50:7.332nM)
log [Cisplatin], nM

B

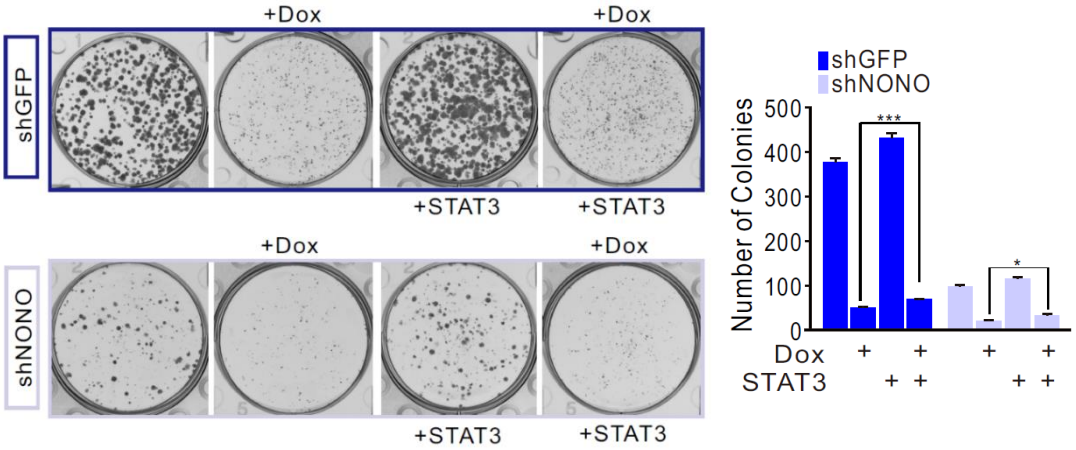
+Dox
+Dox
shGFP
+STAT3
+STAT3
+Dox
+Dox
shNONO
+STAT3
+STAT3
shGFP
shNONO
Number of Colonies
***
*
Dox
STAT3

C

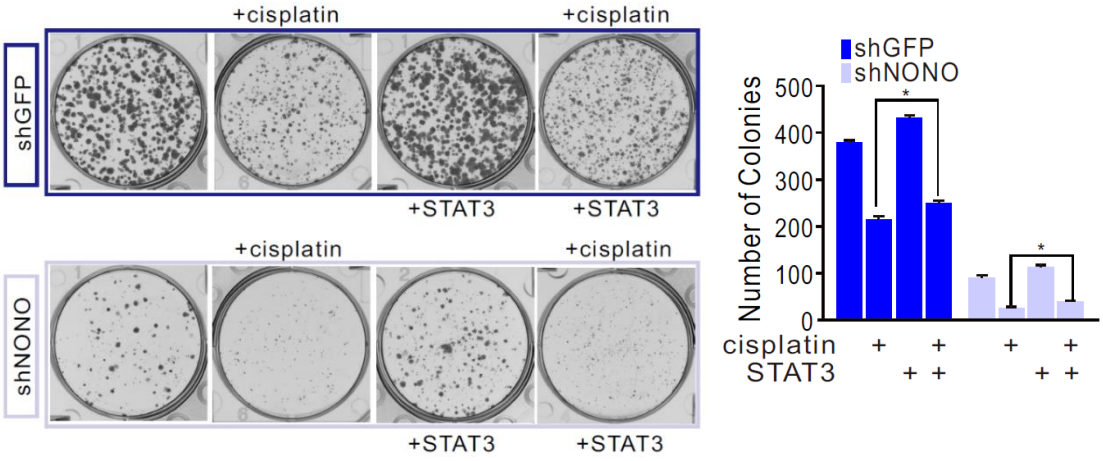
+cisplatin
+cisplatin
shGFP
+STAT3
+STAT3
+cisplatin
+cisplatin
shNONO
+STAT3
+STAT3
shGFP
shNONO
Number of Colonies
*
*
cisplatin
STAT3

Figure 27. NONO induces drug resistance in TNBC cells through the regulation of the STAT3 gene.

(A) MDA-MB-231 cells were transfected with shNONO or shGFP to achieve stable knockdown of NONO expression. Subsequently, the cells were treated with the specified drugs. The cells were then analyzed for IC50 calculation. Error bar displays SD value. (B-C) and after a duration of 14 days, the cells were utilized for a colony formation assay. Cells with silenced NONO expression were subjected to treatment with Dox, and the cells were stained and counted to confirm the reintroduction of STAT3. Data presented are the mean ± SD of three independent experiments. Statistical analysis was performed using one-way ANOVA with Tukey's post hoc analysis, (*$p < 0.05$, and ***$p < 0.005$).

Drug screening for inhibitors targeting NONO in TNBC

Given the association of NONO with TNBC cell growth and its impact on clinical outcomes, we investigated whether directly targeting NONO could effectively inhibit cellular proliferation in TNBC. To discover potential drugs that could target NONO, we conducted high-throughput screening of a compound library comprising 770 compounds (Screen-Well ® FDA approved drug library V2) that are approved by the food and drug administration (FDA). These compounds have been extensively utilized for their safety profile, biological activity, and functional properties. MDA-MB-231 cells were transduced with GFP-NONO and treated with puromycin for selection. Subsequently, the cells were treated in the drug library, and the fluorescence intensity of GFP was quantified (Figure 28A). Initial screening revealed 12 compounds in the library that exhibited inhibition of GFP-NONO signal intensity. Upon further validation, 11 of these compounds consistently demonstrated the suppression of the GFP-NONO signal (Figure 28B). To further test the effects of 4 of the selected compounds, auranofin, digoxin, colchicine, and podophyllotoxin, we examined their ability to suppress NONO expression and downstream STAT3 gene expression. Auranofin demonstrated significant suppression of NONO expression, as well as the mRNA and protein levels of STAT3 in MDA-MB-231 cells (Figures 29A–C). Furthermore, treatment with auranofin resulted in decreased NONO expression in murine 4T1.2 syngeneic model, which reflects TNBC phenotypes [120] and the xenograft model utilizing MDA-MB-231 cells (Figure 29D). To confirm the dependency of NONO gene expression on cell growth inhibition, a rescue experiment was conducted. The re-introduction of NONO partially restored the suppressive effects of auranofin on TNBC cell growth (Figures 29E and F), indicating that auranofin growth inhibitory effects are mediated through the targeting of NONO expression.

Finally, we performed computational analysis using protein structure models and an *in silico* molecular docking technique (Figures 30A and B). NONO/STAT3 complex modeling indicated greater binding affinity (ΔG) of auranofin and digoxin (-7.7 kcal/mol and -7.8 kcal/mol) than either podophyllotoxin or colchicine (-5.7 and -6.2 kcal/mol). This analysis suggested, however, that all four compounds rank highly in their interaction with NONO or the NONO/STAT3 complex. The *in vitro*, *in vivo*, and *in silico* assays indicate that auranofin is a particularly strong candidate as an anti-cancer therapeutic.

A

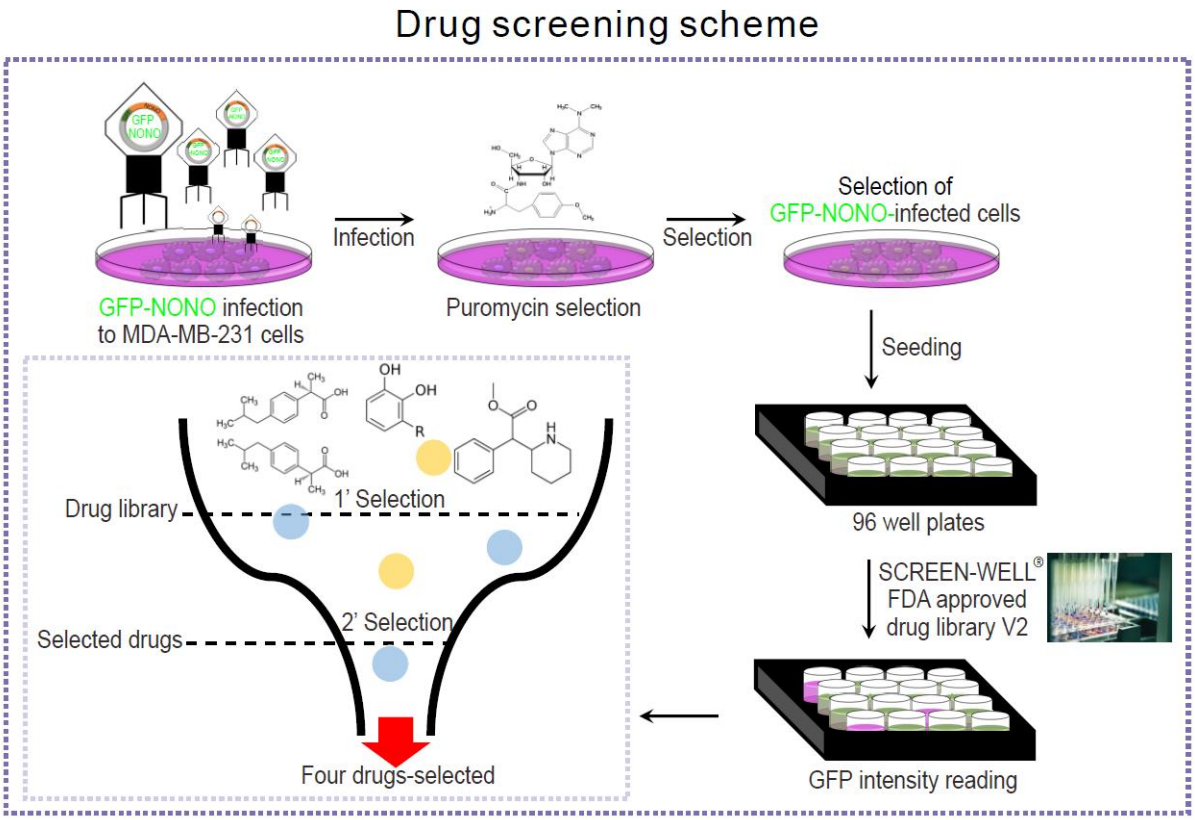
Drug screening scheme
GFP-NONO infection to MDA-MB-231 cells
Infection
Puromycin selection
Selection
Selection of GFP-NONO-infected cells
Seeding
96 well plates
SCREEN-WELL® FDA approved drug library V2
GFP intensity reading
Drug library
1' Selection
2' Selection
Selected drugs
Four drugs-selected

B

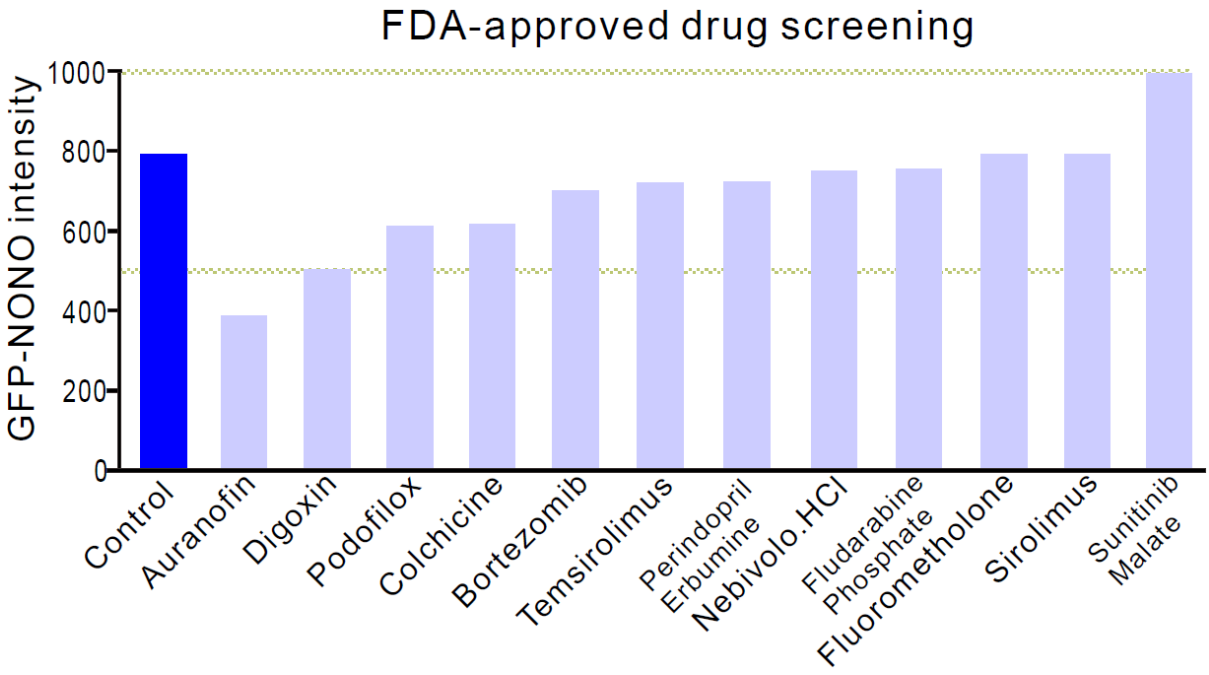
FDA-approved drug screening
GFP-NONO intensity
1000
800
600
400
200
0
Control
Auranofin
Digoxin
Podofilox
Colchicine
Bortezomib
Temsirolimus
Perindopril Erbumine
Nebivolo.HCl
Fludarabine Phosphate
Fluorometholone
Sirolimus
Sunitinib Malate

Figure 28. FDA-approved drug screening for NONO inhibitors in TNBC.

(A) Overview of the drug screening process. (B) Drug screening results showing the relative fluorescence intensity of GFP-NONO compared to control samples.

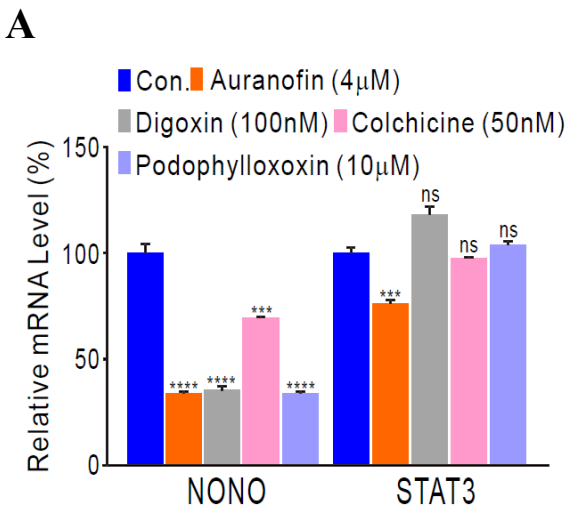
A
Con.
Auranofin (4μM)
Digoxin (100nM)
Colchicine (50nM)
Podophylloxoxin (10μM)
Relative mRNA Level (%)
150
100
50
0
ns
ns
ns
NONO
STAT3

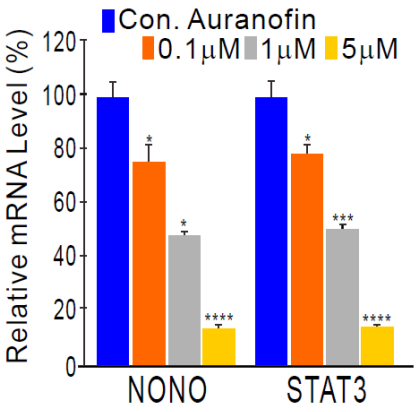
B
Con.
Auranofin
0.1μM
1μM
5μM
Relative mRNA Level (%)
120
100
80
60
40
20
0
NONO
STAT3

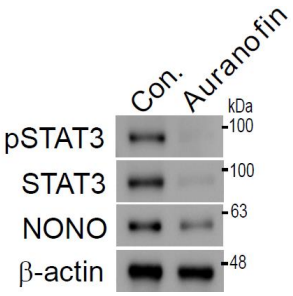
C
Con.
Auranofin
kDa
pSTAT3
100
STAT3
100
NONO
63
β-actin
48

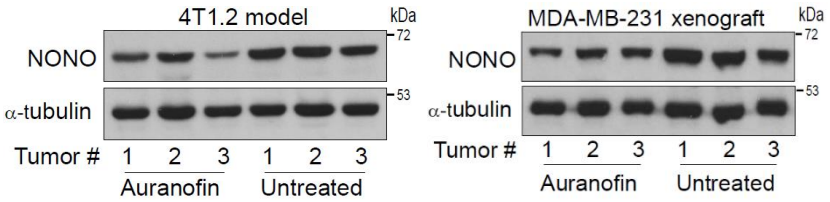
D
4T1.2 model
kDa
NONO
72
α-tubulin
53
Tumor #
1 2 3 1 2 3
Auranofin
Untreated
MDA-MB-231 xenograft
kDa
NONO
72
α-tubulin
53
Tumor #
1 2 3 1 2 3
Auranofin
Untreated

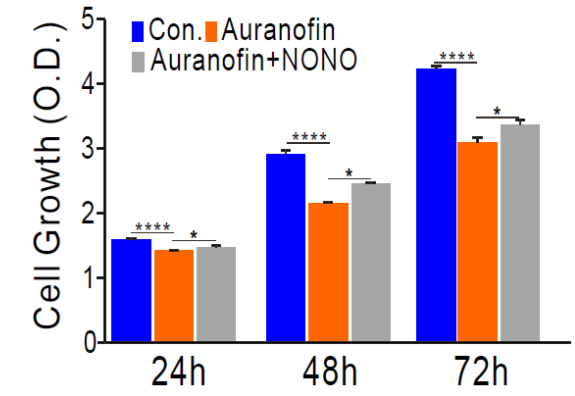
E
Con.
Auranofin
Auranofin+NONO
Cell Growth (O.D.)
5
4
3
2
1
0
24h
48h
72h

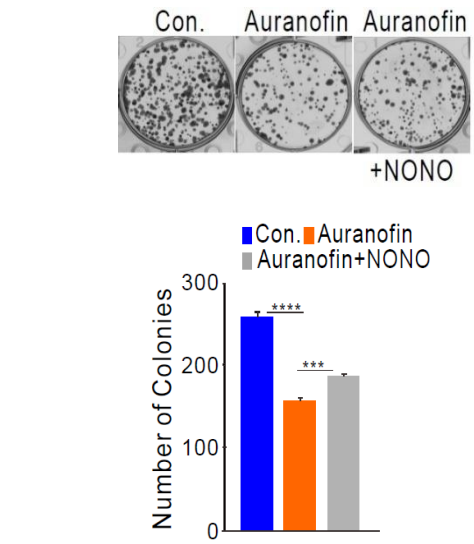
F
Con.
Auranofin
Auranofin
+NONO
Con.
Auranofin
Auranofin+NONO
Number of Colonies
300
200
100
0

Figure 29. NONO inhibitory effect of Auranofin in TNBC.

(A-B) MDA-MB-231 cells were treated with the specified drugs, and subsequent analysis was performed using qPCR with the designated primers. Data presented are the mean ± SD of three independent experiments. Statistical analysis was performed using one-way ANOVA with Tukey's post hoc analysis, (*$p < 0.05$, ***$p < 0.005$, and ****$p < 0.001$ *vs* Con). (C) WB analysis was conducted to examine the expression of STAT3-associated genes in MDA-MB-231 cells treated with the indicated drug. (D) WB analysis was performed on the specified tumor tissues [120]. (E and F) MDA-MB-231 cells were subjected to auranofin treatment, followed by transfection with NONO cDNA, and subsequently evaluated using a CCK8 assay (E). Data presented are the mean ± SD of three independent experiments. Statistical analysis was performed using one-way ANOVA with Tukey's post hoc analysis, (*$p < 0.05$, and ****$p < 0.001$). (F) and colony formation assay. Data presented are the mean ± SD of three independent experiments. Statistical analysis was performed using one-way ANOVA with Tukey's post hoc analysis, (***$p < 0.005$, and ****$p < 0.001$).

A

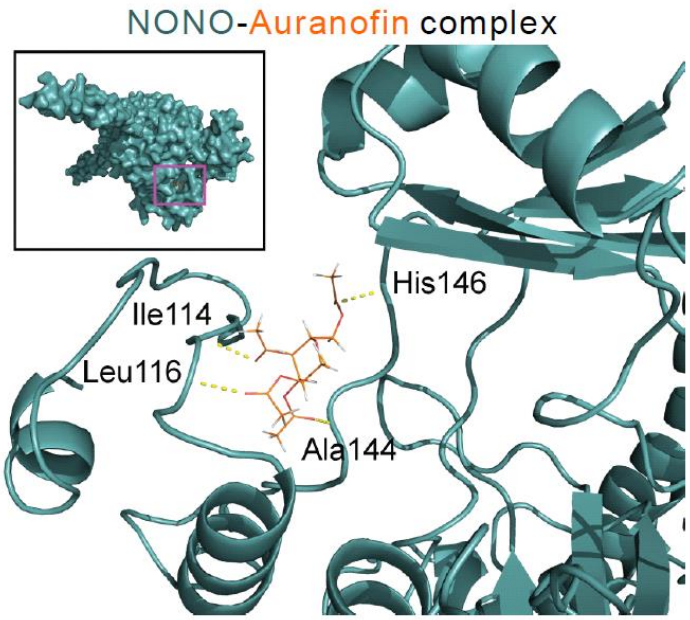
NONO-Auranofin complex
His146
Ile114
Leu116
Ala144

B

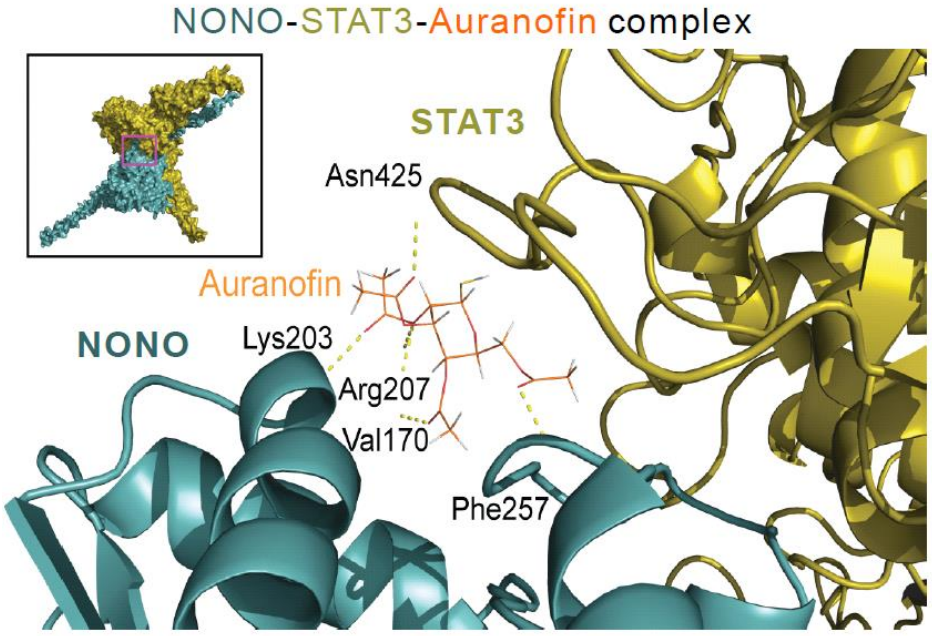
NONO-STAT3-Auranofin complex
STAT3
Asn425
Auranofin
NONO
Lys203
Arg207
Val170
Phe257

Figure 30. Modeling of the structure prediction of drug-target interaction.

(A and B) A computational docking model for human NONO and auranofin (A) and a NONO, STAT3, and auranofin complex (B) which were predicted using ClusPro and Autodock Vina.

Discussion

Identification of the molecular function of NONO in TNBC

Current TNBC treatments include chemotherapy targeting both cancer cells and normal cells. However, chemotherapy has limited effectiveness and can cause serious side effects [10]. Because TNBC lacks ER, PR, and HER2 receptors, it exhibits resistance to established hormone therapies for BC such as tamoxifen or aromatase inhibitors, as well as HER2-targeted therapies like trastuzumab [121]. TNBC treatments therefore involve the use of anticancer agents that target specific proteins that contribute to the cancer cell survival, growth, and resistance to drugs [122]. Targeted anticancer drugs that target proteins can reduce side effects and improve tolerability to chemotherapy. Understanding the molecular mechanisms of oncogenic property genes is essential to the discovery of molecular targets and therapeutic approaches for various cancer types. The emerging functions of the RBPs in cancer are now identified as factors that can directly drive tumorigenesis. Moreover, the aberrant expression or dysfunction of RBPs are commonly observed in diverse cancer types and these molecules can contribute to the initiation, progression, and metastasis of cancer, acting as either oncoproteins or tumor suppressors [100].

In the current study, we uncovered that novel functions of NONO are pivotal RBPs that play a critical role in regulating the growth of TNBC cells. In addition, we found that a NONO-STAT3 axis is clearly involved in cancer cell proliferation and enhancing drug sensitivity in TNBC (Figures 1–30). While upstream regulators of NONO such as ets proto-oncogene 1 (Ets-1) [105] and CREB-regulated transcription coactivator (CRTC)/long intergenic non-protein coding RNA 473 (LINC00473) [123] mediating cancer cell growth have been defined, a downstream target of NONO driving tumorigenesis has not been adequately characterized. Our genomic analysis demonstrates that STAT3 is directly targeted by NONO (Figures 10-18). We observed that the bind between NONO and STAT3 plays a significant role in regulating cancer cell growth and drug sensitivity in TNBC. NONO exerts its function by interacting with both STAT3 RNA and protein. Previous research has demonstrated that STAT3 plays a role in promoting cancer cell growth, invasion, and migration [110].

STAT3 directly regulates the expression of several oncogenes including *COX2* and the DNA binding 1 (*ID1)* inhibitor, *CCND1*, vascular endothelial growth factor *(VEGF)*, matrix metalloproteinase *(MMP),* and interleukins (*ILs)* families. These downstream targets are involved in driving the processes of carcinogenesis, including cell proliferation, angiogenesis, and extracellular matrix remodeling [124].

Therefore, STAT3 targeting is a promising strategy for treating various malignant tumors [125]. The data strongly indicate that the oncogenic potential of NONO relies heavily on the expression of STAT3 (Figures 10–27). To fulfill its typical role as an RBP, it directly interacts with specific RNA sequences that individual RBPs preferentially recognize and RBPs are involved in various processes including transcription, translation, RNA stability, subcellular localization, and degradation. [100]. We found that NONO directly bound to the putative binding site on the STAT3 3' UTR region (Figures 13A–B and 14A). Interestingly, apart from its known function in stabilizing STAT3 RNA, NONO directly binds to the STAT3 protein, which enhances its stability and activity. Through multiple cooperative mechanisms, NONO can modulate the function of STAT3 as illustrated in Figures 13–18.

A comprehensive analysis of genomic data revealed differential expression of various RBPs between TNBC and non-TNBC samples as shown in Figure 1B. However, recent genomic analysis with transcriptome reveals that the expression of RBPs is significantly higher in tumor tissues than in normal tissues [54]. The identification of differentially expressed RBPs across specific cancer subtypes has been limited. We found that 10 RBPs exhibited significant upregulation in TNBC and were strongly correlated with chemotherapy responsiveness although the p-value was not significant depending on chemotherapy types. The expression of NONO is correlated with the response to anticancer drugs, as demonstrated by the ROC curve analysis (Figures 3B and 26A). Although the current study focused on NONO function, other RBPs are worth investigating further because they may play crucial roles in maintaining the oncogenic properties in cancer. Recent studies evidence the interplay between RBPs and ER-positive BC. For instance, the RBP MSI2 is involved in the regulation of the estrogen receptor 1 (ESR1) gene [98]. Meanwhile, RNA-binding region-containing protein 1 (RNPC1) RBP has been identified as a modulator of ESR1 stabilization [126]. While a previous study suggested that RBPs play a role in TNBC [127], the mechanisms underlying their involvement and their clinical relevance were not comprehensively understood and the clinical relevance was unclear. However, our study findings clearly illustrate that NONO expression is significantly increased in TNBC and exhibits a functional association between RBP and cell proliferation. We utilized MDA-MB-231 and Hs 578T cells. However, drug resistant TNBC cell lines were excluded in our experiments. To enhance the clinical relevance of our findings, additional experiments using drug resistant TNBC cell lines, such as those resistant to DOX or cisplatin, should be performed. By incorporating a drug resistance model, we can comprehensively assess the impact of NONO RBPs and other RBPs on drug resistance. Although further validation is required before the application of NONO as a molecular marker, the facilitation of NONO as a therapeutic target in TNBC warrants further research. Because NONO has an oncogenic

function, suppressing NONO function using molecular inhibitors is therapeutically essential in cancer management. The disruption of NONO-target RNA is now common because the target RNA and function of NONO have not been comprehensively elucidated. The development of effective targeting systems may be advanced.

Previous studies demonstrated that STAT3 activated by interleukin-6 (IL-6) and janus kinase (JAK) is frequently associated with drug resistance in various cancers [128, 129]. These findings suggest that the NONO-STAT3 axis plays a critical role in determining drug responsiveness and clinical outcomes for patients with cancer. Therefore, the inhibition of NONO in TNBC cells downregulated the expression of the STAT3 gene, resulting in increased sensitivity to chemotherapeutic drugs (Figures 23–27). To improve drug-sensitization in TNBC, targeting NONO might be a very effective way of inhibiting the oncogenic properties of STAT3. While STAT3 participates in gene regulation of TF, thus contributing to gene transcription and expression, the association of STAT3 with RBP to coordinate oncogenic function is unclear. NONO targeting using neutralizing antibodies is ineffective owing to the cellular localization of RBP. As shown in Figure 9A, the use of siNONO-targeting NONO would be a suitable way of enhancing drug sensitization in TNBC. Downregulation of NONO using antisense RNA or proteolysis-targeting chimeras is a promising therapeutic strategy that is currently being explored in diverse clinical settings for the treatment of TNBC. Proof-of-concept experiments have demonstrated the potential of small-molecule inhibitors or oligonucleotides to disrupt RBP-RNA interactions [74]. Crystal structure analysis revealed that NONO forms a heterodimer with SFPQ [130]. However, the functional implications of this heterodimerization in cancer development and the assembly of the NONO-STAT3-SFPQ triple complex are unclear. Whether disrupting either the heterodimer or the complex would effectively suppress the functions of NONO is currently unknown.

NONO as therapeutic targets for TNBC

Based on the study results, we investigated the potential of the use of NONO inhibitors in TNBC. A drug screening experiment identified auranofin as one of the potential inhibitors targeting NONO in TNBC (Figures 28–30). Auranofin, an oral gold compound, is FDA-approved for the treatment of rheumatoid arthritis. it primarily functions by inhibiting the enzyme thioredoxin reductase (TrxR), thus increasing oxidative stress and impairing cellular adaptive responses, and consequently reducing pain and inflammation [131]. TrxR is an important protein involved in the regulation of cellular redox responses, and inhibition of TrxR disrupts the balance of cellular redox homeostasis [132]. Recent studies utilizing the concept of drug repurposing have indicated that auranofin exhibits antiproliferative

effects in cancer cells [120, 133]. In addition, auranofin can inhibit cancer cell growth and impede cancer progression by suppressing the activation of STAT3, a TF that plays an important role in diverse cellular processes [134, 135]. Therefore, the inhibition of the NONO-STAT3 axis by auranofin in TNBC suggests a mechanism of action that differs from previously known effects of auranofin. For TNBC, experimental results provided insight into the effects of auranofin on cancer cells (Figure 29). Inhibition of the NONO-STAT3 axis by auranofin was confirmed in TNBC (Figure 29), confirming that auranofin's mechanism of action is consistent across cancer types. Although the present results suggest that auranofin may modulate NONO activity, further research is required to comprehensively elucidate the molecular interactions and subsequent effects resulting from the inhibition of the NONO-STAT3 axis by auranofin.

NONO inhibition yields anticancer effects through the modulation of the STAT3 signaling pathway in TNBC (Figure 29). Alternative or complementary treatment options can be offered to patients who do not respond favorably to chemotherapy or who relapse. TNBC is resistant to chemotherapy, whose effectiveness is limited over time. Therefore, NONO inhibition may help overcome drug resistance by interfering with pathways that support the survival and proliferation of cancer cells. NONO inhibition can be combined with chemotherapy or other targeted therapies to enhance the overall efficiency of treatment [136]. These methods may have a synergistic effect on increased therapeutic efficacy and overcome drug resistance, particularly in TNBC. If NONO is used as a therapeutic target, the inhibition of NONO can also be used for TNBC diagnosis and treatment monitoring, allowing for more optimized prediction of the treatment outcome and allowing for tailored treatment. Summarily, inhibiting NONO presents an approach toward TNBC treatment that addresses the limitations of existing therapies, such as lack of target specificity and drug resistance. However, additional research is required to comprehensively elucidate the potential benefits, safety, and efficacy of NONO inhibition in TNBC compared to conventional treatments.

Assessing the expression level of NONO can help identify a patient subgroup that is likely to exhibit a positive response to anticancer drug treatment. Moreover, the activation of STAT3, an oncogenic TF, through NONO expression provides an opportunity to target STAT3 activity using auranofin, an inhibitor of NONO expression. By inhibiting NONO expression, auranofin can achieve a similar effect to directly inhibiting STAT3 activity using established STAT3 inhibitors. This suggests that targeting NONO could potentially inhibit the oncogenic function induced by STAT3 activation. In addition, by targeting NONO, a highly expressed in TNBC and among the various genes that regulate STAT3, and

suppressing STAT3 activity, precise and effective treatment outcomes can be achieved for TNBC compared to other anticancer drugs that do not target NONO. This underscores the potential of NONO as a targeted therapeutic option specifically for TNBC. Notably, while this information is based on available research findings, further studies and clinical trials are needed to comprehensively elucidate the therapeutic potential and clinical implications of targeting NONO in TNBC.

Small molecule inhibitors are compounds used to block the activity of a target protein [137]. Cancer progression can be effectively slowed down by targeting proteins that significantly contribute to the initiation and advancement of cancer [138]. However, this can be particularly problematic when proteins essential for functioning in normal cells or tissues are inhibited. These side effects can lead to drug toxicity and damage to vital organs such as the kidneys, liver, and heart. NONO is involved in various cellular processes, thus exerting significant functional roles [139] including transcription, RNA splicing, mRNA stability, and maintenance of cellular homeostasis [140, 141]. Inhibiting NONO can disrupt these processes, leading to abnormal cellular function and apoptosis. It can also affect other proteins owing to off-target effects, causing unpredictable side effects [137]. Therefore, pre-evaluating the potential effects of NONO inhibition using animal or cell models is crucial.

The inhibition of NONO exerts distinct anti-cancer effects through different mechanisms in two cancer types. Specifically, it targets STAT3 in TNBC and nicotinamide phosphoribosyltransferase (NAMPT) in lung cancer [142]. While STAT3 and NAMPT mechanisms regulated by NONO may not be directly related, separate pathways may be involved in promoting cancer cell survival, proliferation, and therapy resistance [143, 144]. RBPs, including NONO, eIF4E, HuR, MSI, and LIN28, can regulate gene expression at multiple levels, such as transcription, splicing, translation, and RNA decay [66]. Consequently, the target molecules and downstream pathways influenced by NONO can vary based on the cell type and the context of the cancer being studied.

For instance, the RBP HuR has been extensively studied in breast, lung, liver, and colorectal cancers [58]. In breast cancer, HuR promotes tumor growth and progression by stabilizing and increasing the expression of several oncogenes, including Cyclin D1 and VEGF [145, 146]. In lung cancer, HuR contributes to tumorigenesis and drug resistance by regulating specific target genes including Bcl-2 and COX2 [147-149]. In liver cancer, HuR has been implicated in tumor progression, invasion, and metastasis through the regulation of target genes including MMP9 and VEGF [150]. Finally, in colorectal cancer, HuR is involved in the development and progression of tumors by controlling the expression of specific target genes including COX2 and VEGF [71]. The specific targets and

mechanisms may differ across different cancer contexts, underscoring the complexity and diversity of the role of RBPs in cancer biology.

The context-dependent functions and diverse roles of RBPs in cancer highlight the significance of developing therapeutic strategies tailored to the specific molecular landscape of each cancer type. Additional research is needed to elucidate the intricate interactions between proteins and their target pathways in various cancer contexts.

Conclusions

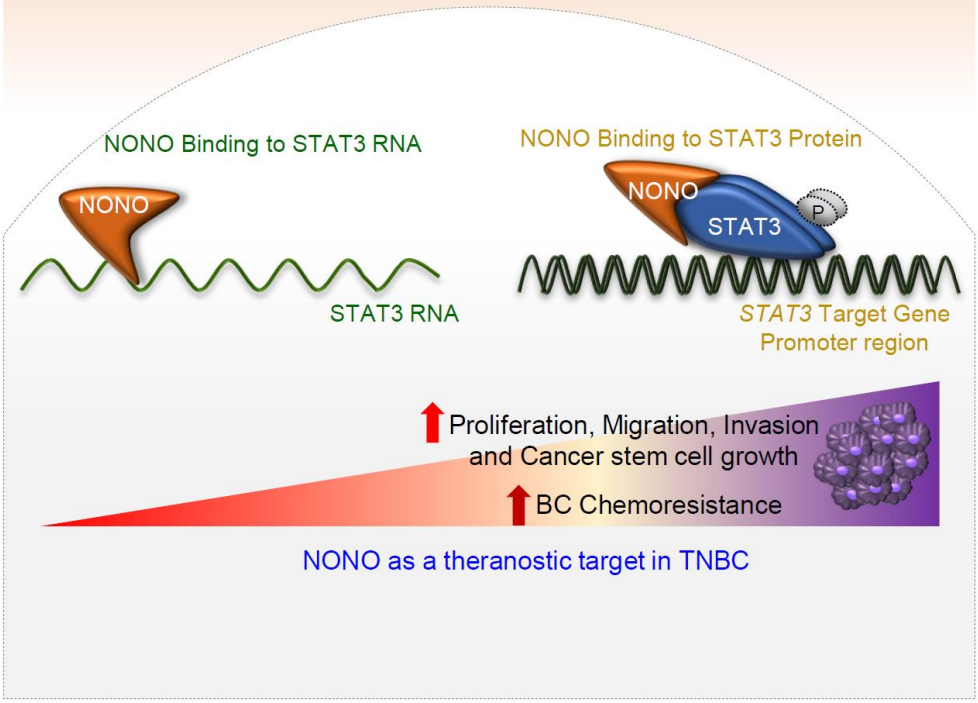

This study identifies a novel function for the NONO RBP in TNBC. We novelly illustrate that NONO is a TNBC-specific RBP that regulates oncogenic signaling pathways. Although RBPs are potential cancer therapeutic targets, the mechanisms underlying their role in specific cancer lineages need to be elucidated to fulfill this therapeutic promise.

To identify lineage specific RBPs, we analyzed TNBC gene expression data and found that NONO expression is linked to clinical outcomes in TNBC. Importantly, NONO increases the transcription and stability of STAT3, thereby increasing STAT3 activity. A knockdown of NONO with nanoparticle-encapsulated siRNA markedly suppressed the growth of TNBC. Drug screening to determine the chemical inhibitor targeting NONO reveals that auranofin is a potent NONO inhibitor. Finally, the study demonstrates that NONO-STAT3 axis is crucial for maintaining the oncogenic property.

The current study thus provides new molecular insights into the regulation of TNBC cell growth induced by RBPs and supports NONO as a viable therapeutic target in these cancers. The study findings significantly elucidate TNBC development at the molecular and therapeutic levels and will be of significant general interest to the biomedical research community.

References

1. Miller KD, Nogueira L, Devasia T, Mariotto AB, Yabroff KR, Jemal A, et al. Cancer treatment and survivorship statistics, 2022. CA Cancer J Clin. 2022; 72: 409-36.
2. Ghoncheh M, Pournamdar Z, Salehiniya H. Incidence and Mortality and Epidemiology of Breast Cancer in the World. Asian Pac J Cancer Prev. 2016; 17: 43-6.
3. Morrow PK, Hortobagyi GN. Management of breast cancer in the genome era. Annu Rev Med. 2009; 60: 153-65.
4. Clark GM, Osborne CK, McGuire WL. Correlations between estrogen receptor, progesterone receptor, and patient characteristics in human breast cancer. J Clin Oncol. 1984; 2: 1102-9.
5. Mohammed H, Russell IA, Stark R, Rueda OM, Hickey TE, Tarulli GA, et al. Progesterone receptor modulates ERalpha action in breast cancer. Nature. 2015; 523: 313-7.
6. Li Z, Wei H, Li S, Wu P, Mao X. The Role of Progesterone Receptors in Breast Cancer. Drug Des Devel Ther. 2022; 16: 305-14.
7. Slamon DJ, Clark GM, Wong SG, Levin WJ, Ullrich A, McGuire WL. Human breast cancer: correlation of relapse and survival with amplification of the HER-2/neu oncogene. Science. 1987; 235: 177-82.
8. Agarwal G, Nanda G, Lal P, Mishra A, Agarwal A, Agrawal V, et al. Outcomes of Triple-Negative Breast Cancers (TNBC) Compared with Non-TNBC: Does the Survival Vary for All Stages? World J Surg. 2016; 40: 1362-72.
9. Borri F, Granaglia A. Pathology of triple negative breast cancer. Semin Cancer Biol. 2021; 72: 136-45.
10. Bianchini G, Balko JM, Mayer IA, Sanders ME, Gianni L. Triple-negative breast cancer: challenges and opportunities of a heterogeneous disease. Nat Rev Clin Oncol. 2016; 13: 674-90.
11. Palma G, Frasci G, Chirico A, Esposito E, Siani C, Saturnino C, et al. Triple negative breast cancer: looking for the missing link between biology and treatments. Oncotarget. 2015; 6: 26560-74.
12. Cinkaya A, Akin M, Sengul A. Evaluation of treatment outcomes of triple-negative breast cancer. J Cancer Res Ther. 2016; 12: 150-4.
13. Early Breast Cancer Trialists' Collaborative G, Davies C, Godwin J, Gray R, Clarke M, Cutter D, et al. Relevance of breast cancer hormone receptors and other factors to the efficacy of adjuvant tamoxifen: patient-level meta-analysis of randomised trials. Lancet. 2011; 378: 771-84.
14. Goodwin PJ. Extended Aromatase Inhibitors in Hormone-Receptor-Positive Breast Cancer. N Engl J Med. 2021; 385: 462-3.
15. Robertson JF, Llombart-Cussac A, Rolski J, Feltl D, Dewar J, Macpherson E, et al. Activity of

fulvestrant 500 mg versus anastrozole 1 mg as first-line treatment for advanced breast cancer: results from the FIRST study. J Clin Oncol. 2009; 27: 4530-5.

16. DeVita VT, Lawrence TS, Rosenberg SA. DeVita, Hellman, and Rosenberg's Cancer: Principles & Practice of Oncology: Wolters Kluwer/Lippincott Williams & Wilkins; 2008.

17. Longo D, Fauci A, Kasper D, Hauser S, Jameson J, Loscalzo J. Harrison's Principles of Internal Medicine, 18th Edition: McGraw-Hill Education; 2011.

18. Chabner BA, Roberts TG, Jr. Timeline: Chemotherapy and the war on cancer. Nat Rev Cancer. 2005; 5: 65-72.

19. Fong PC, Boss DS, Yap TA, Tutt A, Wu P, Mergui-Roelvink M, et al. Inhibition of poly(ADP-ribose) polymerase in tumors from BRCA mutation carriers. N Engl J Med. 2009; 361: 123-34.

20. Davies BR, Guan N, Logie A, Crafter C, Hanson L, Jacobs V, et al. Tumors with AKT1E17K Mutations Are Rational Targets for Single Agent or Combination Therapy with AKT Inhibitors. Mol Cancer Ther. 2015; 14: 2441-51.

21. Richon VM, Emiliani S, Verdin E, Webb Y, Breslow R, Rifkind RA, et al. A class of hybrid polar inducers of transformed cell differentiation inhibits histone deacetylases. Proc Natl Acad Sci U S A. 1998; 95: 3003-7.

22. Emens LA, Ascierto PA, Darcy PK, Demaria S, Eggermont AMM, Redmond WL, et al. Cancer immunotherapy: Opportunities and challenges in the rapidly evolving clinical landscape. Eur J Cancer. 2017; 81: 116-29.

23. Slamon DJ, Leyland-Jones B, Shak S, Fuchs H, Paton V, Bajamonde A, et al. Use of chemotherapy plus a monoclonal antibody against HER2 for metastatic breast cancer that overexpresses HER2. N Engl J Med. 2001; 344: 783-92.

24. Gianni L, Pienkowski T, Im YH, Tseng LM, Liu MC, Lluch A, et al. 5-year analysis of neoadjuvant pertuzumab and trastuzumab in patients with locally advanced, inflammatory, or early-stage HER2-positive breast cancer (NeoSphere): a multicentre, open-label, phase 2 randomised trial. Lancet Oncol. 2016; 17: 791-800.

25. Anders CK, Carey LA. Biology, metastatic patterns, and treatment of patients with triple-negative breast cancer. Clin Breast Cancer. 2009; 9 Suppl 2: S73-81.

26. Dent R, Trudeau M, Pritchard KI, Hanna WM, Kahn HK, Sawka CA, et al. Triple-negative breast cancer: clinical features and patterns of recurrence. Clin Cancer Res. 2007; 13: 4429-34.

27. Carey LA, Dees EC, Sawyer L, Gatti L, Moore DT, Collichio F, et al. The triple negative paradox: primary tumor chemosensitivity of breast cancer subtypes. Clin Cancer Res. 2007; 13: 2329-34.

28. Debela DT, Muzazu SG, Heraro KD, Ndalama MT, Mesele BW, Haile DC, et al. New

approaches and procedures for cancer treatment: Current perspectives. SAGE Open Med. 2021; 9: 20503121211034366.

29. Baskar R, Lee KA, Yeo R, Yeoh KW. Cancer and radiation therapy: current advances and future directions. Int J Med Sci. 2012; 9: 193-9.

30. Li Z, Qiu Y, Lu W, Jiang Y, Wang J. Immunotherapeutic interventions of Triple Negative Breast Cancer. J Transl Med. 2018; 16: 147.

31. Valencia GA, Rioja P, Morante Z, Ruiz R, Fuentes H, Castaneda CA, et al. Immunotherapy in triple-negative breast cancer: A literature review and new advances. World J Clin Oncol. 2022; 13: 219-36.

32. Holohan C, Van Schaeybroeck S, Longley DB, Johnston PG. Cancer drug resistance: an evolving paradigm. Nat Rev Cancer. 2013; 13: 714-26.

33. Mansoori B, Mohammadi A, Davudian S, Shirjang S, Baradaran B. The Different Mechanisms of Cancer Drug Resistance: A Brief Review. Adv Pharm Bull. 2017; 7: 339-48.

34. Housman G, Byler S, Heerboth S, Lapinska K, Longacre M, Snyder N, et al. Drug resistance in cancer: an overview. Cancers (Basel). 2014; 6: 1769-92.

35. Hashem S, Ali TA, Akhtar S, Nisar S, Sageena G, Ali S, et al. Targeting cancer signaling pathways by natural products: Exploring promising anti-cancer agents. Biomed Pharmacother. 2022; 150: 113054.

36. Qin H, Ni H, Liu Y, Yuan Y, Xi T, Li X, et al. RNA-binding proteins in tumor progression. J Hematol Oncol. 2020; 13: 90.

37. Boo SH, Kim YK. The emerging role of RNA modifications in the regulation of mRNA stability. Exp Mol Med. 2020; 52: 400-8.

38. Kovarik P, Bestehorn A, Fesselet J. Conceptual Advances in Control of Inflammation by the RNA-Binding Protein Tristetraprolin. Front Immunol. 2021; 12: 751313.

39. Baralle FE, Giudice J. Alternative splicing as a regulator of development and tissue identity. Nat Rev Mol Cell Biol. 2017; 18: 437-51.

40. Chao Y, Jiang Y, Zhong M, Wei K, Hu C, Qin Y, et al. Regulatory roles and mechanisms of alternative RNA splicing in adipogenesis and human metabolic health. Cell Biosci. 2021; 11: 66.

41. Thelen MP, Kye MJ. The Role of RNA Binding Proteins for Local mRNA Translation: Implications in Neurological Disorders. Front Mol Biosci. 2019; 6: 161.

42. Morris C, Cluet D, Ricci EP. Ribosome dynamics and mRNA turnover, a complex relationship under constant cellular scrutiny. Wiley Interdiscip Rev RNA. 2021; 12: e1658.

43. Turner-Bridger B, Caterino C, Cioni JM. Molecular mechanisms behind mRNA localization in axons. Open Biol. 2020; 10: 200177.

44. Idler RK, Yan W. Control of messenger RNA fate by RNA-binding proteins: an emphasis on mammalian spermatogenesis. J Androl. 2012; 33: 309-37.
45. Gerstberger S, Hafner M, Tuschl T. A census of human RNA-binding proteins. Nat Rev Genet. 2014; 15: 829-45.
46. Wang ZL, Li B, Luo YX, Lin Q, Liu SR, Zhang XQ, et al. Comprehensive Genomic Characterization of RNA-Binding Proteins across Human Cancers. Cell Rep. 2018; 22: 286-98.
47. Lukong KE, Chang KW, Khandjian EW, Richard S. RNA-binding proteins in human genetic disease. Trends Genet. 2008; 24: 416-25.
48. Kang D, Lee Y, Lee JS. RNA-Binding Proteins in Cancer: Functional and Therapeutic Perspectives. Cancers (Basel). 2020; 12.
49. Darnell RB. RNA regulation in neurologic disease and cancer. Cancer Res Treat. 2010; 42: 125-9.
50. Neelamraju Y, Hashemikhabir S, Janga SC. The human RBPome: from genes and proteins to human disease. J Proteomics. 2015; 127: 61-70.
51. Busa R, Paronetto MP, Farini D, Pierantozzi E, Botti F, Angelini DF, et al. The RNA-binding protein Sam68 contributes to proliferation and survival of human prostate cancer cells. Oncogene. 2007; 26: 4372-82.
52. Degrauwe N, Suva ML, Janiszewska M, Riggi N, Stamenkovic I. IMPs: an RNA-binding protein family that provides a link between stem cell maintenance in normal development and cancer. Genes Dev. 2016; 30: 2459-74.
53. Wurth L, Papasaikas P, Olmeda D, Bley N, Calvo GT, Guerrero S, et al. UNR/CSDE1 Drives a Post-transcriptional Program to Promote Melanoma Invasion and Metastasis. Cancer Cell. 2016; 30: 694-707.
54. Dang H, Takai A, Forgues M, Pomyen Y, Mou H, Xue W, et al. Oncogenic Activation of the RNA Binding Protein NELFE and MYC Signaling in Hepatocellular Carcinoma. Cancer Cell. 2017; 32: 101-14 e8.
55. Jang HH, Lee HN, Kim SY, Hong S, Lee WS. Expression of RNA-binding Motif Protein 3 (RBM3) and Cold-inducible RNA-binding protein (CIRP) Is Associated with Improved Clinical Outcome in Patients with Colon Cancer. Anticancer Res. 2017; 37: 1779-85.
56. Mohibi S, Chen X, Zhang J. Cancer the'RBP'eutics-RNA-binding proteins as therapeutic targets for cancer. Pharmacol Ther. 2019; 203: 107390.
57. Majumder M, Chakraborty P, Mohan S, Mehrotra S, Palanisamy V. HuR as a molecular target for cancer therapeutics and immune-related disorders. Adv Drug Deliv Rev. 2022; 188: 114442.
58. Wang J, Guo Y, Chu H, Guan Y, Bi J, Wang B. Multiple functions of the RNA-binding protein

HuR in cancer progression, treatment responses and prognosis. Int J Mol Sci. 2013; 14: 10015-41.
59. Anczukow O, Krainer AR. Splicing-factor alterations in cancers. RNA. 2016; 22: 1285-301.
60. Zhao Y, Mir C, Garcia-Mayea Y, Paciucci R, Kondoh H, ME LL. RNA-binding proteins: Underestimated contributors in tumorigenesis. Semin Cancer Biol. 2022; 86: 431-44.
61. Li Y. Modern epigenetics methods in biological research. Methods. 2021; 187: 104-13.
62. Bonasio R, Tu S, Reinberg D. Molecular signals of epigenetic states. Science. 2010; 330: 612-6.
63. Zhou L, Wu Y, Xin L, Zhou Q, Li S, Yuan Y, et al. Development of RNA binding proteins expression signature for prognosis prediction in gastric cancer patients. Am J Transl Res. 2020; 12: 6775-92.
64. Jonas K, Calin GA, Pichler M. RNA-Binding Proteins as Important Regulators of Long Non-Coding RNAs in Cancer. Int J Mol Sci. 2020; 21.
65. Yao ZT, Yang YM, Sun MM, He Y, Liao L, Chen KS, et al. New insights into the interplay between long non-coding RNAs and RNA-binding proteins in cancer. Cancer Commun (Lond). 2022; 42: 117-40.
66. Cen Y, Chen L, Liu Z, Lin Q, Fang X, Yao H, et al. Novel roles of RNA-binding proteins in drug resistance of breast cancer: from molecular biology to targeting therapeutics. Cell Death Discov. 2023; 9: 52.
67. Cencic R, Hall DR, Robert F, Du Y, Min J, Li L, et al. Reversing chemoresistance by small molecule inhibition of the translation initiation complex eIF4F. Proc Natl Acad Sci U S A. 2011; 108: 1046-51.
68. Moerke NJ, Aktas H, Chen H, Cantel S, Reibarkh MY, Fahmy A, et al. Small-molecule inhibition of the interaction between the translation initiation factors eIF4E and eIF4G. Cell. 2007; 128: 257-67.
69. Konicek BW, Stephens JR, McNulty AM, Robichaud N, Peery RB, Dumstorf CA, et al. Therapeutic inhibition of MAP kinase interacting kinase blocks eukaryotic initiation factor 4E phosphorylation and suppresses outgrowth of experimental lung metastases. Cancer Res. 2011; 71: 1849-57.
70. Wang J, Hjelmeland AB, Nabors LB, King PH. Anti-cancer effects of the HuR inhibitor, MS-444, in malignant glioma cells. Cancer Biol Ther. 2019; 20: 979-88.
71. Blanco FF, Preet R, Aguado A, Vishwakarma V, Stevens LE, Vyas A, et al. Impact of HuR inhibition by the small molecule MS-444 on colorectal cancer cell tumorigenesis. Oncotarget. 2016; 7: 74043-58.
72. Clingman CC, Deveau LM, Hay SA, Genga RM, Shandilya SM, Massi F, et al. Allosteric

inhibition of a stem cell RNA-binding protein by an intermediary metabolite. Elife. 2014; 3.
73. Minuesa G, Albanese SK, Xie W, Kazansky Y, Worroll D, Chow A, et al. Small-molecule targeting of MUSASHI RNA-binding activity in acute myeloid leukemia. Nat Commun. 2019; 10: 2691.
74. Roos M, Pradere U, Ngondo RP, Behera A, Allegrini S, Civenni G, et al. A Small-Molecule Inhibitor of Lin28. ACS Chem Biol. 2016; 11: 2773-81.
75. Lin Z, Radaeva M, Cherkasov A, Dong X. Lin28 Regulates Cancer Cell Stemness for Tumour Progression. Cancers (Basel). 2022; 14.
76. Julio AR, Backus KM. New approaches to target RNA binding proteins. Curr Opin Chem Biol. 2021; 62: 13-23.
77. Corley M, Burns MC, Yeo GW. How RNA-Binding Proteins Interact with RNA: Molecules and Mechanisms. Mol Cell. 2020; 78: 9-29.
78. Meyer SM, Williams CC, Akahori Y, Tanaka T, Aikawa H, Tong Y, et al. Small molecule recognition of disease-relevant RNA structures. Chem Soc Rev. 2020; 49: 7167-99.
79. Kok VJT, Tang JY, Eng GWL, Tan SY, Chin JTF, Quek CH, et al. SFPQ promotes RAS-mutant cancer cell growth by modulating 5'-UTR mediated translational control of CK1alpha. NAR Cancer. 2022; 4: zcac027.
80. Rogoyski O, Gerber AP. RNA-binding proteins modulate drug sensitivity of cancer cells. Emerg Top Life Sci. 2021; 5: 681-5.
81. Xue YC, Ng CS, Xiang P, Liu H, Zhang K, Mohamud Y, et al. Dysregulation of RNA-Binding Proteins in Amyotrophic Lateral Sclerosis. Front Mol Neurosci. 2020; 13: 78.
82. Singh R, Gupta SC, Peng WX, Zhou N, Pochampally R, Atfi A, et al. Regulation of alternative splicing of Bcl-x by BC200 contributes to breast cancer pathogenesis. Cell Death Dis. 2016; 7: e2262.
83. Vo DT, Abdelmohsen K, Martindale JL, Qiao M, Tominaga K, Burton TL, et al. The oncogenic RNA-binding protein Musashi1 is regulated by HuR via mRNA translation and stability in glioblastoma cells. Mol Cancer Res. 2012; 10: 143-55.
84. Lin GL, Ting HJ, Tseng TC, Juang V, Lo YL. Modulation of the mRNA-binding protein HuR as a novel reversal mechanism of epirubicin-triggered multidrug resistance in colorectal cancer cells. PLoS One. 2017; 12: e0185625.
85. Ramesh-Kumar D, Guil S. The IGF2BP family of RNA binding proteins links epitranscriptomics to cancer. Semin Cancer Biol. 2022; 86: 18-31.
86. Chen HM, Lin CC, Chen WS, Jiang JK, Yang SH, Chang SC, et al. Insulin-Like Growth Factor 2 mRNA-Binding Protein 1 (IGF2BP1) Is a Prognostic Biomarker and Associated with Chemotherapy Responsiveness in Colorectal Cancer. Int J Mol Sci. 2021; 22.
87. Warner KD, Hajdin CE, Weeks KM. Principles for targeting RNA with drug-like small

molecules. Nat Rev Drug Discov. 2018; 17: 547-58.
88. Jankowsky E, Harris ME. Specificity and nonspecificity in RNA-protein interactions. Nat Rev Mol Cell Biol. 2015; 16: 533-44.
89. Park YY, Kim K, Kim SB, Hennessy BT, Kim SM, Park ES, et al. Reconstruction of nuclear receptor network reveals that NR2E3 is a novel upstream regulator of ESR1 in breast cancer. EMBO Mol Med. 2012; 4: 52-67.
90. Park YY, Jung SY, Jennings NB, Rodriguez-Aguayo C, Peng G, Lee SR, et al. FOXM1 mediates Dox resistance in breast cancer by enhancing DNA repair. Carcinogenesis. 2012; 33: 1843-53.
91. Kang MH, Choi H, Oshima M, Cheong JH, Kim S, Lee JH, et al. Estrogen-related receptor gamma functions as a tumor suppressor in gastric cancer. Nat Commun. 2018; 9: 1920.
92. Kim H, Suh JM, Hwang ES, Kim DW, Chung HK, Song JH, et al. Thyrotropin-mediated repression of class II trans-activator expression in thyroid cells: involvement of STAT3 and suppressor of cytokine signaling. J Immunol. 2003; 171: 616-27.
93. Kharade SS, Parekh VI, Agarwal SK. Functional Defects From Endocrine Disease-Associated Mutations in HLXB9 and Its Interacting Partner, NONO. Endocrinology. 2018; 159: 1199-212.
94. Budczies J, Klauschen F, Sinn BV, Gyorffy B, Schmitt WD, Darb-Esfahani S, et al. Cutoff Finder: a comprehensive and straightforward Web application enabling rapid biomarker cutoff optimization. PLoS One. 2012; 7: e51862.
95. Arnold K, Bordoli L, Kopp J, Schwede T. The SWISS-MODEL workspace: a web-based environment for protein structure homology modelling. Bioinformatics. 2006; 22: 195-201.
96. Porter KA, Xia B, Beglov D, Bohnuud T, Alam N, Schueler-Furman O, et al. ClusPro PeptiDock: efficient global docking of peptide recognition motifs using FFT. Bioinformatics. 2017; 33: 3299-301.
97. Trott O, Olson AJ. AutoDock Vina: improving the speed and accuracy of docking with a new scoring function, efficient optimization, and multithreading. J Comput Chem. 2010; 31: 455-61.
98. Kang MH, Jeong KJ, Kim WY, Lee HJ, Gong G, Suh N, et al. Musashi RNA-binding protein 2 regulates estrogen receptor 1 function in breast cancer. Oncogene. 2017; 36: 1745-52.
99. Almousa AA, Morris M, Fowler S, Jones J, Alcorn J. Elevation of serum pyruvate kinase M2 (PKM2) in IBD and its relationship to IBD indices. Clin Biochem. 2018; 53: 19-24.
100. Pereira B, Billaud M, Almeida R. RNA-Binding Proteins in Cancer: Old Players and New Actors. Trends Cancer. 2017; 3: 506-28.
101. van de Vijver MJ, He YD, van't Veer LJ, Dai H, Hart AA, Voskuil DW, et al. A gene-expression signature as a predictor of survival in breast cancer. N Engl J Med. 2002; 347: 1999-2009.
102. Oh DS, Troester MA, Usary J, Hu Z, He X, Fan C, et al. Estrogen-regulated genes predict

survival in hormone receptor-positive breast cancers. J Clin Oncol. 2006; 24: 1656-64.
103. Zhao Y, Simon R. BRB-ArrayTools Data Archive for human cancer gene expression: a unique and efficient data sharing resource. Cancer Inform. 2008; 6: 9-15.
104. Mihaly Z, Kormos M, Lanczky A, Dank M, Budczies J, Szasz MA, et al. A meta-analysis of gene expression-based biomarkers predicting outcome after tamoxifen treatment in breast cancer. Breast Cancer Res Treat. 2013; 140: 219-32.
105. Li D, Chen Y, Mei H, Jiao W, Song H, Ye L, et al. Ets-1 promoter-associated noncoding RNA regulates the NONO/ERG/Ets-1 axis to drive gastric cancer progression. Oncogene. 2018; 37: 4871-86.
106. Yamamoto R, Osawa T, Sasaki Y, Yamamoto S, Anai M, Izumi K, et al. Overexpression of p54(nrb)/NONO induces differential EPHA6 splicing and contributes to castration-resistant prostate cancer growth. Oncotarget. 2018; 9: 10510-24.
107. Yu T, Zhao Y, Hu Z, Li J, Chu D, Zhang J, et al. MetaLnc9 Facilitates Lung Cancer Metastasis via a PGK1-Activated AKT/mTOR Pathway. Cancer Res. 2017; 77: 5782-94.
108. Zhu Z, Zhao X, Zhao L, Yang H, Liu L, Li J, et al. p54(nrb)/NONO regulates lipid metabolism and breast cancer growth through SREBP-1A. Oncogene. 2016; 35: 1399-410.
109. Balanis N, Carlin CR. Stress-induced EGF receptor signaling through STAT3 and tumor progression in triple-negative breast cancer. Mol Cell Endocrinol. 2017; 451: 24-30.
110. Moreira MP, da Conceicao Braga L, Cassali GD, Silva LM. STAT3 as a promising chemoresistance biomarker associated with the CD44(+/high)/CD24(-/low)/ALDH(+) BCSCs-like subset of the triple-negative breast cancer (TNBC) cell line. Exp Cell Res. 2018; 363: 283-90.
111. Yang B, Shen JW, Zhou DH, Zhao YP, Wang WQ, Zhu Y, et al. Precise discovery of a STAT3 inhibitor from Eupatorium lindleyanum and evaluation of its activity of anti-triple-negative breast cancer. Nat Prod Res. 2019; 33: 477-85.
112. Jing N, Tweardy DJ. Targeting Stat3 in cancer therapy. Anticancer Drugs. 2005; 16: 601-7.
113. Benegiamo G, Mure LS, Erikson G, Le HD, Moriggi E, Brown SA, et al. The RNA-Binding Protein NONO Coordinates Hepatic Adaptation to Feeding. Cell Metab. 2018; 27: 404-18 e7.
114. Clevenger CV. Roles and regulation of stat family transcription factors in human breast cancer. Am J Pathol. 2004; 165: 1449-60.
115. Dassi E. Handshakes and Fights: The Regulatory Interplay of RNA-Binding Proteins. Front Mol Biosci. 2017; 4: 67.
116. McDaniel JM, Varley KE, Gertz J, Savic DS, Roberts BS, Bailey SK, et al. Genomic regulation of invasion by STAT3 in triple negative breast cancer. Oncotarget. 2017; 8: 8226-38.
117. Lee JS, Heo J, Libbrecht L, Chu IS, Kaposi-Novak P, Calvisi DF, et al. A novel prognostic subtype of human hepatocellular carcinoma derived from hepatic progenitor cells. Nat Med. 2006; 12:

410-6.
118. Kuo WY, Hwu L, Wu CY, Lee JS, Chang CW, Liu RS. STAT3/NF-kappaB-Regulated Lentiviral TK/GCV Suicide Gene Therapy for Cisplatin-Resistant Triple-Negative Breast Cancer. Theranostics. 2017; 7: 647-63.
119. Galoczova M, Coates P, Vojtesek B. STAT3, stem cells, cancer stem cells and p63. Cell Mol Biol Lett. 2018; 23: 12.
120. Raninga PV, Lee AC, Sinha D, Shih YY, Mittal D, Makhale A, et al. Therapeutic cooperation between auranofin, a thioredoxin reductase inhibitor and anti-PD-L1 antibody for treatment of triple-negative breast cancer. Int J Cancer. 2020; 146: 123-36.
121. Masoud V, Pages G. Targeted therapies in breast cancer: New challenges to fight against resistance. World J Clin Oncol. 2017; 8: 120-34.
122. Garrido-Castro AC, Lin NU, Polyak K. Insights into Molecular Classifications of Triple-Negative Breast Cancer: Improving Patient Selection for Treatment. Cancer Discov. 2019; 9: 176-98.
123. Chen Z, Li JL, Lin S, Cao C, Gimbrone NT, Yang R, et al. cAMP/CREB-regulated LINC00473 marks LKB1-inactivated lung cancer and mediates tumor growth. J Clin Invest. 2016; 126: 2267-79.
124. Kim BH, Yi EH, Ye SK. Signal transducer and activator of transcription 3 as a therapeutic target for cancer and the tumor microenvironment. Arch Pharm Res. 2016; 39: 1085-99.
125. Gelain A, Mori M, Meneghetti F, Villa S. Signal Transducer and Activator of Transcription Protein 3 (STAT3): An Update on its Direct Inhibitors as Promising Anticancer Agents. Curr Med Chem. 2019; 26: 5165-206.
126. Shi L, Xia TS, Wei XL, Zhou W, Xue J, Cheng L, et al. Estrogen receptor (ER) was regulated by RNPC1 stabilizing mRNA in ER positive breast cancer. Oncotarget. 2015; 6: 12264-78.
127. Mehta M, Basalingappa K, Griffith JN, Andrade D, Babu A, Amreddy N, et al. HuR silencing elicits oxidative stress and DNA damage and sensitizes human triple-negative breast cancer cells to radiotherapy. Oncotarget. 2016; 7: 64820-35.
128. Huang LL, Rao W. SiRNA interfering STAT3 enhances DDP sensitivity in cervical cancer cells. Eur Rev Med Pharmacol Sci. 2018; 22: 4098-106.
129. Wang TY, Yu CC, Hsieh PL, Liao YW, Yu CH, Chou MY. GMI ablates cancer stemness and cisplatin resistance in oral carcinomas stem cells through IL-6/Stat3 signaling inhibition. Oncotarget. 2017; 8: 70422-30.
130. Huang J, Casas Garcia GP, Perugini MA, Fox AH, Bond CS, Lee M. Crystal structure of a SFPQ/PSPC1 heterodimer provides insights into preferential heterodimerization of human DBHS family proteins. J Biol Chem. 2018; 293: 6593-602.
131. Zhang X, Selvaraju K, Saei AA, D'Arcy P, Zubarev RA, Arner ES, et al. Repurposing of

auranofin: Thioredoxin reductase remains a primary target of the drug. Biochimie. 2019; 162: 46-54.
132. Jastrzab A, Skrzydlewska E. Thioredoxin-dependent system. Application of inhibitors. J Enzyme Inhib Med Chem. 2021; 36: 362-71.
133. Gamberi T, Chiappetta G, Fiaschi T, Modesti A, Sorbi F, Magherini F. Upgrade of an old drug: Auranofin in innovative cancer therapies to overcome drug resistance and to increase drug effectiveness. Med Res Rev. 2022; 42: 1111-46.
134. Kim NH, Park HJ, Oh MK, Kim IS. Antiproliferative effect of gold(I) compound auranofin through inhibition of STAT3 and telomerase activity in MDA-MB 231 human breast cancer cells. BMB Rep. 2013; 46: 59-64.
135. Kim NH, Lee MY, Park SJ, Choi JS, Oh MK, Kim IS. Auranofin blocks interleukin-6 signalling by inhibiting phosphorylation of JAK1 and STAT3. Immunology. 2007; 122: 607-14.
136. Lee A, Djamgoz MBA. Triple negative breast cancer: Emerging therapeutic modalities and novel combination therapies. Cancer Treat Rev. 2018; 62: 110-22.
137. Yap TA, Workman P. Exploiting the cancer genome: strategies for the discovery and clinical development of targeted molecular therapeutics. Annu Rev Pharmacol Toxicol. 2012; 52: 549-73.
138. Zhang J, Yang PL, Gray NS. Targeting cancer with small molecule kinase inhibitors. Nat Rev Cancer. 2009; 9: 28-39.
139. Knott GJ, Bond CS, Fox AH. The DBHS proteins SFPQ, NONO and PSPC1: a multipurpose molecular scaffold. Nucleic Acids Res. 2016; 44: 3989-4004.
140. Shav-Tal Y, Zipori D. PSF and p54(nrb)/NonO--multi-functional nuclear proteins. FEBS Lett. 2002; 531: 109-14.
141. Dong X, Sweet J, Challis JR, Brown T, Lye SJ. Transcriptional activity of androgen receptor is modulated by two RNA splicing factors, PSF and p54nrb. Mol Cell Biol. 2007; 27: 4863-75.
142. Kim SJ, Ju JS, Park SS, Suh YA, Yoo HJ, Choi EK, et al. An RNA-binding-protein, NONO governs energy metabolism by regulating NAMPT in lung cancer. Biochem Biophys Res Commun. 2020; 528: 376-82.
143. Shackelford RE, Bui MM, Coppola D, Hakam A. Over-expression of nicotinamide phosphoribosyltransferase in ovarian cancers. Int J Clin Exp Pathol. 2010; 3: 522-7.
144. Lin TC. Updated Functional Roles of NAMPT in Carcinogenesis and Therapeutic Niches. Cancers (Basel). 2022; 14.
145. Yuan Z, Sanders AJ, Ye L, Wang Y, Jiang WG. Knockdown of human antigen R reduces the growth and invasion of breast cancer cells in vitro and affects expression of cyclin D1 and MMP-9. Oncol Rep. 2011; 26: 237-45.
146. Gubin MM, Calaluce R, Davis JW, Magee JD, Strouse CS, Shaw DP, et al. Overexpression of

the RNA binding protein HuR impairs tumor growth in triple negative breast cancer associated with deficient angiogenesis. Cell Cycle. 2010; 9: 3337-46.

147. Muralidharan R, Mehta M, Ahmed R, Roy S, Xu L, Aube J, et al. HuR-targeted small molecule inhibitor exhibits cytotoxicity towards human lung cancer cells. Sci Rep. 2017; 7: 9694.

148. Raguraman R, Shanmugarama S, Mehta M, Elle Peterson J, Zhao YD, Munshi A, et al. Drug delivery approaches for HuR-targeted therapy for lung cancer. Adv Drug Deliv Rev. 2022; 180: 114068.

149. Kim GY, Lim SJ, Kim YW. Expression of HuR, COX-2, and survivin in lung cancers; cytoplasmic HuR stabilizes cyclooxygenase-2 in squamous cell carcinomas. Mod Pathol. 2011; 24: 1336-47.

150. Lachiondo-Ortega S, Delgado TC, Banos-Jaime B, Velazquez-Cruz A, Diaz-Moreno I, Martinez-Chantar ML. Hu Antigen R (HuR) Protein Structure, Function and Regulation in Hepatobiliary Tumors. Cancers (Basel). 2022; 14.

국문요약

유방암은 여성에서 가장 발병율이 높은 암의 하나로, 에스트로겐 수용체, 프로게스테론 수용체와 표피 성장 인자 수용체 (HER2)는 대표적인 유방암 치료 표적으로 알려져 있다. 그런데, 이들 3종의 수용체를 발현하지 않는 삼중음성 유방암의 경우 전체 유방암 한자의 10~15% 정도를 차지하고 있으며, 삼중음성 유방암 환자는 임상에서 적용 가능한 치료제가 극히 제한적이며, 림프절 전이율이 높은 반면, 치료제에 대한 약제내성이 강하고, 반응이 좋지 않아 평균 5년 생존율이 65%이며, 종양이 전이된 경우 11%로 매우 낮다. 최근 연구에 따르면, 현재 최신 치료제의 옵션은 제한적인 부분에만 사용되고 있으며, 특정군에서만 치료효과를 보이기 때문에 치료제가 많이 부족하다고 보고되고 있다. 따라서, 삼중음성 유방암의 치료효과를 높이기 위해서는 새로운 치료 표적을 발굴하는 것이 반드시 필요하다.

RNA 결합 단백질(RBP)은 mRNA 안정성, RNA 이어맞추기, 번역 효율 및 단백질 세포 내 위치를 제어하여 다양한 세포 기능을 조절하는데 필수적이다. 인간 게놈 프로젝트를 통해 구조적, 기능적 다양성을 가진 1500개 이상의 RBP가 확인되었다. 최근, RNA 결합 단백질이 유전자의 발현을 조절하는 기능이 알려지면서 유방암을 포함한 다른 암에서도 발암유전자 발현조절에 RNA 결합 단백질이 관여하는 것으로 보고되고 있다. 이것은 RNA 결합 단백질이 항암 치료의 잠재적인 분자적 표적이 될 수 있음을 제시하고 있다. 본 연구에서는 유전자 분석을 통해 삼중음성 유방암 환자에서 RNA 결합 단백질인 NONO가 특이적으로 발현됨을 확인하였다. 삼중음성 유방암에서 NONO의 발현과 환자의 생존율간 음의 상관성을 가지는 것을 확인하였다. NONO 결핍 세포주를

확립하고, 유전자 발현 프로파일 분석을 통해 NONO가 삼중음성 유방암에서 세포 사멸, 세포 증식, 세포 주기 및 세포 이동과 연관성이 있음을 확인하였다. 특히, 삼중음성 유방암에서 NONO가 STAT3 mRNA에 결합하여 발현을 증가시키고 STAT3 단백질과 직접적인 상호 작용을 통해 안정성을 높여 발암 기능을 유지한다는 것을 발견하였다. 본 연구에서는 FDA 승인 라이브러리를 이용한 NONO 표적 항암제에 대한 고효율 스크리닝을 통해 오라노핀이 잠재적인 NONO 억제제이고, 삼중음성 유방암에서 세포 증식을 억제하는 것을 규명하였다. 본 연구의 결과를 종합하면, 삼중음성 유방암에서 NONO가 RNA와 단백질 수준에서 STAT3의 상위에서 발현 및 기능을 조절하여 전이 및 치료제 내성에 관여할 것으로 추측할 수 있다. 결론적으로 본 연구는 약제 내성 삼중음성 유방암에서 NONO가 새로운 치료 표적이 될 수 있음을 제시하고 있다.

중심 단어: RNA-결합 단백질; 삼중음성 유방암; NONO; STAT3; Auranofin